

# **Extrusion-based 3D Printing and Characterization of Edible Materials**

by

Chu Yin Huang

A thesis  
presented to the University of Waterloo  
in fulfillment of the  
thesis requirement for the degree of  
Master of Applied Science  
in  
Chemical Engineering

Waterloo, Ontario, Canada, 2018

© Chu Yin Huang 2018

## **Author's declaration**

I hereby declare that I am the sole author of this thesis. This is a true copy of the thesis, including any required final revisions, as accepted by my examiners.

I understand that my thesis may be made electronically available to the public.

## Abstract

3D printing food offers the ability to customize shapes, texture, as well as nutritional content. In addition, it can automate the cooking process to save time and produce meals on-demand to minimize waste. One potential application is to 3D print food for those suffering from dysphagia, a condition that affects one's ability to swallow. Texture modified food products for dysphagia often lose their shape and have limited visual appeal. 3D printing could provide shape to these texture modified food products and ultimately improve nutrient intake. One of the limitations that are currently preventing wider adoption of this technology is the lack of understanding of how food properties affect the 3D printing process and quality of the printed object.

In this thesis, room temperature extrusion-based 3D printing was investigated using a desktop 3D printer with a syringe extrusion system. Two hydrocolloids, modified starch and xanthan gum, were used as model material to study room temperature extrusion-based 3D printing.

The relationship between the 3D printer settings and the extrusion process variables, extrusion rate and nozzle speed, was obtained by investigating the machine command (G-code). The nozzle speed could be controlled by the extrusion multiplier while the extrusion rate could be controlled by the stepper motor speed. In addition, extrusion tests showed that the syringe extrusion system displayed a lag time around 2 to 5 minutes before stable extrusion rate was reached. The extrusion lag time increased with increased material yield stresses and decreased with increased syringe motor speed.

Xanthan gum paste, modified starch pastes, and puréed carrot were selected as model inks. Oscillatory rheology measurements including strain and frequency sweep were conducted to study the range of properties suitable for 3D printing. The range of yield stress suitable for extrusion was between 60-730 Pa and around 0.1-0.2 for the loss tangent ( $\tan \delta$ ). The printable range of complex modulus ( $G^*$ ) was from 320 to 1200 Pa. Furthermore, data from the frequency sweep of xanthan gum and modified starch pastes was fitted to power law models and compared to published data of foods to assess their potential suitability as food inks for 3D printing. Puréed carrot had higher  $G^*$  compared to xanthan gum and modified starch pastes but had lower elasticity. Puréed carrot was suitable for 3D printing because of its stiffness and low elasticity. In addition, food texture measurements based on the methods described in the International Dysphagia Diet Standardisation Initiative (IDDSI) were also conducted. Printable inks were able to retain its shape on a fork without dripping through the prongs and slide off a spoon with minimal residue.

Two printed objects were considered, a line and a cylinder. The line printing was conducted to find the optimal settings of volumetric extrusion rate, nozzle speed, and layer height. The cylinder printing was

conducted to assess the effects of ink rheology and infill levels, the fraction of the interior of the object to be filled with material when printed, on maximum build height. Continuous lines and sharp angles were able to be 3D printed when the line diameter was 130% of the nozzle diameter. Slightly thicker lines ensure proper layer adhesion. The layer height of the printed line, determined from the aspect ratio (height over width), ranged from 50% to 80% of the nozzle diameter. Lower aspect ratio indicated spreading of the ink. The cylinder printing experiments indicated that an ink with storage modulus ( $G'$ ) around 300 Pa produced cylinder up to 20 mm height before collapse, while an ink with  $G'$  around 900 Pa produced a cylinder up to twice the height. Increasing infill levels from 0 to 50% provided additional internal support to the structure but subjected the object to more stress due to nozzle movement.

The work presented in this thesis generated information on how rheological characteristics affect the food's suitability for room temperature extrusion-based 3D printing as well as the quality of the printed object. The relationships between the 3D printer, slicer setting, and G-code were investigated to understand how extrusion rates and nozzle speeds can be controlled for 3D printing paste type inks. Food texture measurements based on the methods described in the International Dysphagia Diet Standardisation Initiative (IDDSI) were conducted with fork and spoon to assess the ink's consistency and adhesiveness. Rheological characterization of the inks provided upper and lower limit of a printable ink. Power law models were used to analyze the rheology data and the models parameters of the inks were compared to published data of foods to assess their potential suitability as food inks for 3D printing.

## **Acknowledgements**

I would like to express my earnest gratitude to my supervisor Dr. Christine Moresoli for her support, mentorship, and providing the opportunities to help me develop into a better researcher.

Thanks to my fellow lab members Huayu Niu, Joseph Khouri, Nikole Lyn, Omar Mustafa Al-Kubaisi, and Rasool Nasser, for their advice, valuable discussions, and friendship.

I would like to thank Madhu Sharma and Dr. Lisa Duizer at University of Guelph for conducting the oscillatory rheology experiments.

Thanks to Andrew Finkle and Charles Mire at Structur3D for their technical advice regarding the 3D printer and extruder.

I would like to express my earnest gratitude to my readers Dr. Evelyn Yim and Dr. Boxin Zhao for their time to review my thesis.

I am grateful to the University of Waterloo and the Natural Sciences and Engineering Research Council of Canada for their financial support in scholarships and grants.

Last but not least, I would like to thank my parents for their unending love and support. Their decision to move to Canada offered me the opportunities to expand my horizons and become the person I am today.

## Table of Contents

Author's declaration.....	ii
Abstract.....	iii
Acknowledgements.....	v
List of Tables .....	ix
List of Figures.....	x
List of Abbreviations .....	xii
List of Symbols.....	xiii
Chapter 1. Research motivation and objective .....	1
1.1. Research motivation.....	1
1.2. Project Objectives .....	2
1.3. Thesis Structure .....	2
Chapter 2. Literature review .....	3
2.1. 3D Printer and extruder set-up.....	3
2.1.1. 3D printer configuration.....	3
2.1.2. Extruder.....	5
2.1.3. Ink extrusion conditions.....	6
2.2. Food Hydrocolloids .....	7
2.2.1. Xanthan gum.....	7
2.2.2. Starch .....	8
2.3. Viscosity and viscoelasticity .....	10
2.3.1. Steady shear viscosity .....	10
2.3.2. Oscillatory rheology.....	11
2.4. Applications of extrusion-based 3D printing.....	13
2.4.1. Printer configuration and extruder type for paste .....	15
2.4.2. Rheology and extrusion-based 3D printing of foods .....	16
2.4.3. Inks and printing methods.....	18

2.4.4.	Print object quality .....	19
2.5.	Commercial and government sponsored food printing systems .....	22
Chapter 3.	Materials and experimental methods .....	26
3.1.	3D printing and extrusion system .....	26
3.2.	G-code and slicer settings .....	27
3.3.	Printing tests and image analysis .....	30
3.3.1.	Extrusion test .....	30
3.3.2.	Line printing test .....	30
3.3.3.	Cylinder printing test .....	32
3.3.4.	Image analysis.....	32
3.4.	Data Analysis .....	34
Chapter 4.	Rheological characterization of 3D printable pastes.....	35
4.1.	Introduction.....	35
4.2.	Materials and methods .....	36
4.2.1.	Sample preparation .....	36
4.2.2.	Oscillatory rheology.....	36
4.2.3.	Analysis of rheology data .....	36
4.3.	Results.....	37
4.3.1.	Strain sweep.....	37
4.3.2.	Frequency sweep.....	38
4.3.3.	Yield stress determination.....	41
4.4.	Discussion .....	44
4.4.1.	Rheology as constraints for design of 3D printable food inks .....	44
4.4.2.	Rheology of XG and MS paste and texture-modified food for dysphagia.....	44
4.4.3.	Rheology of XG and MS paste and general types of foods .....	46
4.5.	Conclusion .....	50
Chapter 5.	3D printing of hydrocolloids and texture modified food .....	51

5.1.	Introduction.....	51
5.2.	Material and methods.....	52
5.2.1.	Materials and paste preparation .....	52
5.2.2.	Rheology measurement.....	53
5.2.3.	Food texture .....	53
5.2.4.	3D printing .....	53
5.3.	Results and discussion .....	56
5.3.1.	Rheology of starch and xanthan gum pastes .....	56
5.3.2.	Texture measurement.....	59
5.3.3.	3D Printing test .....	61
5.4.	Conclusions.....	67
Chapter 6.	Conclusions and recommendations.....	68
6.1.	Conclusions.....	68
6.2.	Recommendations for future work .....	70
	Letters of Copyright Permission .....	71
	Bibliography .....	75
	Appendix A. Slicer setting design of experiments.....	90
	Appendix B. 3D printing experiment slicer settings.....	94



## List of Tables

Table 1 Health Canada approved chemically modified starch and their properties adapted from (Singh et al., 2007) with permission.....	9
Table 2 Overview of extrusion-based 3D printing cells, flexible polymer, inorganic materials, and food applications (Hinton et al., 2016; Kirchmajer et al., 2015; Li et al., 2015; Yang et al., 2015).....	14
Table 3 Viscosity and shear rates of inks during extrusion and at rest in literature.....	17
Table 4 Yield stress and $G'$ of printable food inks in literature.....	17
Table 5 Commercial or government sponsored 3D food printing systems.....	23
Table 6 Extruder characteristics.....	29
Table 7 Predicted $Q$ (Equation 3-4) at different stepper motor speeds (Equation 3-3) for $f = 600$ mm/min .....	29
Table 8 Critical strain ( $\gamma_c$ ) for XG and MS pastes at different concentrations. Values reported as average $\pm$ standard deviation ( $N = 3$ ) .....	38
Table 9 $G'$ and $G''$ fitted to Equation 4-1 & 4-2. Fitted parameters are reported as average $\pm$ one standard deviation errors on the parameters ( $N = 3$ ) .....	40
Table 10 $G^*$ for XG and MS pastes fitted to Equation 4-3. Fitted parameters are reported as average $\pm$ one standard deviation error ( $N = 3$ ).....	41
Table 11 Shear stress ramp analysis of XG and MS pastes .....	43
Table 12 Parameters of the power law model for different food reported in the literature. Rheology measurement conducted at 20 - 25 °C. Parameters not reported in paper are listed as N/A.....	46
Table 13 Parameters of the weak gel model for different food reported in the literature. Rheology measurement conducted at 20 - 25 °C .....	47
Table 14 Oscillatory stress sweep (1-1000 Pa) at 25 C for XG and MS pastes. $G'$ and $G''$ are values within LVR. Results reported as average $\pm$ standard deviation. ( $N = 3$ ).....	58
Table 15 Parameters obtained when fitting extrusion rates to Equation 5-1 for XG and MS pastes and carrot purée. Extrusion lag time ( $t_{lag}$ ) calculated with Equation 5-2 .....	62
Table 16 Aspect ratios ( $c$ ) for XG and MS pastes and carrot purée obtained from linear regression of the line widths for $\sqrt{Q/v}$ from 1 to 2.5.....	64

## List of Figures

Figure 1 Types of 3D printer configuration according to movement: A. Cartesian type printer (Prusa i3 MK2) credits: Josef Prusa, B. Delta type printer ( $\mu$ Delta) credits: eMotion Tech, and C. SCARA type printer (Wally) credits: Nicholas Seward. The arrows indicate direction of the moving parts. Images reused under CC-BY SA.....	3
Figure 2 Different types of extrusion mechanisms reproduced with permission from (Sun et al., 2017) ....	5
Figure 3 Structure of xanthan gum (XG), credits: NEUROtiker reuse under public domain.....	7
Figure 4 Structure of amylose and amylopectin in starch (Sweedman et al., 2013). Reproduced with permission.....	8
Figure 5 Evaluating 3D printability of gel through image analysis of lattice structures (Ouyang et al., 2016). Reproduced with permission of IOP Publishing in the format Thesis/Dissertation via Copyright Clearance Center.....	21
Figure 6 Schematics of the extrusion system (left) and the desktop 3D printer (right) .....	26
Figure 7 Diagram of the extruder showing the stepper motor, gear box, and threaded rod. The stepper motor drives the two gears which in turn move the rod in the vertical direction which pushed the piston of the extruder. ....	28
Figure 8 Side-view and front-view of the nozzle and ink for over-extrusion, under-extrusion, and desired extrusion.....	31
Figure 9 Top-down view of cylinders at 0, 25, and 50% infill using line pattern .....	32
Figure 10 Examples of threshold settings where the darker portion of the image is selected. Hue/ Saturation/ Brightness thresholds were manipulated to exclude the background.....	33
Figure 11 Examples of image analysis. The two 1 mm wide rectangles measure the width of the printed lines (left) and the line drawn down the center of the cylinder measures the height of the printed cylinder (right). ....	33
Figure 12 Amplitude sweep of (A) xanthan gum (XG) and (B) modified starch (MS). Each point represents the average of 3 measurements with standard deviation represented as error bars .....	37
Figure 13 Frequency sweep of (A) XG and (B) MS. Each point represents the average of 3 measurements with standard deviation represented as error bars .....	39
Figure 14 Shear stress ramp for (A) XG and (B) MS pastes and methods of identifying yield stress. Each point represents average yield stress of 3 measurements with standard deviation represented by horizontal error bars.....	42
Figure 15 (A) Complex modulus ( $G^*$ ) and (B) loss tangent ( $\tan \delta$ ) for XG and MS pastes compared to five classes of dysphagia-oriented products. Data for different dysphagia classes obtained from (Casanovas et al., 2011).....	45

Figure 16 Oscillatory stress sweep for (A) xanthan gum (XG) and (B) modified starch (MS) pastes. Each data point is the average of three measurements and the dotted lines are the fitted cubic spline functions 57

Figure 17 Results of fork drip and spoon tilt test based on IDDSI for (A) XG and MS pastes and (B) carrot purée. .... 60

Figure 18 Extrusion rate over time for (A) and carrot purée samples (B). Each point represents the average of 3 measurements with standard deviation represented as error bars..... 61

Figure 19 Line width as a function of extrusion rate ( $Q$ ) and nozzle speed ( $v$ ) for a syringe with a 1.54 mm diameter nozzle. Images represent typical printed lines at each condition. The solid line ( $c = 1$ ) represents the aspect ratio of a line with a circular cross-section. The dotted line ( $c = 0.5$ ) represents aspect ratio for a line with an elliptical cross-section (height is half the width of the line). Each point represents the average of 6 measurements with standard deviation represented as error bars..... 63

Figure 20 Images of cylinder printing experiments for XG and MS pastes and carrot purée at three infill levels ..... 65

Figure 21 Height of printed cylinders before collapse at three infill levels. Each column represents the average with standard deviation represented as error bars ( $N = 3$ ). ..... 66

## List of Abbreviations

3D	Three dimensional
FDM	Fused deposition modeling
PLA	Polylactic acid
ABS	Acrylonitrile butadiene styrene
SCARA	Selective Compliance Articulated Robot Arm
OSA	Octenyl succinic anhydride
MRE	Meals ready to eat
EEPROM	Electrically erasable programmable read-only memory
XG	Xanthan gum
MS	Modified starch
IDDSI	International Dysphagia Diet Standardisation Initiative
LVR	Linear viscoelastic region

## List of Symbols

$G^*$	Complex modulus (Pa)
$G'$	Storage modulus (Pa)
$G''$	Loss modulus (Pa)
$\tan \delta$	Loss tangent
$Q$	Volumetric extrusion rate ( $\text{mm}^3/\text{s}$ )
$v$	Nozzle speed (mm/s)

## **Chapter 1. Research motivation and objective**

### **1.1. Research motivation**

We are what we eat. What one consumes affects their overall health and poor dietary choices are the cause of many diseases. In Canada, 54% of the population are obese and over 2 million people were diagnosed with diabetes in 2014 (Statistics Canada, 2016). It is often difficult to maintain a healthy diet due to the efforts needed in tracking one's food intake and the convenience of processed meals. Most people have trouble adjusting their diets through self-advocacy alone. What is needed is a way to automatically adjust foods to the consumers' needs and preferences (Lipton, 2017).

Some diseases affect the ability to eat. Dysphagia, for example, is a disease which affects one's ability to swallow. Over 16 million people in the USA and over 40 million people in Europe are affected and most of them are the elderly (Takizawa et al., 2016). A study of patients in long term care facilities show that the odds of being malnourished are nearly double in those showing signs of dysphagia (Namasivayam-MacDonald et al., 2017). Attempts have been made to improve meal appearance through the use of food molds; however, it is time consuming and not practical for many long term care facilities due to limited food budgets (Keller et al., 2014).

3D printing food may be the solution to these problems. 3D printing is a type of additive manufacturing which involves building an object in a layer by layer manner. The technology can offer mass customization, on-demand production, as well as personalized nutrition. The first patent on 3D printing food was granted over a decade ago to Nanotek Instruments (Yang et al., 2001) although no printer was made commercially available. A few years later the open source Fab@Home project drew interest to 3D printing paste (Malone and Lipson, 2007). In the recent years there has been a notable increase of interest in 3D printing food both in academia and commercial use.

Currently, food inks suitable for extrusion-based 3D printing are formulated by trial and error which is time consuming and may not generate an optimal ink formulation. Physical properties such as rheology may have the ability to provide a framework for the formulation of food inks that could reduce the time requirements and may lead to improved food ink formulation.

## **1.2. Project Objectives**

The goal of this project is to identify optimal conditions and material rheology for room temperature extrusion-based 3D printing of food purée, paste, and gel. Specific objectives are:

- 1) Determine the relationship between the 3D printer settings and the extrusion rate and nozzle speed.
- 2) Identify rheological characteristics and texture of inks as potential criteria for the development of formulation suitable for extrusion-based 3D printing. Two hydrocolloids, modified corn starch and xanthan gum, and modified purée carrot were selected as model inks.
- 3) Determine 3D printer settings for extrusion-based printing and achieving good quality of printed objects.

## **1.3. Thesis Structure**

The thesis is broken down into the following chapters and their rationale is as follows:

Chapter 2 provides background on 3D printers and extrusion systems and reviews properties and food specific applications of xanthan gum and starch. Literature review was conducted on extrusion-based 3D printing of biological materials, flexible polymer, inorganic materials such as ceramic and metal, and food.

Chapter 3 describes the methodology which includes relevant 3D printer settings that enable extrusion of viscoelastic pastes, as well as 3D printing tests developed to evaluate the quality of printed objects.

Chapter 4 presents the investigation of the rheological characteristics of modified starch and xanthan gum pastes. The framework of rheological characteristics established for the two model hydrocolloids was then used to analyze published rheological characteristics of foods and assess their potential suitability as food inks for 3D printing. The chapter concludes on approach to design 3D printable food that combines rheology, sensory properties, and food composition.

Chapter 5 focuses on the 3D printability of the hydrocolloid pastes and modified carrot purée. Rheology measurements, texture measurement with fork and spoon, and 3D printing tests were conducted. The relationship between material rheology and quality of the printed object is discussed.

## Chapter 2. Literature review

3D printing, also known as additive manufacturing, involves building an object in a layer by layer manner. Traditional fused deposition modeling (FDM) involves melting a filament that solidifies as it is pushed out of the nozzle (N. Turner et al., 2014). For FDM the material is limited to thermoplastics with the most popular choices being either polylactic acid (PLA) or acrylonitrile butadiene styrene (ABS) (C. C. Kuo et al., 2016). Extrusion-based 3D printing expands the range of printable ink to include pastes and gels such as silicone, clay, and hydrogel. As long as the ink can be extruded through a nozzle and maintain its shape upon deposition it can be 3D printed. This versatility allows 3D printing to be used for a great variety of applications ranging from cell scaffold (Ouyang et al., 2016) to flexible electronics (Shin et al., 2016).

This chapter reviews 3D printer and extruder configurations, xanthan gum and starch properties, basic concepts of viscosity and oscillatory rheology, and reviews recent literature for extrusion-based 3D printing. The literature review focuses on the characteristics of a printable ink and methods used to evaluate printability. Lastly the commercial research on 3D food printing is also be discussed.

### 2.1. 3D Printer and extruder set-up

#### 2.1.1. 3D printer configuration

3D printer can be classified by their movements. The three main types include Cartesian, Delta, and selective compliance assembly robot arm (SCARA) (Figure 1).

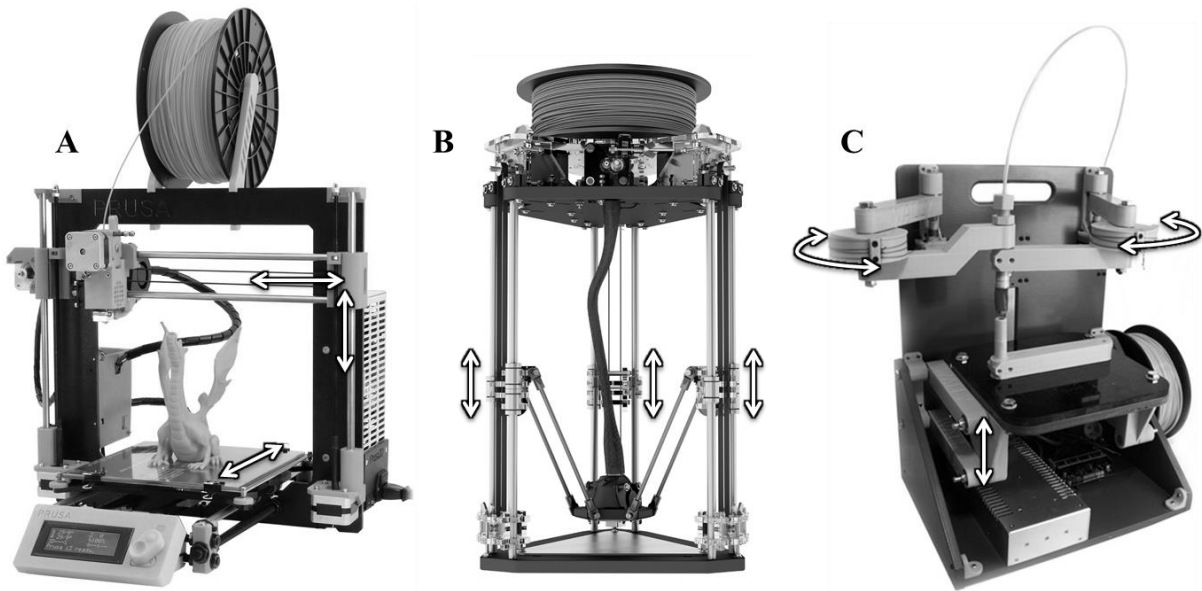


Figure 1 Types of 3D printer configuration according to movement: A. Cartesian type printer (Prusa i3 MK2) credits: Josef Prusa, B. Delta type printer ( $\mu$ Delta) credits: eMotion Tech, and C. SCARA type printer (Wally) credits: Nicholas Seward. The arrows indicate direction of the moving parts. Images reused under CC-BY SA.



The Cartesian printer system is the most commonly used due to its simplicity and intuitive control. Movement in the x, y, and z-direction are controlled by moving the print nozzle, the print platform, or both simultaneously. This type of printer is widely available and can be purchased for a few hundred dollars. There are also dedicated maker communities that aim to create, improve, and modify open-source 3D printers (Wittbrodt et al., 2013).

In the delta printer system, the print nozzle is mounted on a base at the intersection of three carriages. Movement is controlled by the position of the three carriages relative to each other. This configuration carries very little weight on the base and can move faster than the Cartesian design (Horvath, 2014). Additionally, it is possible to create reversible delta designs that can switch from free moving tool for printing thermoplastic filaments to fixed tool for extruding paste (Anzalone et al., 2015). In general this type of printer is more complicated to calibrate and modify than Cartesian printers.

The SCARA system is a relatively new design to be used in 3D printers (Refer to Figure 1 C). This design has linked arms that move in an arc by rotating the elbows. Movement in the z-direction can be achieved by mounting the shoulder on the z-axis or raising and lowering the printer platform. Creative Machines Lab at University of Columbia proposed a conceptual design for a food printer based on the SCARA configuration (Creative Machines Lab, 2017). This configuration is more compact since the arms can be folded flat for storage and portability. SCARA 3D printers are more expensive since their components are not as widely available as Cartesian and delta 3D printers.

### 2.1.2. Extruder

For extrusion-based 3D printer there are two major components: the printer which controls movement and position of the nozzle and the extruder which controls the material flow. Three common types of extrusion systems include stepper motor driven piston, pneumatic, and conveying screw (Figure 2).

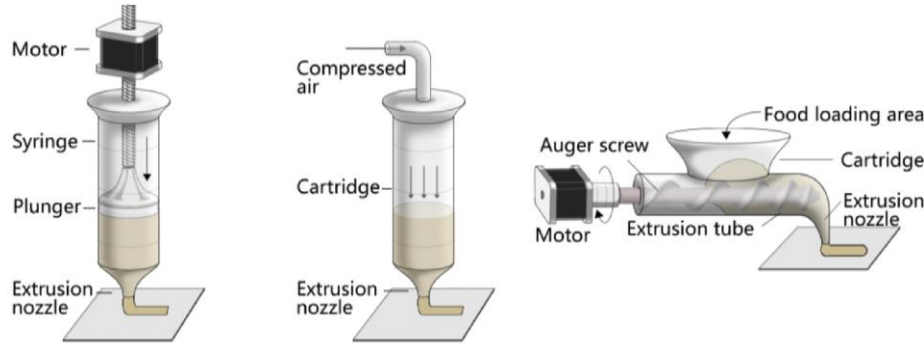


Figure 2 Different types of extrusion mechanisms reproduced with permission from (Sun et al., 2017)

In the stepper motor driven piston system, there is physical contact between the material and the piston. This mechanism provides better control of the extrusion rate since there is constant volume displacement. One disadvantage with this set up is the time delay to start and stop the extrusion process which may result in inaccurate print (Li et al., 2015).

The pneumatic extrusion system utilizes compressed gas as a driving force for extrusion. Air is commonly used but nitrogen can also be used if sterility is required such as in the case of printing biological inks (Hinton et al., 2015). Pneumatic extrusion is capable of extruding a wide range of viscoelastic inks (Hözl et al., 2016). It also has faster response time since the cartridge can be pressurized and depressurized quickly. This type of system is more complicated to build and operate than motor driven systems since it involves the use of compressed gas.

The conveying screw extrusion system uses a single screw extruder to deliver material from the hopper to the nozzle. One benefit of this design is that it allows for continuous printing since the material can be loaded as required (L. Wang et al., 2017). The rotating screw also helps mix the material as it is being printed to ensure homogeneity and prevent phase separation. Some disadvantages of this design include the possibility of cross-contamination since the materials are not stored in separate cartridges. Additionally, delicate materials such as cells are not suitable for conveying screw extrusion since shear force would damage cell membrane (Ouyang et al., 2016).

### **2.1.3. Ink extrusion conditions**

Inks can be grouped into three categories depending on the extrusion techniques applicable: cold extrusion, hot-melt extrusion, and gel-forming extrusion (Lipton, 2017). Both hot-melt and gel-forming extrusion involves some kind of phase change of the ink whereas cold extrusion generally occurs at room temperature with no phase transition (Godoi et al., 2016).

Cold extrusion or room temperature extrusion relies solely on the inks' rheology for printing. In contrast to hot-melt extrusion, there is no manipulation of temperature. The ink should be both extrudable and capable of forming self-supporting layers (Godoi et al., 2016). Ink rheology may be modified through the addition of thickeners or changing the composition.

Hot-melt extrusion involves an initial heating step to allow the ink to flow out of the nozzle followed by a cooling step to solidify the ink. In general the ink in hot melt extrusion is not heated to the same degree as FDM. The melting temperature for ABS filaments is around 200 °C (N. Turner et al., 2014). In comparison, gelation point for gelatin and agar is around 30-40 °C (Williams, 2006). The ink is kept a few degrees above the material's gelation point such that the ink can gel rapidly once extruded. For inks with gelation point around or below room temperature the printing platform or chamber may be cooled with an ice bath (Furukawa et al., 2015) or a Peltier device (He et al., 2016) to induce gelation. The ink itself may also be modified. In one study, Schutyser and colleagues (2017) increase the gelation temperature of sodium caseinate solution from 15 °C to 31 °C by crosslinking with transglutaminase. The ink is kept in a heated chamber slightly above the gelation temperature (31.5 °C) to print multi-layer structures (Schutyser et al., 2017).

Gel-forming extrusion involves the chemical or physical crosslinking of the ink. Instead of relying on manipulation of temperature to induce gelation like the case of hot-melt extrusion, addition of ionic species or ultra-violet light is used to trigger gelation (Wang et al., 2015). For example, alginate can be crosslinked in the presence of divalent ions such as calcium to form thermally irreversible gels (Williams, 2006). Photopolymers such as gelatin methacrylate can be cured by UV light to form mechanically robust structures (Wang et al., 2015).

## 2.2. Food Hydrocolloids

Hydrocolloids are important food additives that have diverse function due to their ability to interact and bind with water. Some commonly used ones include starch, xanthan gum, beta-glucan, guar gum, locust bean gum, konjac glucomannan, pectin, alginate, carrageenan, and inulin (Funami, 2011). They can serve as gelling agent, thickener, or stabilizer. For extrusion-based 3D printing, hydrocolloids can be added to the inks to modify ink rheology. This section will focus on the properties of xanthan gum and starch.

### 2.2.1. Xanthan gum

Xanthan gum (XG) contains linear  $\beta$  (1-4) linked glucose backbone (similar to cellulose) with tri-saccharide side chains on every other glucose (Sworn, 2009) (Figure 3). It is an anionic polysaccharide due to the carboxylic acid groups on its side chains. It has high molecular weight ( $>3 \times 10^6$  Da) (Williams, 2006) and forms highly viscous solution at low concentrations. XG can dramatically increase the viscosity of food bolus. High viscosity effectively slows down the digestion process and prevents spike in blood glucose level (Yi et al., 2015). Currently there is no government approved health claims associated with the consumption of XG by itself; however, Health Canada recently accepted the health claims by PGX®, a dietary supplement which consists of XG, konjac glucomannan, and sodium alginate, as effective in reducing post-prandial glycaemic responses (Brand-Miller et al., 2010). In addition, Health Canada restricts the amount of XG used in some foods (e.g. 0.5% in cheese, margarine, or sour cream, 0.1% for ice cream and sherbet) (Health Canada, 2016).

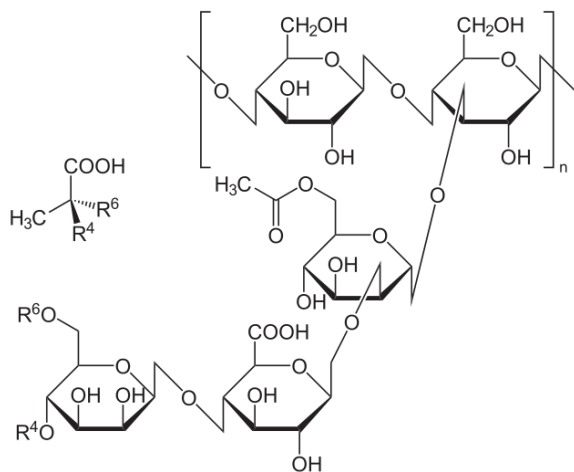


Figure 3 Structure of xanthan gum (XG), credits: NEUROtiker reuse under public domain

XG is produced by the aerobic fermentation of glucose or sucrose by *Xanthomona campestris* (Viebke et al., 2014). In terms of price, it is more expensive than starch. The average price for XG was \$5.17/kg in 2010 compared to \$0.92/kg for starch (Seisun, 2012). However, XG is a popular choice for thickener due to its excellent thickening ability at low concentration and stability in a wide range of temperature, pH, and salt concentrations.

XG molecules form intermolecular aggregates through hydrogen bonding and polymer entanglements. Solution of XG is highly pseudo-plastic and gel-like at rest for concentration above 1% by weight (Sworn, 2009). Furthermore, XG has good synergy with galactomannans such as guar gum or locust bean gum and can gel due to interactions with the unsubstituted “smooth” region of galactomannan (Sworn, 2009).

### 2.2.2. Starch

Starch contains repeating glucose units linked by  $\alpha$  (1-4) and  $\alpha$  (1-6) glycosidic bond. Amylose is short chain starch with relative linear structure while amylopectin is highly branched (Figure 4). The typical molecular weight for amylose is  $10^5$ - $10^6$  Daltons and  $10^7$ - $10^9$  Daltons for amylopectin (Dupuis et al., 2014). The amylose and amylopectin present in starch depends on the plant source. Starch extracted from cultivars of corn, potato, rice, wheat, or tapioca would have different compositions (Potter and Hassid, 1948). Consumption of resistant starch, portion of starch that is not digested in the small intestine, slows down the process of digestion and prevents spikes in blood glucose level (Dupuis et al., 2014).

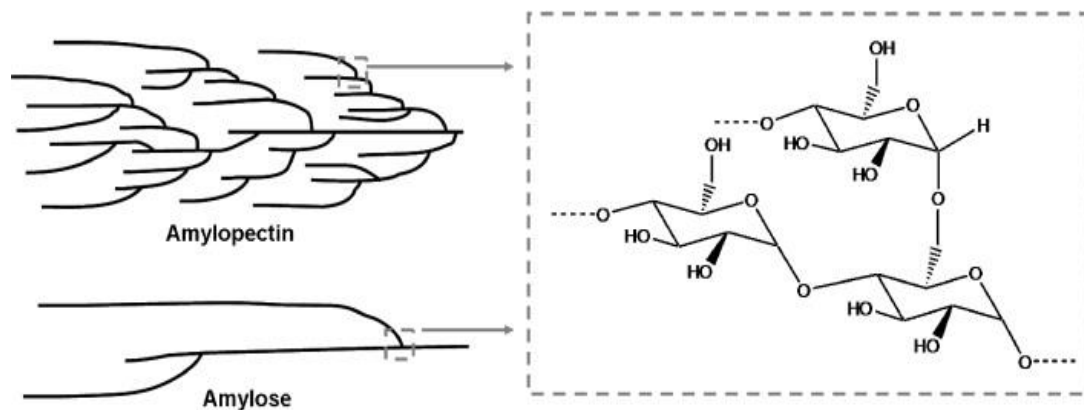


Figure 4 Structure of amylose and amylopectin in starch (Sweedman et al., 2013). Reproduced with permission.

Native starch exists as granules that contain alternating layers of semi-crystalline amylopectin and amorphous amylose (Sweedman et al., 2013). At first glance, it may seem counter-intuitive that the branched molecule is crystalline while the short, linear molecule is amorphous. The arrangement is possible since starch granules are synthesized by plants as part of their growth and not produced in a stirred tank reactor like synthetic polymers. Because of the granule structure, native starch can be

dispersed but not dissolved in cold water. Native starch granules need to be hydrated and heated above its gelatinization temperature (~90 °C) to form a solution.

Starch molecules contain many hydroxyl groups that can interact with water through hydrogen bonding. The interactions lead to increase in viscosity. The amylopectin component exists as free coils in solution due to its highly branched structure and high molecular weight. The amylose component, on the other hand, may aggregate to form a gel (i.e. retrogradation). Retrogradation may be undesirable since it alters the food texture during storage. The process is reversible by heating or shearing the gel.

Starch can be modified physically, chemically, or enzymatically to alter its properties (Dupuis et al., 2014; Singh et al., 2007). The use of chemically modified starch in the food industry is regulated. Table 1 shows some of the modification available and their effect.

Table 1 Health Canada approved chemically modified starch and their properties adapted from (Singh et al., 2007) with permission

<b>Treatment</b>	<b>Permitted starch-modifying chemicals</b> (Health Canada, 2016)	<b>Properties</b>
<b>Acid hydrolysis</b>	Hydrochloric acid Nitric acid Sulphuric acid	Reduced molecular weight Reduced viscosity Increased retrogradation
<b>Oxidation</b>	Calcium hypochlorite Hydrogen peroxide Sodium hypochlorite Potassium permanganate	Low viscosity High clarity Low temperature stability
<b>Crosslinking</b>	Sodium trimetaphosphate Sodium tripolyphosphate Potassium tripolyphosphate	Higher stability of granules towards swelling, high temperature, high shear, and acidic conditions
<b>Esterification</b>	Acetic anhydride Succinic anhydride Octenyl succinic anhydride	Lower gelatinization temperature Lower tendency to form gels Higher clarity
<b>Etherification</b>	Propylene oxide	Higher clarity Higher viscosity Reduced syneresis and freeze-thaw stability

Both acid-treated and oxidized starches have lower viscosity compared to native starch. For acid hydrolysis, inorganic acids are used to breakdown the starch molecule into smaller segments to increase gelling. For oxidation reactions, peroxide and hypochlorite are used to convert the hydroxyl groups on the starch to either aldehyde or carboxyl groups.

Starch can also be crosslinked to increase its stability in acidic conditions and its resistance to digestive enzymes such as amylase (Singh et al., 2007). Phosphorylation is the most common reaction for crosslinking food grade starch. Recently a crosslinking agent, epichlorohydrin, was removed from the list of permitted chemicals citing concerns with safety (Health Canada, 2016).

Succinic anhydride and octenyl succinic anhydride (OSA) can also crosslink starch molecules through the formation of ester linkages. OSA treated starch contains hydrophobic octenyl groups and is therefore more suited for use as emulsifiers due to its amphiphilic nature (Sweedman et al., 2013).

Propylene oxide is used for hydroxypropylation of starch. The reaction creates bulky substituted groups on the starch that interferes with hydrogen bonding between starch molecules and reduces syneresis (also known as “weeping” where water separates from a gel) (Dupuis et al., 2014).

Other types of modified starch include pre-gelatinized starch and enzyme hydrolyzed starch. Pre-gelatinized starch is produced by heating native starch in water above its gelatinization point and then dried (Singh et al., 2007). The process is conducted to achieve cold water soluble starch. Enzyme hydrolyzed starch is produced by dispersing starch in an aqueous solution with food grade amylolytic enzymes at a temperature below the gelatinization point (Sweedman et al., 2013). Amylase has lower hydrolysis rate compared to mineral acid but is effective at ambient conditions and less corrosive to equipment (Li et al., 2013). Enzyme treated starch has similar properties to those treated with mineral acids.

### **2.3. Viscosity and viscoelasticity**

Rheology is the study of how materials deform and flow. It is applicable to all kind of viscoelastic materials including food, polymer, and ceramic pastes. This section reviews the concepts of steady shear viscosity and oscillatory rheology measurements since 3D printing studies often use one or both methods to characterize the ink.

#### **2.3.1. Steady shear viscosity**

The inks’ resistance to flow or deformation is its viscosity. It can be defined as the ratio of shear stress over shear rate. The viscosity of a Newtonian fluid is constant since the shear stress changes linearly with shear rate. For non-Newtonian fluids, the shear stress varies non-linearly with shear rate and can be described with the power law (Equation 2-1) or the Herchel-Bulkley model (Equation 2-2).

$$\tau = K \dot{\gamma}^n \quad \text{Equation 2-1}$$

$$\tau = \tau_y + K \dot{\gamma}^n \quad \text{Equation 2-2}$$

Where  $\tau$  is the shear stress (Pa),  $\dot{\gamma}$  is the shear rate ( $\text{s}^{-1}$ ),  $K$  is the consistency coefficient ( $\text{Pa s}^n$ ),  $n$  is the flow behavior index (dimensionless), and  $\tau_y$  is the yield stress.

The flow behavior index ( $n$ ) describes how the shear stress changes with shear rate. If  $n > 1$ , the ink is shear thickening and if  $0 < n < 1$ , the ink is shear thinning. The Herchel-Bulkley model describes inks that are solid-like at rest and only starts to flow after the applied stress exceeds the yield stress  $\tau_y$ .

Steady shear viscosity is measured with stationary tests. Stationary tests involve subjecting the ink to a certain stress and measuring the resulting strain or vice versa. For example, a simple rotational test can be performed with a Brookfield viscometer. The ink is subjected to a constant shear rate (i.e. speed) and the viscosity of the sample is calculated from the amount of torque (i.e. force) required to turn the spindle. Viscosity can be reported at some standard conditions (e.g. shear rate of  $50 \text{ s}^{-1}$  is the standard for thickened food developed for dysphagia (Zargaraan et al., 2013)) or over a range of shear rates to generate a flow curve. The shape of the curve depends on the type of fluid. For Newtonian fluid the viscosity is a constant. Non-Newtonian fluid may display increase or decrease in viscosity as shear rate increases.

Some inks' viscosity is also time-dependant. In those cases, viscosity can be recorded over time at a single shear rate to show whether the sample is thixotropic (i.e. viscosity decreases with time) or rheopectic (i.e. viscosity increases with time). Most inks for 3D printing behave as a non-Newtonian fluid with a yield stress and exhibits shear thinning behavior.

### **2.3.2. Oscillatory rheology**

In addition to viscosity, the inks used for 3D printing also exhibit viscoelastic behaviours which means they have both fluid and solid like behaviors. Viscoelasticity is measured by oscillatory tests.

For oscillatory tests, the sample is subjected to sinusoidal oscillatory stress to measure both the elastic and the viscous response of the ink. The rheometer can operate under two modes: controlled stress or controlled rate. Controlled stress rheometers apply a torque and measure the strain rate whereas controlled rate rheometers are the opposite.

The sample's entire resistance against deformation is known as the complex modulus ( $G^*$ ). For a perfectly elastic material such as a spring, the deformation is in phase with the applied shear stress (phase angle  $\delta = 0^\circ$ ). For a purely viscous material, the deformation is out of phase with applied shear stress (phase angle  $\delta = 90^\circ$ ). Therefore the complex modulus can be split into its respective components (McKenna and Lyng, 2003):



$$G' = G^* \cos(\delta) \quad \text{Equation 2-3}$$

$$G'' = G^* \sin(\delta) \quad \text{Equation 2-4}$$

Storage modulus ( $G'$ ) measures the elastic response. The applied energy is stored and the material springs back into its original form once the stress is removed. The loss modulus ( $G''$ ) measures the viscous response. The applied energy is dissipated due to the material flowing. Other important parameters include the loss tangent ( $\tan \delta = G''/G'$ ) which is the ratio of the two moduli and the complex viscosity ( $\eta^* = G^*/\text{angular frequency}$ ).  $\tan \delta$  indicates if the material is behaving more like a solid or a liquid.

One type of oscillatory test is an amplitude sweep. The amplitude of deformation slowly increases over a number of cycles to identify when the material's internal structure starts to break down. Within the linear viscoelastic region (LVR), the viscoelastic parameters ( $G'$ ,  $G''$ ,  $\delta$ ) are independent of applied stress or strain (Steffe, 1996). The point where  $G'$  starts to deviate from linearity is the material yield point. The yield point estimated by oscillatory measurements is the static yield stress (i.e. minimum shear stress or strain required to initiate flow) whereas the yield stress obtained from flow curves is the dynamic yield stress (i.e. shear stress required to maintain flow at low shear rates) (Steffe, 1996).

Another type of oscillatory test is a frequency sweep. The amplitude of deformation is constant but the frequency of oscillation increases. Frequency sweep is conducted within the LVR. It helps to better understand the internal structure of the material and the time-dependant shear behavior (McKenna and Lyng, 2003). For instance, high frequency represents short term behavior like mixing or extruding while low frequency represents long term behavior such as settling. The frequency where  $G'$  and  $G''$  will crossover is the inverse of the relaxation time which is defined as the length of time at rest required for the sample to relax a stress received from an external body (Norton et al., 2011).

## 2.4. Applications of extrusion-based 3D printing

The goal of this section is to review typical extruder and printer configurations, suitable range of rheology parameters for a 3D printable ink, modification of the material and printing process, as well as methods of characterizing printability.

Applications of extrusion-based 3D printing with food is recent; however, 3D printing with hydrogels (Hölzl et al., 2016; Kirchmayer et al., 2015; Wang et al., 2015), elastomers (Hinton et al., 2016; Hung et al., 2014; Lipton and Lipson, 2016; O'Bryan et al., 2017), and colloidal inks of ceramic (Cai et al., 2012; Faes et al., 2015; Feilden et al., 2016; Ghazanfari et al., 2017; Li et al., 2015; Wang and Shaw, 2005), glass (Avery et al., 2014; Dorj et al., 2012; Gao et al., 2013; P. W. Wang et al., 2016), and metal (Jakus et al., 2015b; Ren et al., 2017) are well established.

Table 2 provides an overview on 3D printing with these inks and their similarities and differences compared to food inks. Bio-printing involves printing cells or bacteria embedded in hydrogel. It allows for precise positioning of the cells and better degree of control over pore size and distribution compared to traditional scaffold fabrication techniques (Ouyang et al., 2016). The print resolution may range from 100-500  $\mu\text{m}$  depending on the size of the nozzle tip used. The printed objects can be subjected to post-processing steps such as crosslinking by ions to improve mechanical properties. Hydrogels such as alginate, gelatin, and agarose are often used since they can be extruded as liquid and gel once printed in order to minimize shear-induced damage to cells (Hölzl et al., 2016; Kirchmayer et al., 2015).

Inorganic inks such as metal, glass, or ceramic are generally suspended in a polymer solution to create an ink that can be used for 3D printing. The printed objects are subjected to a heating step to remove the polymer binder and a high temperature sintering step to fuse the particles together. The print resolution can range from 100 to 2000  $\mu\text{m}$  depending on the application. For example, printing a custom fitted denture would require higher precision than printing a decorative flower vase. In order for the printed object to have good mechanical strength, the ink needs to have high solid loading. If the solid content of the ink is too low, the final structure might shrink unevenly or have poor mechanical properties due to high porosity. Thickeners such as methyl-cellulose are sometimes added to make the ink more shear thinning and to prevent the inorganic particles from settling (Ghazanfari et al., 2017).

Flexible polymers such as silicone and polyurethane as well as composite materials such as carbon nanotubes or graphene dispersed in polymer binder can be 3D printed. The ink is similar to the inorganics inks in that it is a heterogeneous mixture of particles and binder. The main difference is that the polymer binder is not removed in the final printed object. Some post-processing steps may include crosslinking or solvent evaporation.

3D printing food allows for product design, personalized nutrition, and rapid experimentation with various flavour and texture combinations (Sun et al., 2015a). 3D printing also produces less waste since only what is needed is printed. In addition, the deconstruction and reconstruction of food allows for incorporation of functional ingredients such as vitamins and minerals (Rodgers, 2016). After the food paste, purée, or gel is printed, it may be subjected to post-processing steps such as steaming, baking, deep frying or freezing. The print resolution is usually in the range of a few millimeters. In the case of food, speed is favored over accuracy since the shapes are mostly for aesthetic purposes. Food-pathogens might be of concern if printing takes too long. Starch, gelatin, or xanthan gum can be used to modify the ink to make it suitable for 3D printing.

Table 2 Overview of extrusion-based 3D printing cells, flexible polymer, inorganic materials, and food applications (Hinton et al., 2016; Kirchmajer et al., 2015; Li et al., 2015; Yang et al., 2015)

	Bio-Printing	Inorganics	Polymer blends	Food Printing
Ink	Cells in hydrogel	Metal, ceramic, glass suspension	carbon composites silicone, polyurethane	Food paste, gel, purée
Post-processing	Crosslink Cell seeding	High temperature sintering to remove binder	Crosslinking	Steam, bake, deep fry, freeze
Restrictions	Bio-compatible Good cell viability Shear and heat sensitive	High solid loading needed for good fusing	Drying to remove volatile solvent	Safe for human consumption Good mouthfeel
Print Resolution	100-500 $\mu\text{m}$	100-2000 $\mu\text{m}$	100-1000 $\mu\text{m}$	>1 mm
Objective	Cell propagation and migration	Control porosity and shape Good mechanical strength	Appropriate mechanical and electrical properties Flexible and robust structure	Customize shape, taste, and nutrition
Rheology Modifier	Gelling agent such as alginate or gelatin	Thickener such as methyl-cellulose to prevent phase separation	Concentration of filler particles	Food thickener like starch or xanthan gum

#### **2.4.1. Printer configuration and extruder type for paste**

This section reviews printer configuration and extruder types used for 3D printing paste in literature and their typical operating conditions.

The Cartesian type 3D printer configuration has been the most common type reported in literature. Some printers are custom builds (Ouyang et al., 2016; Zhao et al., 2015) while others are modified from an existing commercial 3D desktop printer (Hinton et al., 2015). Commercially available printers include 3D-Bioplotter by EnvisionTEC and Bioscaffolder by Gesim (Hölzl et al., 2016). The nozzle is usually the moving component; however, if the cartridge containing the paste is too heavy, a stationary extruder configuration (i.e. fixed nozzle and moving print bed) is preferred (Anzalone et al., 2015).

Both stepper motor driven piston and pneumatic extrusion are used to extrude pastes. Piston-based extruders may be custom-built (Shin et al., 2016) or modified from a syringe pump (Hinton et al., 2016; O'Bryan et al., 2017). The volumetric extrusion rate is controlled by the piston which is driven by a stepper motor. The reported extrusion rate ranges from 10 to  $10^4$   $\mu\text{L}/\text{hour}$  (Lehner et al., 2017; O'Bryan et al., 2017; Ouyang et al., 2016; Zhao et al., 2015). The combination of extrusion rates and nozzle speeds can create a wide range of filament sizes. Piston-based extrusion systems offer more consistent extrusion compared to pneumatic extrusion (Bégin-Drolet et al., 2017). Piston setup has been used to print chocolate (Khot et al., 2017), food hydrocolloids such as pectin (Vancauwenberghe et al., 2017b), alginate (D'Angelo et al., 2016), agar, and gelatin (Serizawa et al., 2014; Vesco et al., 2009), as well as processed food like cheese (Le Tohic et al., 2017), tofu (Mizrahi et al., 2016), and meat purée (Lipton et al., 2010).

Pneumatic extrusion is usually chosen when quick response is required. Extrusion pressures are reported instead of the volumetric extrusion rate. For bio-printing it can range from 5-65 kPa depending on gel concentration (Akkineni et al., 2016; Chung et al., 2013; He et al., 2016). For ceramic, metal, or glass, the extrusion pressure reported ranges from 50-500 kPa which is higher than the range reported for bio-printing (Barui et al., 2017; Gao et al., 2013; Jakus et al., 2015a, 2015b). For instance, the extrusion pressure for printing carbon grease and silicone is 344 kPa and 480 kPa, respectively (Lipton and Lipson, 2016; Muth et al., 2014). For bio-printing, the extrusion pressure is limited by the cell viability whereas for other applications, the extrusion pressure can be as high as the equipment limits. Pneumatic extrusion has been used to print food paste with a wide range of consistency. Soft foods like fish, pumpkin, and beet purée as well as egg white foam can be extruded at a low pressure of 20 to 50 kPa (Kouzani et al., 2017, 2016). For stiffer pastes such as vegemite, food spread made from yeast extracts, the extrusion pressure ranges from 100-170 kPa depending on printing temperature (Hamilton et al., 2017). Mixtures

that are rich in protein, fiber, or have low water content have thicker consistency and require higher pressure from 300 kPa to 600 kPa (Derossi et al., 2017; Gong et al., 2014; Lille et al., 2017; Schutyser et al., 2017; Severini et al., 2016).

Conveying screw-based extruder systems have been used to print mashed potato (Liu et al., 2017), fish gel (L. Wang et al., 2017), and chocolate (Hao et al., 2010).

In addition to the aforementioned setups, Ghazanfari and colleagues (2017) designed a novel system that combines both pneumatic and conveying screw extrusion. Pressurized air delivers paste to a chamber and the paste is extruded by a progressive cavity pump based extruder (Ghazanfari et al., 2017). Similar setup also used in the modular printer xPrint, developed by MIT media lab for dispensing liquids (G. Wang et al., 2016).

#### **2.4.2. Rheology and extrusion-based 3D printing of foods**

This section reviews key rheology parameters used for characterizing inks in literature and the typical range of printable inks.

For inks that undergo phase transition, the rheology would be measured as function of time and temperature. An important parameter is the characteristic  $\tan \delta$  which shows whether the ink is predominately elastic or viscous. It also helps determine the conditions under which the phase change occurs. The gelation point will help researcher determine the optimal printing conditions such as printing temperature. Strong gels that are covalently or ionically bonded have moduli that are independent of frequency within the linear viscoelastic region and if  $\tan \delta$  is below 0.1 (Vancauwenberghe et al., 2017b). The high gel strength helps the object to hold its shape but results in inconsistent extrusion due to gel fracturing. Similar print results were observed for 3D printing of fish gels (L. Wang et al., 2017). On the other hand, weak gels have  $\tan \delta$  higher than 0.1 and their  $G'$  and  $G''$  show power-law like behavior during frequency sweep. The weaker gel shows more uniform extrusion but may spread during printing (Vancauwenberghe et al., 2017b).

For inks that do not undergo phase change, the rheology is focused on the ink's behavior as a function of shear rate ( $\dot{\gamma}$ ). Both viscosity measurements and oscillatory rheology measurements are important. Viscosity measurements at different shear rates are usually reported. The ideal ink should be shear-thinning and have high near-zero viscosity (Faes et al., 2015). Power law parameters such as the consistency coefficient ( $K$ ) and the shear thinning coefficient ( $n$ ) are also useful for comparison between inks.

Ink viscosity can range from 0.030 Pa s to  $6 \times 10^4$  Pa s for extrusion-based systems (Hölzl et al., 2016). However the range doesn't provide information on how the ink behaves during and after extrusion. Table 3 summarizes changes in ink viscosity during 3D printing extrusion process.

Table 3 Viscosity and shear rates of inks during extrusion and at rest in literature

Extrusion viscosity (Pa s)	Extrusion shear rate ( $s^{-1}$ )	Rest viscosity (Pa s)	Rest shear rate ( $s^{-1}$ )	References
28.6	26	400	0	Faes et al., 2015
40	30	$4 \times 10^4$	0.01	Cai et al., 2012
35	28.34	2560	0.14	Derossi et al., 2017
100-400	30	2000-6000	0	Feilden et al., 2016

Low viscosity during extrusion and high viscosity at rest is desirable to prevent spreading; however, if the zero shear viscosity is too high, extrusion might be difficult. Wang and colleagues (2017) found that fish gel with zero-shear viscosity of  $3 \times 10^4$  Pa s was not suitable for 3D printing. Uniform extrusion is possible once the viscosity was reduced to  $10^4$  Pa s by adding table salt (L. Wang et al., 2017).

In addition to viscosity, rheological parameters such as yield stress and storage modulus ( $G'$ ) are equally important in defining ideal ink behavior. These rheological parameters indicate whether the material is capable of producing self-supporting layers. The yield stress of a printable paste should be at least 200-300 Pa and can be as high as 1000 to 2000 Pa (Cai et al., 2012; Zhong et al., 2017). Table 4 summarizes typical range of yield stress and  $G'$  of 3D printable food inks in literature.

Table 4 Yield stress and  $G'$  of printable food inks in literature

Inks	Yield stress (Pa)	$G'$ (Pa)	References
Vegemite and marmite	419-1419	N/A	Hamilton et al., 2017
Mashed potatoes	312	N/A	Liu et al., 2017
Protein and fiber paste	60	1500	Lille et al., 2017

In a recent study, vegemite and marmite are 3D printed under temperatures ranging from 37 to 4 °C. The ink yield stress ranged from 419 to 1419 Pa and was able to retain its shape in all cases (Hamilton et al., 2017). Liu et al (2017) found that for mashed potatoes the best printing results was obtained for mashed potatoes with yield stress of 312 Pa. The mashed potatoes with yield stress of 370 Pa and low  $\tan \delta$  was hard to extrude and the one with yield stress of 195.90 Pa ended up spreading (Liu et al., 2017). In contrast, Lille et al (2017) found the best food paste has yield stress of 60 Pa. The value is much lower than the ones reported in other studies and may be explained by the high  $G'$  value of 1500 Pa. High  $G'$  is desirable for building objects with high shape fidelity. Inks with yield stress of 100 Pa and  $G'$  of 36000

Pa were deemed too hard to extrude while those with yield stress of 8 Pa and  $G'$  of 300 Pa ended up spreading (Lille et al., 2017). Both yield stress and  $G'$  contribute to the ink's ability to hold its shape. The minimum and maximum yield stress for a 3D printable ink will change depending on the  $G'$  of the ink.

Postiglione and colleagues (2015) determined the printability window of their ink by defining a maximum allowable shear stress (2900 Pa) based on the extruder capabilities and finding the corresponding range of shear rates. The shear rates were converted to extrusion speeds for the printer. For example, the viscous paste with high solid loading is limited to printing speed of 0.1 mm/s without exceeding the maximum shear stress. On the other hand, paste with lower solid loading can print as fast as 5 mm/s and remained extrudable (Postiglione et al., 2015).

### **2.4.3. Inks and printing methods**

This section reviews several potential modifications to both the ink composition and the printing process in literature. Modifications of ink composition include addition of crosslinkers or volatile solvents. If the ink composition cannot be altered, the printing process can be modified to enable 3D printing. Techniques including laser curing, frozen deposition, support gel bath, and coaxial extrusion will be discussed.

Addition of crosslinkers enabled Lehner et al (2017) to print alginate solution on a calcium chloride treated surface and constructed multi-layer objects by pausing for 40 seconds in-between layers to allow for diffusion of calcium ions (Lehner et al., 2017). Solutions of alginate and pectin crosslinked with calcium ions have also been successfully 3D printed. It was found that gel strength increases with calcium ion concentration (D'Angelo et al., 2016; Vancauwenberghe et al., 2017b). Orange juice mixed with calcium gluconate lactate was successfully 3D printed in a bath of alginate solution (D'Angelo et al., 2016).

The use of volatile solvent such as dichloromethane enabled 3D printing of carbon nanotube, graphene, and metal oxide pastes (Jakus et al., 2015a, 2015b; Postiglione et al., 2015). The purpose is two-fold: the volatile ingredient (e.g. water, alcohol, vinegar) acts as solvent to make extrusion easier and helps harden the deposition through evaporation (Yang et al., 2001). The described technique was also used to create self-folding pasta. The pasta consists of gelatin film and stripes of ethyl cellulose printed on top of the film that modulate folding behavior. Ethyl cellulose was dissolved in ethanol to form 3D printable ink. The ethanol evaporates during printing to solidify the structure (W. Wang et al., 2017).

Laser densification or infrared heating can be used to solidify the paste in-between each layer. The paste can be extruded into an oil bath to prevent drying and cracking at the object (Feilden et al., 2016; Ghazanfari et al., 2017; Wang and Shaw, 2005).

In frozen deposition the ink is printed onto cooled platform (Dorj et al., 2012). Edible objects made of agar, gelatin (Gong et al., 2014; Serizawa et al., 2014) have been 3D printed by frozen deposition. Agar gels around 32-40 °C and melts around 85 °C whereas gelatin forms thermally reversible gel around 30-40 °C (Gong et al., 2014; Serizawa et al., 2014). High gelation temperature is desirable for fast solidification after extrusion. Schutyser and colleagues (2017) were able to increase the gelation point for sodium caseinate dispersion from around 15 °C to 31 °C by crosslinking with transglutaminase. In addition to the gelation of polysaccharides and proteins, the fat content in food also affects the melting and solidification behavior. For example, chocolate solidifies around 30 °C so it is possible to print at room temperature (Hao et al., 2010) although additional fan cooling allows for printing objects with more complex geometry with bridging and overhangs (Lanaro et al., 2017). In a study with processed cheese where the reported melting temperature was 59.5 – 64.2 °C, the cheese was heated to 70 °C prior to printing (Le Tohic et al., 2017).

Support gel bath technique was used to print soft gels and viscous fluids in a support bath consisting of gelatin micro-particles (Hinton et al., 2015). The technique was also applied to print silicone into tubular and helical structures (Hinton et al., 2016). In a different study, O'Bryan and colleagues printed silicone into a support composed of micro-organogel instead of an aqueous gel (O'Bryan et al., 2017). The support bath behaves like a solid at low shear stress to support the deposited material. At high shear stress the support bath flows to allow the nozzle tip to move. The support allows for the printing of objects with complex geometry with overhangs and hollow interiors (Hinton et al., 2015).

For coaxial extrusion, a soft gel is encapsulated inside a stiff shell for mechanical support. The print is further treated by crosslinking with calcium ions or genipin depending on the core material (Akkineni et al., 2016).

Lastly, modification of the printing process can also apply to the movement of the nozzle. Instead of having the nozzle tracing the exact print path, Lipton and Lipson (2016) used viscous thread instability to print silicone foam with cellular structures. The nozzle is lifted off the print surface and the extruded filament coils onto itself as it falls. The structures can be meanders, translated coils, or alternating loops depending on the nozzle travel speed as well as its distance from the print surface (Lipton and Lipson, 2016).

#### **2.4.4. Print object quality**

After the appropriate ink composition and technique are selected to enable 3D printing, the quality of the printed object can be evaluated in several ways. The first method involves qualitative observation of the printing process and object. A wide range of arbitrary designs of the object have been reported in the



literature. Some examples include miniature map of Australia made out of egg white foam (Kouzani et al., 2016), coral reef made out of tofu noodles (Mizrahi et al., 2016), cartoon fish out of pumpkin and fish purée (Kouzani et al., 2017), insect-inspired geometric designs such as honeycomb using insect powder fondant (Soares and Forkes, 2014), apple logo with mashed potato (Liu et al., 2017), Chinese calligraphy characters with molten sugar (Leung, 2017), flower bowls printed with rice paste (Tanaka et al., 2015), and pyramid with vegemite and marmite (Hamilton et al., 2017). The printed object may be assigned a numerical rank that represents print quality based on visual inspection (Lille et al., 2017). Important characteristics noted during the printing process include deposition uniformity, clogged nozzles, lag time, and deformation of the object (Vancauwenberghe et al., 2017b).

The second method involves 3D printing objects with a basic design such as lines, grids, or cubes. The shape of the object is kept simple so its dimensions such as the line diameter and height can be compared to the intended design. Hao and colleagues (2010) measured the printability of chocolate by printing straight lines and hollow cubes. The line diameter, cube length and width, and wall thickness are used to judge print accuracy (Hao et al., 2010). In a similar study with chocolate, Lanaro and colleagues (2017) conducted bridging test in addition to printing lines. The chocolate is extruded over gaps with increasing distance to determine the maximum distance that can be printed without collapse in absence of support (Lanaro et al., 2017). The line printing test can be used to identify the optimal extrusion rate and nozzle speed. The desired combination should produce lines with diameter equal to the nozzle diameter (Hao et al., 2010; L. Wang et al., 2017). Furthermore, the line print test can be modified to print dotted lines to measure accuracy of the extruder (Ghazanfari et al., 2017). The extruder needs time to build up enough force in order to overcome the ink's yield stress. Li and colleagues compared different extruder designs including piston, needle valve, and auger valve and found that auger valve offer the best extrusion start and stop accuracy, as well as flow rate consistency (Li et al., 2015).

Simple 2D designs such as lattices are also used to evaluate print quality (He et al., 2016; Ouyang et al., 2016; Zhao et al., 2015). The width and line spacing of the printed object are measured and compared to the intended design. The line width can be estimated from the volumetric extrusion rate and nozzle speed assuming that the cross-sectional area of the printed filament is an ellipse (O'Bryan et al., 2017). Ouyang et al (2016) proposed a method for quantitatively evaluating printability through image analysis of the pore shapes in a lattice design (Figure 5). The pore shape should be square if the gel is able to hold its shape. If the gel starts spreading, the pore would become more circular. On the other hand, if the gel fractures during printing, irregular pore shapes would be created. In this approach the printability (Pr) is calculated as the ratio of circularity of a perfect square ( $\pi/4$ ) over the actual circularity of the pore shape ( $C = \frac{4\pi A}{L^2}$ ) (Ouyang et al., 2016).

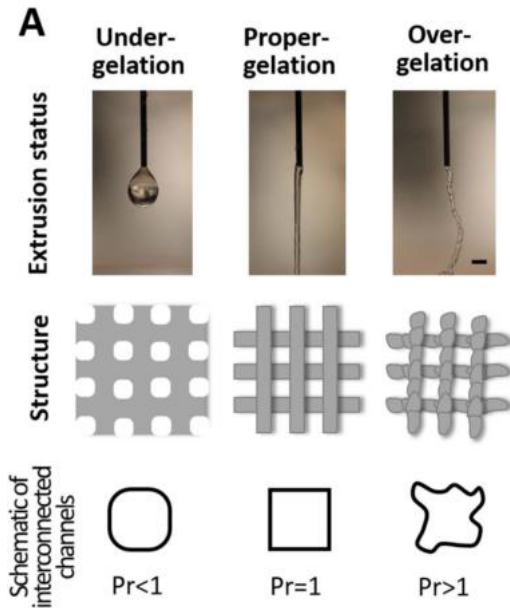


Figure 5 Evaluating 3D printability of gel through image analysis of lattice structures (Ouyang et al., 2016). Reproduced with permission of IOP Publishing in the format Thesis/Dissertation via Copyright Clearance Center.

Multi-layer cube and cylinder geometries are also common choices for assessing the quality of the printed object. The cross-section of the structure can be examined qualitatively to ensure the walls are uniform and there're no slumping or defects in the printed object (Faes et al., 2015; Wang and Shaw, 2005). Some advance techniques such as scanning electron microscopy, confocal microscopy, or X-ray micro-computed tomography can be used to observe the microstructures of the printed objects (Dorj et al., 2012; Gao et al., 2013; Vancauwenberghe et al., 2017a). For printing solid objects with high final density, the line spacing and layer height should be approximately 80-85% of the nozzle diameter to ensure good adhesion between adjacent lines and layers (Feilden et al., 2016).

The third method is focused on the texture of the printed object. Le Tohic and colleagues use texture profile analysis to evaluate 3D printed processed cheese cylinders (Le Tohic et al., 2017). Vesco et al (2009) use mixtures of xanthan gum and gelatin to simulate the texture of common food. The printed object is ranked according to a mouthfeel matrix where one axis is weak – firm and the second axis is smooth – granular (Vesco et al., 2009). Vancauwenberghe and colleagues (2017a) printed cookies with honeycomb or kelvin structure and various degrees of infills. They attempt to manipulate texture of the printed cookie as a function of porosity (Vancauwenberghe et al., 2017a)

## **2.5. Commercial and government sponsored food printing systems**

A significant portion of the research conducted on 3D food printing is outside academia. Table 5 provides an overview of the key participants in the field. There are many start-up companies that sprung from successful crowdsourcing campaigns: Foodini, Bocusini, and Choc Edge. Most of the information on their printer comes from blog posts and company newsletters that are purposely vague to protect proprietary information. Natural Machines Inc, the creator of Foodini, recently submitted a patent application (US 2016/0135493 A1) for their printer which provides more information on their design (C.-J. Kuo et al., 2016). However, the actual printer is not yet available for purchase to the public.

Table 5 Commercial or government sponsored 3D food printing systems

Company/Project	Description
<b>Start-up companies</b>	
Choc Edge	Chocolate printing customized designs, personalized gifts; Choc Creator v2 available for €4500
BeeHex Inc.	3D pizza printer in prototyping phase Pneumatic extrusion system (Contractor et al., 2016)
VormVrij 3D	Designed for clay but since expanded to include food paste (VormVrij 3D, 2016) Maximum working pressure is 8 Full system €4500. Single extruders are sold from €795
Print2Taste GmbH	Food printer for catering and professional chef use; Sells pre-filled chocolate and marzipan, 8 refills (70 mL) for €38.80 Bocusini printer available for €3000
Natural Machines Inc.	Food printer for professional and home use (C.-J. Kuo et al., 2016) Pneumatic extrusion; multiple capsules with heating element Foodini printer has limited initial run for \$4000 USD
<b>University Labs</b>	
Tangible Media Group	Transformative Appetite: MIT (G. Wang et al., 2016; W. Wang et al., 2017) “4D printing” pasta with modular liquid printer xPrint
Creative Machines Lab	Digital food: Cornell University and Columbia University Focus on developing personalized nutrition (Creative Machines Lab, 2017)
<b>Established companies</b>	
Xerox Inc.	Chocolate printer patent (Mantell et al., 2015) Inkjet printing with temperature controlled platform
Stratasys Inc.	Chocolate printer patent (Zimmerman et al., 2015) Extrusion with temperature controlled loop
3DSystems	Acquired The Sugar Lab (von Hasseln et al., 2014) and form Culinary division Partner with Culinary Institute of America and M�elisse restaurant Chefjet Pro; Powder bed with binder jetting
<b>Government Projects and Research Groups</b>	
PERFORMANCE	EU funded project focused on 3D printing soft food for elderly (K�uck, 2015)
NSRDEC	US army research center Personalized nutrition for combat troops (Benson, 2014)
CSIRO	Australia research center Investigating 3D printing food for dysphagia patients (Tyers, 2017)
NAMIC	National Additive Manufacturing Innovation Cluster, Singapore In depth review articles on food printing technologies (Sun et al., 2017, 2015b)
TNO	Netherlands Organization for Applied Scientific Research Extrusion, laser sintering, confectionary, personalized nutrition (Linden, 2015)
<b>Restaurants</b>	
Moto	Haute cuisine recognized for molecular gastronomy (2004-2015) Modified printer to create novel dishes
Food ink	Pop-up restaurant 3D printed food, utensil, and furniture (3DFP Ventures Ltd, 2017)
La Enoteca	Haute cuisine Create “sea coral” dishes with 3D printer (Koenig, 2016)

Some well-established companies working in conventional printing are stepping into the 3D food printing market as well. Xerox Inc. and Stratasys Inc. both hold patents (US 9185923 B2, US 9215882 B2) on 3D printing chocolate (Mantell et al., 2015; Zimmerman et al., 2015). Xerox's design uses a temperature controlled platform while Stratasys's printer use internal temperature controlled loop, respectively. Neither company has officially announced plans for commercial 3D food printer as of yet. In contrast, 3DSystems has a dedicated culinary division. 3DSystems have partnered with Culinary Institute of America and several celebrity chefs. 3DSystems developed the ChefJet Pro which is a printer designed for professional catering services instead of home use.

In addition to private investment, governmental organizations have shown interest in food printing. NASA, NSRDEC, research centers in Singapore, Australia, as well as the Netherlands are all looking to develop their own 3D food printing system.

3D printing food is appealing for NASA and NSRDEC for its ability to eliminate waste and replace meals ready-to-eat (MRE). NASA is looking into long term manned space mission so they need a way to provide food to the astronauts. The current MRE is not feasible due to limited shelf life (3-6 months) and excessive waste generated from packaging (Contractor et al., 2016). 3D printing food could help eliminate waste since it only prints what is needed. It can also extend shelf life when the raw ingredients are stored as powder. Nutritional content can be customized to suit personal needs since the food will be constructed from individual macronutrient components. The food preparation process can be automated to save time. In addition, the cooking step can be integrated in the 3D printer since traditional cooking techniques may not be suitable for given environment.

The army faces a similar issue since the amount of equipment carried out to the field is limited. Troops deployed to remote areas rely mostly on MRE. 3D printing food could provide a variety of food using only a few basic ingredients (Benson, 2014). It could allow for personalized nutrition based on activity levels and can work in conjunction with wearable technology that monitors the user's physiology and nutritional requirements.

3D printing food was the focus of the PERFORMANCE (development of personalised food using rapid manufacturing for the nutrition of elderly consumers) project for its ability to manipulate food texture. People with chewing and swallowing difficulties rely on modified texture food. Texture-modified food is unappetizing as taste and aesthetic is often sacrificed in favor of safety and convenience. 3D printers can reconstruct the purée into more appetizing shapes while still maintaining the texture that is safe to swallow. The visual appeal of food contributes to the enjoyment of food. Furthermore, streamlining the meal preparation process could allow for improved consistency and reduced variation of in-house preparations. Finally, personalized food would be valuable to the elderly to suit their preference and dietary needs.

## Chapter 3. Materials and experimental methods

This chapter will provide information on the 3D printer and extruder used in this thesis. The 3D printing experiments are discussed in section 3.3. In section 3.4, the G-code and the slicer settings are discussed in the context of understanding 3D printer setting and modifying it for printing viscoelastic pastes.

### 3.1. 3D printing and extrusion system

A delta-style desktop 3D printer (Rostock Max V2, SeeMeCNC) and a stepper motor driven paste extrusion system (Discov3ry, Structur3D Printing) were used for all printing experiments. An open-source slicer called MatterControl (MatterHackers) was used to prepare the files for printing.

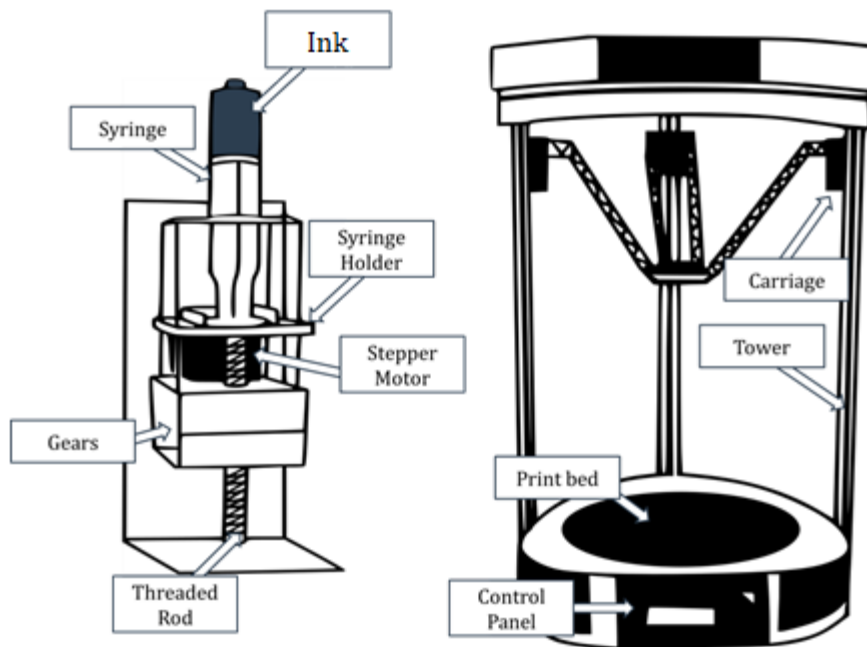


Figure 6 Schematics of the extrusion system (left) and the desktop 3D printer (right)

The 3D printer is controlled by a RepRap Arduino-Mega compatible motherboard (RAMbo) with the Repetier firmware. It controls the temperature, speed, extrusion rates, and other 3D printer settings. It is a delta-style printer where the nozzle is mounted on a base at the intersection of the arms of the three carriages. The movement is controlled by the position of the three carriages relative to each other. The extruder has a stepper motor that drives the gear which moves the threaded rod up or down. The rod drives the plunger which pushes the content in the syringe out. 3D print files can be loaded from a computer connected to the RAMbo. A 1.54 mm diameter polypropylene nozzle was used for all experiments. The nozzle height was set to equal the nozzle diameter unless stated otherwise. All 3D printing tests were conducted at room temperature.

### 3.2. G-code and slicer settings

After reviewing the hardware of the 3D printing system, this section will discuss the software components specific to viscoelastic inks. Most available software is designed for solid plastic filaments as inks. The speed at which filaments are fed into the hot end can be easily controlled by gears. On the other hand, extruding a viscoelastic ink requires modification. Slicer settings and machine commands (G-code) for extrusion-based 3D printing will be examined in the next paragraphs.

The goal was to be able to control extrusion rate and speed independently. The slicer settings were first investigated by changing individual settings in increments to observe their effects on the printing process (Appendix A). Once the key settings were identified, the G-code was investigated in order to understand how the slicer settings were involved. It is important to understand how the slicer generates G-code as well as how the G-code commands are interpreted by the 3D printer and the extruder.

The G-code has the following format: G1 X( $x_i$ ) Y( $y_i$ ) Z( $z_i$ ) E( $e$ ) F( $f$ ). The first element instructs the printer on the type of action to take. For example, G1 is a command for printing and G28 moves all the axes to the home position (RepRapWiki, 2017). The X, Y, and Z fields determine the nozzle position. The E field represents the length of filament extruded ( $e$ ) and the F field represents the filament extrusion speed ( $f$ ). The values of  $e$  and  $f$  are in units of mm and mm/min, respectively.

In general, G-code files are generated by slicers. The slicer takes a 3D model and converts it to printing paths. The  $f$  value is generated by the slicer based on print speed which is a user input. The  $e$  value is also generated by the slicer based on multiple user inputs including nozzle diameter, filament diameter, layer height, and extrusion multiplier (Equation 3-1).

$$e = \frac{(D_{nozzle})^2}{(D_{filament})^2} \times \frac{layer\ height}{D_{nozzle}} \times extrusion\ multiplier \times toolpath \times 1.273 \quad \text{Equation 3-1}$$

In Equation 3-1 the constant 1.273 is a multiplier inherent to the MatterControl slicer since when printing thermoplastics a thicker line will help with layer adhesions.

The nozzle speed ( $v$ , mm/s) is calculated by dividing the toolpath length (i.e. how far the nozzle needs to travel) by the extrusion time (Equation 3-2).

$$v = \frac{toolpath}{(e/f)} = \frac{\sqrt{(x_1 - x_0)^2 + (y_1 - y_0)^2 + (z_1 - z_0)^2}}{(e/f)} \quad \text{Equation 3-2}$$

The toolpath is the distance the nozzle needs to travel to move from its current position ( $x_0, y_0, z_0$ ) to the new coordinate ( $x_1, y_1, z_1$ ). The duration of extrusion in minutes can be calculated from  $e$  and  $f$  values.



The volumetric extrusion rate ( $Q$ ,  $\text{mm}^3/\text{s}$ ) calculation, on the other hand, is more complicated since it involves understanding the extruder mechanisms. For a stepper motor driven piston-based extruder the extrusion rate is controlled by the rotational speed of the stepper motor. Figure 7 shows the different components of the motor moving the threaded rod in the extruder and how they interact with each other.

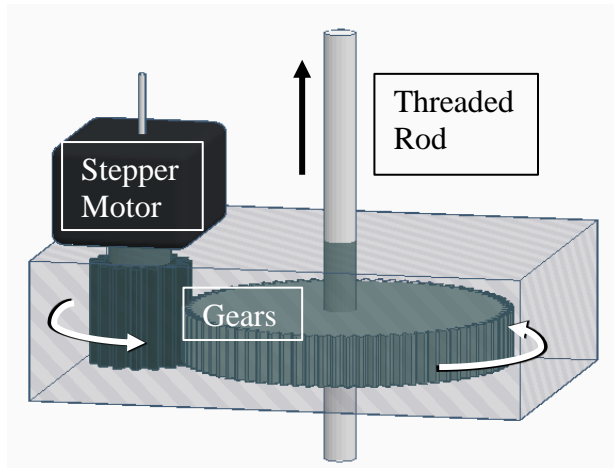


Figure 7 Diagram of the extruder showing the stepper motor, gear box, and threaded rod. The stepper motor drives the two gears which in turn move the rod in the vertical direction which pushed the piston of the extruder.

As shown in Figure 7, the stepper motor is the main driving force of the piston in the extruder. The motor rotational speed can be calculated as follows:

$$\text{motor speed} = \frac{f \times e\text{-step}}{\text{motor steps per rev}} \quad \text{Equation 3-3}$$

Where  $f$  is the print speed ( $\text{mm}/\text{min}$ ),  $e\text{-step}$  is a setting in the printer's temporary electronic memory (EEPROM) that is related to the extruder ( $\text{steps}/\text{mm}$ ), and the motor step per revolution is specific to the model of stepper motor. For the stepper motor in this work, it moves 1.8 degree per full step and has a reduction ratio of 1:100. The stepper motor step per revolution is calculated to be  $\frac{360^\circ}{\text{rev}} / \left( \frac{1.8^\circ}{\text{step}} \times \frac{1}{100} \right) = 20000 \text{ steps}/\text{rev}$ .

The motor speed (RPM) is calculated from the  $f$  and  $e\text{-steps}$  value, both are user inputs to the slicer. Note that the motor speed is for the smaller gear directly attached to the stepper motor out of the two interconnected gears shown in Figure 7.

The predicted volumetric extrusion rate ( $Q_{\text{Predicted}}$ ) is estimated from the stepper motor, speed of the lead screw, and the size of the syringe as listed in Table 6.

Table 6 Extruder characteristics

Stepper motor (steps/rev)	20000
Gear reduction ratio	1:5
Lead screw travel speed (mm/rev)	1/6
Syringe internal diameter (mm)	30

The volumetric flow rate is caused by the threaded rod pushing the piston upwards as the stepper motor rotates. The speed of the piston multiplied by the internal cross-sectional area of the syringe gives the volume of the ink extruded. The predicted volumetric extrusion rate is calculated as:

$$Q_{Predicted} = f \times e\text{-step} \times 1 \frac{1/6 \text{ mm/rev}}{20000 \text{ steps/rev}} \times \frac{1}{5} \times \frac{\pi}{4} (30 \text{ mm})^2 \times \frac{\text{min}}{60 \text{ s}} \quad \text{Equation 3-4}$$

Equation 3-2 and Equation 3-4 both contain  $f$  which means that changing the print speed would affect both  $v$  and  $Q$ . In order to independently vary  $v$  and  $Q$ , the print speed should be constant (e.g. 600 mm/min). The extrusion multiplier is used to change  $v$  and the e-step (listed as “extruder steps per mm” in EEPROM) is manipulated to achieve different  $Q$ .

Table 7 summarizes the predicted volumetric extrusion rate based according to Equation 3-4 which assumes that there is no load and no friction. The experimental extrusion rate might be lower since during printing there is friction along the walls of the syringe as well as resistance from the viscoelastic ink. Extrusion experiments (section 3.3.1) were conducted to measure the actual extrusion rates as well as extrusion lag time.

Table 7 Predicted  $Q$  (Equation 3-4) at different stepper motor speeds (Equation 3-3) for  $f = 600$  mm/min

e-step (steps per mm)	Motor Speed (RPM)	$Q_{Predicted}$ (mm <sup>3</sup> /s)
<b>533</b>	16	6.3
<b>800</b>	24	9.4
<b>1067</b>	32	12.6
<b>1333</b>	40	15.7
<b>1600</b>	48	18.8

### 3.3. Printing tests and image analysis

#### 3.3.1. Extrusion test

The purpose of the extrusion tests was to measure the experimental and steady state extrusion rate and the time required to reach steady state. Since the inks were viscoelastic, time was required for sufficient pressure to build up to push the ink out of the syringe.

The mass of ink exiting the nozzle was recorded over a period of 10 minutes at different stepper motor speeds to investigate changes in extrusion rate over time. The data were fitted to a Weibull distribution function (Equation 3-5). This form of equation is frequently used to model systems that approach steady state over time such as fungal microbial growth (Peleg and Normand, 2013). This model was recently used to represent the changes in height of a stack during the 3D printing of fruit-based snacks (Derossi et al., 2017).

$$M(t) = M_{\infty} [1 - \exp(-kt^n)] \quad \text{Equation 3-5}$$

$M(t)$  is the extrusion rate at time  $t$  and it is measured as mass collected per minute (g/min).  $M_{\infty}$  is the extrusion rate at the plateau (g/min). Initially at  $t = 0$  the stepper motor is not turning so no ink is extruded:  $M(0) = 0$ . After sufficient time,  $M(t)$  approaches the plateau value:  $M(\infty) = M_{\infty}$ . The constants  $k$  ( $s^{-1}$ ) and  $n$  (dimensionless) represent steepness and span of the curve (Peleg and Normand, 2013).

$$t_{lag} = \left( \frac{\ln 0.1}{-k} \right)^{1/n} \quad \text{Equation 3-6}$$

The extrusion lag time ( $t_{lag}$ ) was calculated as the time required for reaching 90% of  $M_{\infty}$ . Equation 3-5 was rearranged to obtain Equation 3-6.

#### 3.3.2. Line printing test

Line printing experiments were conducted to assess the quality of the printed objects. Three different situations could be expected (Figure 8). First, over-extrusion if the line thickness is much larger than the nozzle diameter. The object would be bloated and the finer details of the design would be lost. The nozzle would also flatten the line and drag through previously printed areas. Second, under-extrusion if there is no continuous line. The printed line is broken because the nozzle is moving too fast and not enough ink is extruded. In addition, minor under-extrusion can occur if the line thickness is slightly smaller than the nozzle diameter. There may be a continuous line but the line is stretched and dragged, rounding out any sharp angle in the design. Third situation if the printed line width is equal or slightly larger than the nozzle diameter. The third situation is desired since slightly thicker line help with adhesion between printed layers.

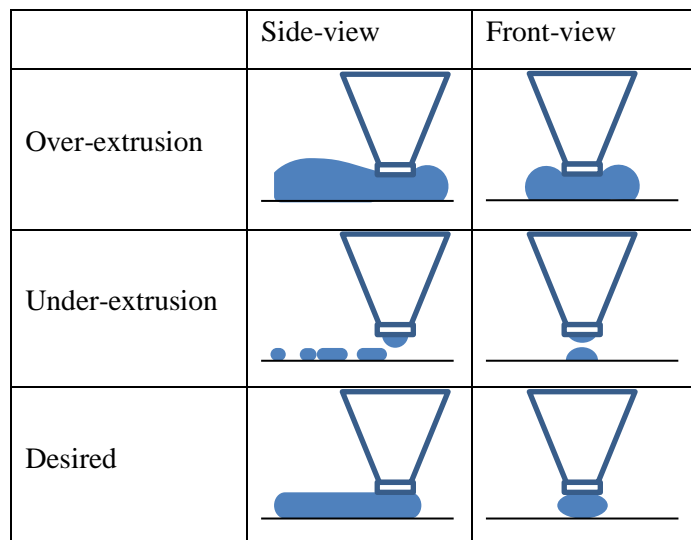


Figure 8 Side-view and front-view of the nozzle and ink for over-extrusion, under-extrusion, and desired extrusion.

Line printing tests were performed at 5 nozzle speeds (2, 4, 6, 8, 10 mm/s) and 5 motor speeds (16, 24, 32, 40, 48 RPM) which provided different predicted volumetric extrusion rates according to Equation 3-3 and 3-4. The lines were photographed and image analysis software ImageJ (National Institutes of Health) was used to estimate the diameters of the printed line.

The diameter of the printed line is controlled by the nozzle speed and the extrusion rate. The line diameter can be predicted using volume conservation and assuming elliptical cross-sectional area of the line (Equation 3-7).

$$\frac{Q}{v} = A = \frac{\pi ab}{4} \quad \text{Equation 3-7}$$

Where  $Q$  is the experimental steady state volumetric extrusion rate ( $\text{mm}^3/\text{s}$ ),  $v$  is the nozzle speed ( $\text{mm}/\text{s}$ ) (Equation 3-2), and  $a$  and  $b$  are the width and height of an elliptical cross-section ( $\text{mm}$ ), respectively.

$$a = \sqrt{\frac{4}{\pi c}} \sqrt{\frac{Q}{v}} \quad \text{Equation 3-8}$$

Equation 3-7 is rearranged to estimate the line width as function of  $Q$  and  $v$  (Equation 3-8), here  $c$  is the aspect ratio defined as height over width ( $c = b/a$ ). If the cross-section is a circle then  $c = 1$ , but if there is horizontal spreading of the line,  $c < 1$ . Linear regression was performed in python to determine the value of  $c$  for each type of ink.

### 3.3.3. Cylinder printing test

The previous two sections provided information on the print settings for accurate prints. A cylinder was selected to assess the effects of ink rheology and infill levels on maximum build height. Infill level is a fraction of the interior to be filled with material when printed. Cylinders 20 mm in diameter and 40 mm in height at 0, 25, and 50% infill were printed using starch and XG pastes (Figure 9). Video of the cylinder printing process was captured with a digital camera. A snapshot was taken before the cylinder collapsed and the height at that point was deemed the maximum build height. All snapshots were analyzed with ImageJ.


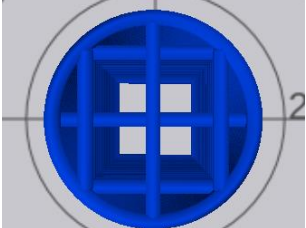
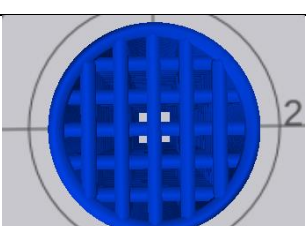
Infill level (%)	Top-down view of cylinder
0	
25	
50	

Figure 9 Top-down view of cylinders at 0, 25, and 50% infill using line pattern

### 3.3.4. Image analysis

Image analysis was used for capturing the shape of the printed line of cylinder. Compared to measurement with a caliper, image analysis doesn't involve direct contact with the printed object so the structure is not affected. Blue food coloring (McCormick Canada) was added to the ink as needed to enhance the contrast between the object and the background. For line printing, the image was taken top down since only one layer was printed. For cylinder printing, the image was taken sideways allowing for the observation of the adhesion between layers.

For line printing, the scale of the image was first set with a ruler. Afterwards, a threshold was obtained by adjusting hue, saturation, or brightness cut-off so only printed lines were selected (Figure 10). For when using blue food coloring, the hue > 85 threshold cut-off was selected. For carrot purée, the saturation > 100 cut-off was selected.

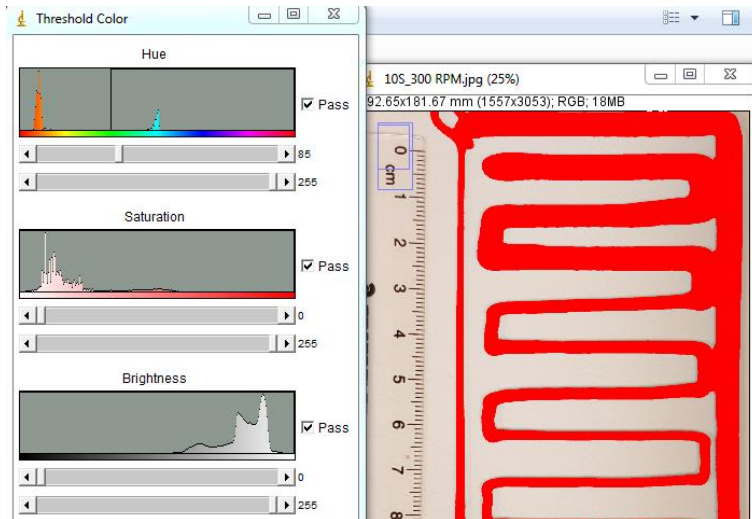


Figure 10 Examples of threshold settings where the darker portion of the image is selected. Hue/ Saturation/ Brightness thresholds were manipulated to exclude the background.

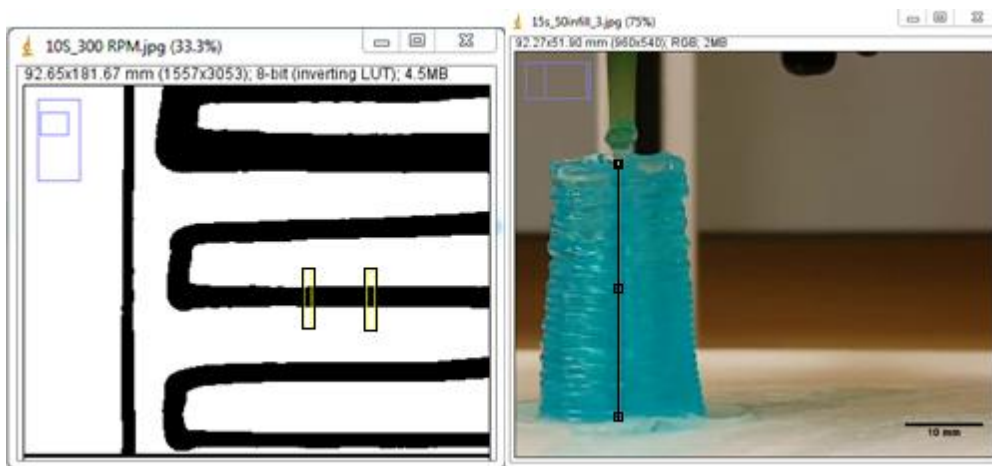


Figure 11 Examples of image analysis. The two 1 mm wide rectangles measure the width of the printed lines (left) and the line drawn down the center of the cylinder measures the height of the printed cylinder (right).

The image was then converted to binary format for measurement. For line printing, rectangles (box) with width of 1 mm were used and the area was taken as printed line width. Two measurements were taken per line towards the center (about 20 mm from the edges) where the line was more uniform (Figure 11). For cylinder printing, the scale was set the same way. The build height was measured directly by drawing a line down the center of the object (about 10 mm from the edges) (Figure 11).

### **3.4. Data Analysis**

Parameter estimation for equation 3-5 and 3-8 was done with Python with its scientific computation library Scipy (Jones et al., 2001). Extrusion rate and line width data were fitted to their respective equations (Equation 3-5, Equation 3-8). The parameters of each equation were obtained by minimizing sum of squared error. The standard deviation errors of the parameters were calculated from the square roots of the diagonal of the covariance matrix. Third-order piecewise polynomial fit was used for analysis of oscillatory rheology data for shear stress ramp.

## **Chapter 4. Rheological characterization of 3D printable pastes**

This chapter addresses the second object, identifying the rheological characteristics of foods as potential criteria for the development of ink formulation suitable for extrusion-based 3D printing. Modified corn starch and xanthan gum were selected as model ink. Rheological characteristics investigated included storage modulus, loss modulus, complex modulus, loss tangent and yield stress. I would like to state the contributions of Madhu Sharma for collecting the rheological experimental data presented in this chapter. This chapter was written as a manuscript intended for submission to publication in the Journal of Food Engineering.

### **4.1. Introduction**

Currently, food inks suitable for extrusion-based 3D printing are formulated by trial and error which is time consuming and may not generate an optimal ink formulation. Physical properties may have the ability to provide a framework for the formulation of food inks that could reduce the time requirements and may lead to improved food ink formulation.

In this study, we have investigated the rheological characteristics of foods as potential criteria for the development of formulation suitable for extrusion-based 3D printing. Two hydrocolloids, modified corn starch and xanthan gum, were selected as model food ink. Rheological characteristics investigated included storage modulus, loss modulus, complex modulus, loss tangent and yield stress. Attention was also given to the estimation and mathematical representation of these characteristics. The framework of rheological characteristics established for the two model hydrocolloids was then used to analyze published rheological characteristics of foods and assess their potential suitability as food inks for extrusion-based 3D printing. The potential of using rheological characteristics and their relationship to the texture sensory attribute for general types of foods and for the special food class, texture modified food for dysphagia management, was examined in the context of developing formulation for food inks suitable for extrusion-based 3D printing.



## 4.2. Materials and methods

### 4.2.1. Sample preparation

Modified corn starch (MS) (Uni-Pure® D2560, Ingredion) and xanthan gum (XG) (Duinkerken Foods, Canada) were mixed with deionized water with a spoon to form pastes. The mixture was blended with a food processor (BlenderPro) for 2 min. Three concentrations of modified starch pastes (10, 15, 20% w/w) and xanthan gum pastes (5, 7.5, 10% w/w) were prepared. The concentration ranges were selected so the paste can both hold its shape after deposition and be extruded. All samples were stored at 4 °C and warmed up to room temperature prior to 3D printing.

### 4.2.2. Oscillatory rheology

Viscoelasticity of the hydrocolloid pastes were analyzed with Paar Physica MCR-301 rheometer (Anton Paar GmbH, Germany). Parallel plates with a diameter of 50 mm and gap distance of 2 mm were used.

Linear viscoelastic region (LVR) was determined by amplitude sweeps conducted at frequency of 1 Hz and strain from 0.1-100%. Frequency sweep was performed at 0.4% strain from 0.1-100 Hz. Shear stress ramp test was performed from 1 to 1000 Pa at frequency of 1 Hz to determine the yield stress. The dependency of the storage modulus ( $G'$ ), loss modulus ( $G''$ ), complex modulus ( $G^*$ ), and loss tangent ( $\tan \delta = G''/G'$ ) on strain, frequency, or stress was analyzed (Section 4.2.3). Analysis was conducted in triplicates at 25 °C.

### 4.2.3. Analysis of rheology data

The rheology data was analyzed with Python with its scientific computation library Scipy (Jones et al., 2001). Cubic spline functions were used to fit  $G'$  or  $G''$  and to determine the point where  $G'$  started to deviate from the LVR.

Two types of mathematical representation were used to analyze the frequency sweep data. The first representation is the power law relationship (Equation 4-1& Equation 4-2) (Steffe, 1996) . The parameters  $K'$  and  $K''$  represent the modulus value at 1 Hz while  $n'$  and  $n''$  reflects the modulus dependency on frequency.

$$G' = K' \omega^{n'} \quad \text{Equation 4-1}$$

$$G'' = K'' \omega^{n''} \quad \text{Equation 4-2}$$

The weak gel model (Equation 4-3) was used to relate  $G^*$  to frequency. The parameter  $A_f$  can be interpreted as the strength of interaction between rheological units (drops, fibres, micelles, etc.) whereas  $z$  is the number of rheological units interacting with one another (Gabriele et al., 2001).

$$G^* = \sqrt{G'^2 + G''^2} = A_f \omega^{1/z}$$

Equation 4-3

All model parameters were estimated with the non-linear least squares method in Python.

### 4.3. Results

#### 4.3.1. Strain sweep

The purpose of the strain sweep was to determine the linear viscoelastic region (LVR). At low strain, the storage modulus ( $G'$ ) and the loss modulus ( $G''$ ) for xanthan gum (XG) and modified starch (MS) paste were constant and parallel according to concentration and  $G' > G''$  for all cases (Figure 12). As strain increased,  $G'$  started to decrease. The critical strain ( $\gamma_c$ ) is defined at the point where  $G'$  shows 5% reduction from its LVR value (Moelants et al., 2013). Strong gels have higher  $\gamma_c$  than weak gels (Steffe, 1996).

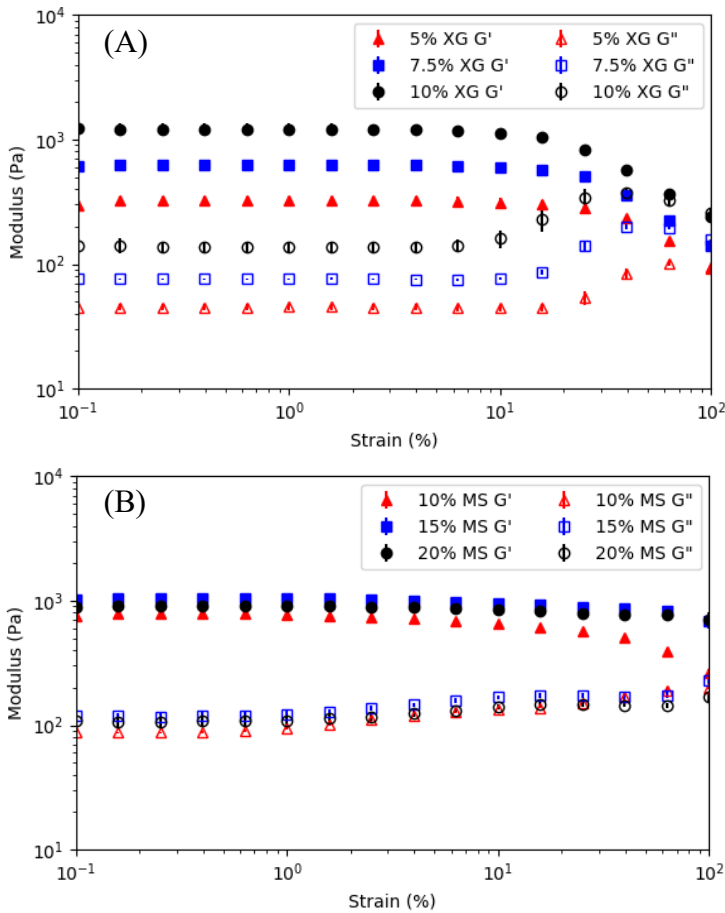


Figure 12 Amplitude sweep of (A) xanthan gum (XG) and (B) modified starch (MS). Each point represents the average of 3 measurements with standard deviation represented as error bars

For XG pastes,  $\gamma_c$  decreased with increasing concentration while the opposite was observed for MS pastes (Table 8). At strain higher than  $\gamma_c$ ,  $G'$  decreased while  $G''$  increased slightly followed by decrease. This behavior is described as weak strain overshoot (Hyun et al., 2002). The behavior may be explained by XG structure. It was proposed that the charged side groups on XG results in their repulsion and the extension of the long backbone (Sworn, 2009). The long XG chains may entangle and form weakly structured material at low strain which result in initial increase in  $G''$ . At high strain, the temporary structure of XG is destroyed and both modulus start to decrease (Carmona et al., 2014; Song et al., 2006).

Table 8 Critical strain ( $\gamma_c$ ) for XG and MS pastes at different concentrations. Values reported as average  $\pm$  standard deviation (N = 3)

Material	$\gamma_c$ (%)
5% XG	13.5 $\pm$ 0.8
7.5% XG	11.8 $\pm$ 0.6
10% XG	8.4 $\pm$ 1.3
10% MS	2.1 $\pm$ 0.3
15% MS	5.4 $\pm$ 1.3
20% MS	8.0 $\pm$ 2.8

#### 4.3.2. Frequency sweep

Frequency sweep studies provided information on the response of the materials to different time-scale of operation. For food studies, the typical frequency range is between 0.1 to 100 Hz which corresponds roughly to the time-scale of industrial processes such as mixing or pumping (Gabriele et al., 2001; Norton et al., 2011).

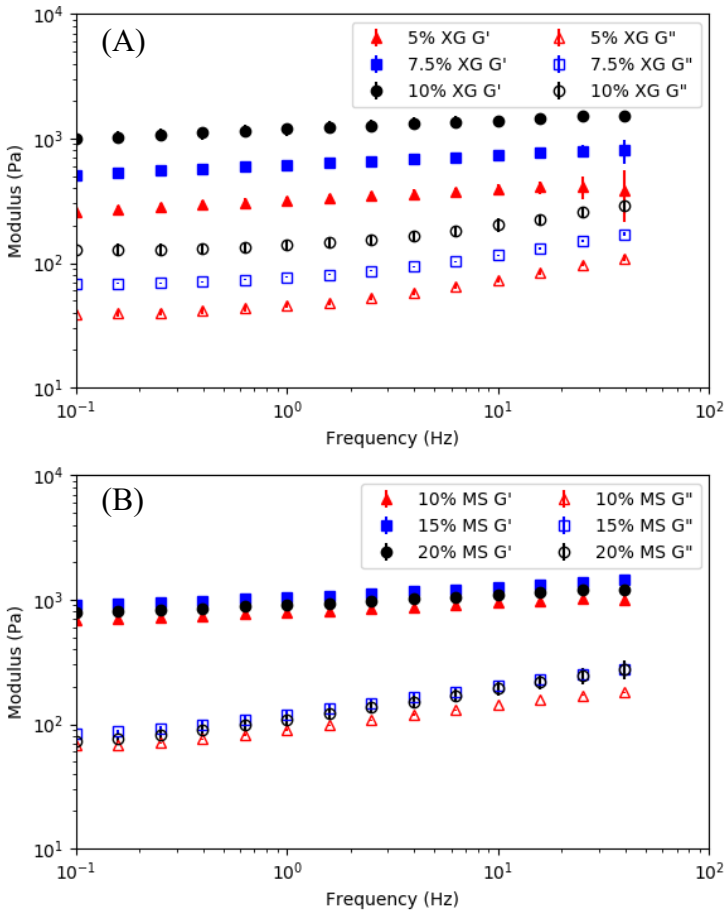


Figure 13 Frequency sweep of (A) XG and (B) MS. Each point represents the average of 3 measurements with standard deviation represented as error bars

Frequency sweep of XG and MS pastes showed  $G' > G''$  for the entire frequency interval tested (Figure 13). No cross-over between  $G'$  and  $G''$  was observed. XG pastes showed more distinct differences in  $G'$  and  $G''$  according to concentration. In contrast, MS pastes had similar  $G'$  and  $G''$  for all concentrations investigated.

The effect of frequency on the modulus was analyzed with the power law and the weak gel model. The models were chosen because of their simplicity and the availability of published data. Alternative methods such as the fractional derivative model (Song et al., 2006) or the generalized Maxwell equations (Meza et al., 2011) were not considered because of the large number of parameters and the limited published data.

The simplicity of the power law model made it easy to interpret the physical meaning of parameters. The constant K was related to the network strength within the LVR and the exponent n was related to modulus' frequency dependency (Table 9). For a perfectly crosslinked gel, n is 0 while for a physical gel with weak interactions, such as hydrogen bonds, n is a small positive number (Norton et al., 2011; Tunick, 2011).

Table 9 G' and G'' fitted to Equation 4-1 & 4-2. Fitted parameters are reported as average  $\pm$  one standard deviation errors on the parameters (N = 3)

Material	G' (Pa)		G'' (Pa)	
	K' (Pa s <sup>n'</sup> )	n'	K'' (Pa s <sup>n''</sup> )	n''
5% XG	319 $\pm$ 0.17	0.09 $\pm$ 0.0004	49 $\pm$ 1.37	0.18 $\pm$ 0.02
7.5% XG	614 $\pm$ 0.32	0.08 $\pm$ 0.0004	82 $\pm$ 1.79	0.13 $\pm$ 0.01
10% XG	1186 $\pm$ 1.59	0.08 $\pm$ 0.0008	148 $\pm$ 3.58	0.13 $\pm$ 0.01
10% MS	795 $\pm$ 2.05	0.072 $\pm$ 0.002	96 $\pm$ 1.04	0.175 $\pm$ 0.005
15% MS	1060 $\pm$ 4.72	0.075 $\pm$ 0.003	125 $\pm$ 1.76	0.190 $\pm$ 0.009
20% MS	920 $\pm$ 3.23	0.07 $\pm$ 0.002	113 $\pm$ 1.42	0.212 $\pm$ 0.008

For XG, the power law model provided a fit with  $R^2 > 0.998$  for G' and  $R^2 = 0.85-0.92$  for G''. The lower  $R^2$  for G'' reflected the slight concave shape of the curve which indicated greater variation in G'' at high frequency as previously observed for thickened salad dressings (Dolz et al., 2006). Both K' and K'' increased with increasing concentration. For MS, the power law model provided a fit of  $R^2 > 0.97$  for both G' and G''. An unusual behavior was observed with higher K' and K'' for the 15% MS compared to the 20% MS. The estimated n' for XG and MS were relatively small (0.07-0.09) which indicates that G' did not vary significantly with frequency. On the other hand, the estimated n'' was higher (0.1-0.2) which indicate that G'' has higher frequency dependence.

The weak gel model (Equation 4-3), which represented food materials as network of aggregates connected by weak strands that may be broken upon deformation (Gabriele et al., 2001), provided information on the gel structure and texture attributes of foods. The model parameters,  $A_f$  and z, have been interpreted as the network strength and the degree of interaction, respectively (Gabriele et al., 2001). The z parameter can also be interpreted as the degree of viscoelasticity since it described the frequency dependency of G\* (Murekatete et al., 2014). For gels exhibiting ideal elastic behavior, the exponent would equal zero so larger z values indicated that the material was more elastic than viscous.

Table 10  $G^*$  for XG and MS pastes fitted to Equation 4-3. Fitted parameters are reported as average  $\pm$  one standard deviation error (N = 3)

Material	$A_f$ (Pa s <sup>1/2</sup> )	z
5% XG	323 $\pm$ 0.69	11 $\pm$ 0.18
7.5% XG	620 $\pm$ 0.38	12 $\pm$ 0.06
10% XG	1194 $\pm$ 3.15	13 $\pm$ 0.20
10% MS	801 $\pm$ 2.42	14 $\pm$ 0.32
15% MS	1069 $\pm$ 5.13	13 $\pm$ 0.45
20% MS	928 $\pm$ 3.44	14 $\pm$ 0.44

The weak gel model provided a good fit for both XG and MS pastes ( $R^2 > 0.99$ ) (Table 10). Since  $G^*$  was considered in the weak gel model, the number of parameters was reduced to two compared to the four parameters of the power law model. For XG pastes, both  $A_f$  and z increased with increasing concentration. The higher concentration of XG was creating stronger gel network that was more elastic. For MS pastes,  $A_f$  was similar for all concentrations and z was higher than XG pastes which indicates a more elastic network for MS compared to XG.

#### 4.3.3. Yield stress determination

The yield stress, defined as the point where the internal structure of the material starts to break down (Steffe, 1996), can be used to assess the suitability of food inks for extrusion-based 3D printing where the yield stress should be low enough so that the ink can be extruded but not too low that once extruded, the ink will spread under its own weight.

There does not seem to be consensus on the method for the estimation of the yield stress from stress ramp measurements. The yield stress point has been considered as the point where  $G'$  starts to deviate from its LVR value since it represents the onset of non-linearity. Alternatively, the yield stress point has been considered as the point where  $G'$  and  $G''$  intersected since it represented solid-liquid transition (Shih et al., 2004). With this in mind, we elected to compare two methods recently proposed in the literature for the estimation of the yield stress and compared the estimated yield stress. Method one uses the intercept of two straight lines fitted to the log-log plot of  $G^*$  vs stress. The first line is fitted to values within the LVR and the second line is fitted to  $G^*$  beyond the LVR (De Graef et al., 2011). In method two, a plot of oscillatory strain vs stress was used. The strain-stress curve is linear at low stress since the response is predominantly elastic. The point where the curve starts to deviate from linearity is determined as the yield stress (Cyriac et al., 2015). We also report the onset of nonlinearity identified as the yield point and calculated as the point where  $G'$  deviated 10% from its LVR value (Sharma et al., 2017) and the

intersection point identified as the flow point. These estimates were illustrated in Figure 14 and presented in Table 9.

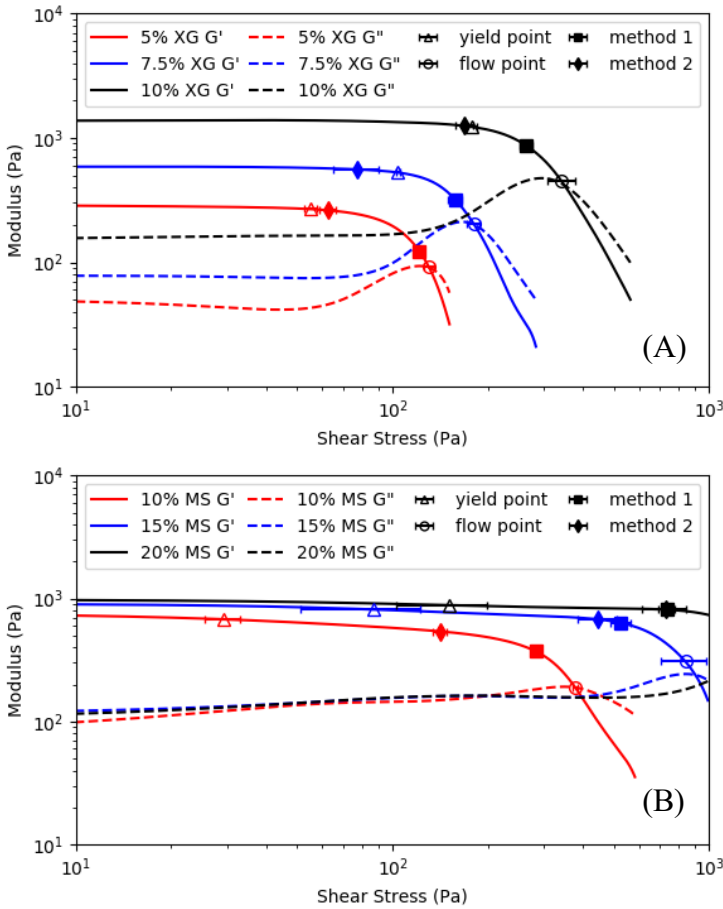


Figure 14 Shear stress ramp for (A) XG and (B) MS pastes and methods of identifying yield stress. Each point represents average yield stress of 3 measurements with standard deviation represented by horizontal error bars.

Within the LVR, both  $G'$  and  $G''$  were relatively constant with  $G' > G''$  for all samples which indicated a predominantly elastic response (Figure 14). For all XG pastes,  $G''$  had a slight increase before its intersection with  $G'$ . For MS pastes, strain overshoot was observed at 15% and 20%.

Table 11 Shear stress ramp analysis of XG and MS pastes

Material	Yield Stress Method 1 (Pa)	Yield Stress Method 2 (Pa)	Yield point (Pa)	Flow Point (Pa)	G' LVR (Pa)	G'' LVR (Pa)
5% XG	122 ± 0.3	62 ± 4	55 ± 3	130 ± 4	283 ± 17	47 ± 9
7.5% XG	158 ± 8	78 ± 13	104 ± 1	181 ± 8	572 ± 29	80 ± 9
10% XG	264 ± 12	169 ± 11	178 ± 7	342 ± 34	1350 ± 146	175 ± 28
10% MS	284 ± 4	141 ± 8	29 ± 4	377 ± 7	755 ± 7	82 ± 4
15% MS	526 ± 39	446 ± 63	87 ± 36	841 ± 137	899 ± 119	138 ± 31
20% MS	735 ± 46	730 ± 116	150 ± 47	N/A	925 ± 102	140 ± 21

For XG pastes, the yield stress estimated by method 1 was similar to the flow point and while yield stress estimated by method 2 was similar to the yield point. For MS, the yield stress estimated by method 1 and 2 were within the yield point and flow point. The yield stress estimates were higher than the yield point for all samples and lower than the flow point for the 10% and 15% MS pastes. Note that the flow point for 20% MS was above 1000 Pa as crossover was not observed within the range tested.

The estimation of the yield stress from the yield point and the flow points is the most straightforward method; however, it may not be the most accurate. Simply using a set percent deviation from LVR may underestimate the yield stress as observed for the MS pastes. When G' and G'' crossover, the material may already be flowing such that the yield stress may be overestimated.

The effect of concentration on the yield stress estimates was similar for both methods. The yield stress increased with increasing concentration. In contrast, the magnitude of the yield stress estimate was higher for method 1 compared to method 2 except the 20% MS paste. Both methods attempt to locate the onset of structural breakdown. Method 1 consists of a visual approach based on tangents in a log-log graph of G\* vs shear stress. This method can locate the point where G' start to decrease rapidly; however, it is not the most robust since the slope of the lines is sensitive to the number of data points selected. The number of data points for the linear and non-linear region is at the researcher's discretion. In contrast, method 2 determines the number of data points for the initial linear portion by removing points until  $R^2 > 0.99$  and the whole data set is fitted to a cubic spline. Although more complicated to implement initially, the iterative approach of method 2 is more rigorous. Therefore yield stress estimated using method 2 will be used in the discussion.



## **4.4. Discussion**

### **4.4.1. Rheology as constraints for design of 3D printable food inks**

Rheology is critical for extrusion-based 3D printing in terms of operation and product quality. Yield stress and  $\tan \delta$  are related to the paste's ability to be extruded while  $G^*$  is related to the paste's stiffness and its ability to hold its shape after 3D printed (Liu et al., 2017). In this study, rheological characterization of XG and MS pastes show that a printable paste should have  $\tan \delta$  around 0.1 to 0.2, yield stress between 60 to 730 Pa, and  $G^*$  between 300 to 1200 Pa at 1 Hz. The rheology studies on XG and MS pastes provided the upper and lower limit of a printable paste.

Other studies have used rheological properties to understand and predict texture, composition and mechanical properties of foods. For example, a study on carrot purée show statistically significant ( $p \leq 0.01$ ) correlation between its rheological parameters,  $\tan \delta$  and yield point, and sensory panel results such as oily mouth-coating and adhesiveness (Sharma et al., 2017). Mathematical relationships have been proposed to relate the rheological characteristics of foods to their composition. The  $G'$  and yield stress characteristics of carrot purée have been related to their pulp content with a power law relationship (Moelants et al., 2013). The  $G'$  and  $G''$  characteristics of potato foods have been related to the potato flakes, butter, milk, and salt content by quadratic polynomial equations (Alvarez and Canet, 1999). In a similar approach, Ađar and colleagues have related the texture (hardness, chewiness, gumminess, and cohesiveness) for meat emulsions to the  $A_f$  from the weak gel model (Ađar et al., 2016).

One can envision that predictive models could be used for the design of food inks suitable for 3D printing by extrusion. The rheological characteristics can be constraints in the food ink formulation development and optimization. One example is the optimization of flour blend in reduced fat burgers. Optimization targets (color, texture, and juiciness) are specified and the flour blend is optimized with mixture experiment approach (Shahiri Tabarestani and Mazaheri Tehrani, 2014).

### **4.4.2. Rheology of XG and MS paste and texture-modified food for dysphagia**

Texture modified food for dysphagia management are differentiated based on their consistency. In the context of the development of a classification system of food products that are suitable for 3D printing, the dysphagia classification system provides a good starting point. The  $G^*$  and  $\tan \delta$  of XG and MS pastes were compared to the five dysphagia product classes: nectar, honey, pudding, purée, and pâté (Figure 15).

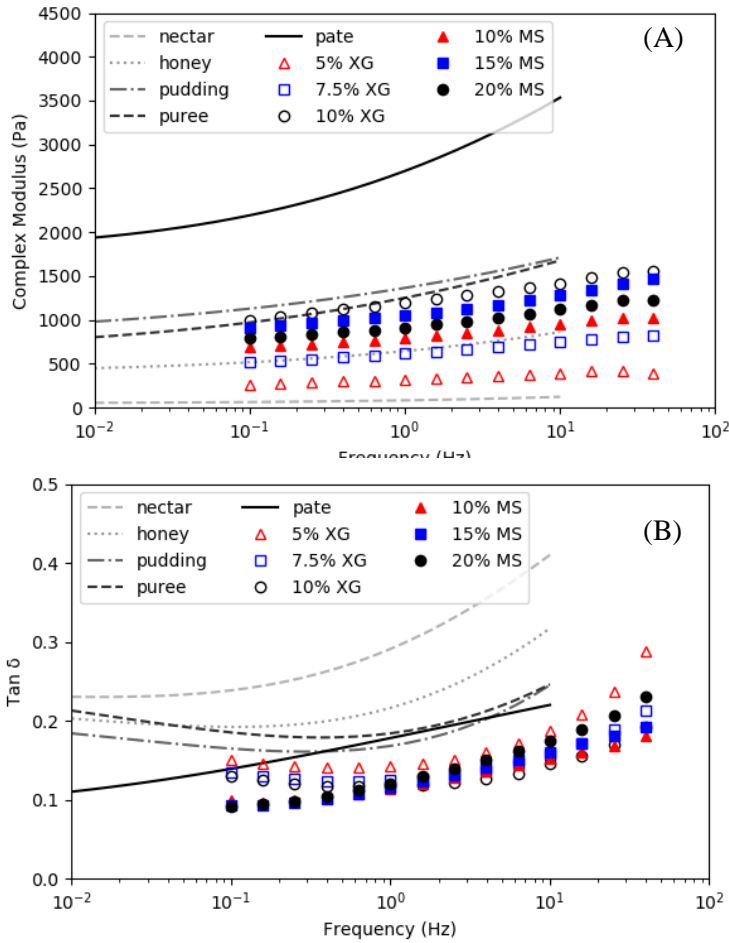


Figure 15 (A) Complex modulus ( $G^*$ ) and (B) loss tangent ( $\tan \delta$ ) for XG and MS pastes compared to five classes of dysphagia-oriented products. Data for different dysphagia classes obtained from (Casanovas et al., 2011)

The  $G^*$  of the 5% and 7.5% XG is close to of the honey class. In contrast, the  $G^*$  of the 10% XG is close to the purée class at low frequency.  $G^*$  of MS pastes was between the honey and purée classification. The XG and MS pastes appear to be less frequency dependent compared to pudding, purée, and pâté classes since  $G^*$  remains relatively constant instead of increasing at high frequency.

XG and MS pastes have lower  $\tan \delta$  than any of the dysphagia product classes. For all XG pastes, a minimum  $\tan \delta$  was observed around frequency of 0.5 Hz. The profile of the  $\tan \delta$  for the XG paste indicates a stronger effect of the frequency similar to the honey and pudding classes. In contrast,  $\tan \delta$  for MS pastes increases linearly similar to the pâté class.

The comparison of the rheological behavior of XG and MS pastes according to the dysphagia product classes indicate that the pudding and purée type products could be produced by extrusion-based 3D printing.

#### 4.4.3. Rheology of XG and MS paste and general types of foods

Due to its relative simplicity, the power law representation of the shear modulus according to frequency (equations 4-1 and 4-2) is widely used in food texture studies. One has to keep in mind rheometer setup and testing conditions may have been used; nonetheless, it is still useful to compare approximate ranges of the power law parameters. Note that parameter estimates are affected by the units of the frequency. In this study hertz (hz, s<sup>-1</sup>) was used. When frequency is expressed as radian per second (rad/s), K' and K'' estimates will be different by a factor of (2π)<sup>n</sup> while n' and n'' estimates will remain the same. Data from other publications were converted to units consistent with this study.

Table 12 Parameters of the power law model for different food reported in the literature. Rheology measurement conducted at 20 - 25 °C. Parameters not reported in paper are listed as N/A

Material	G' (Pa)		G'' (Pa)		References
	K' (Pa s <sup>n'</sup> )	n'	K'' (Pa s <sup>n''</sup> )	n''	
XG paste	319-1186	0.08-0.09	49-148	0.13-0.18	This study
MS paste	795-1060	0.07-0.075	96-125	0.17-0.21	
Cocoa drink	1-4	0.2	N/A	N/A	Zargaraan et al., 2015
Pudding	70-300	0.2	N/A	N/A	
Fruit and sweet potato purée	200-400	0.05-0.07	30-70	0.17-0.27	Ahmed and Ramaswamy, 2007a, 2006
Rice pastes	1100-2800	0.072-0.137	N/A	N/A	Li et al., 2016

Cocoa drink and Ferni have lower K' and higher n' compared to XG and pastes. Cocoa drink is considered a thickened liquid and has much lower K' compared to Ferni which is considered a type of pudding. For both foods, n' is around 0.2 (Zargaraan et al., 2015). The foods are likely not suitable for extrusion-based 3D printing due to its low stiffness.

Sweet potato and fruit purées have power law parameters similar to 5% and 7.5% XG. Puréed fruit and sweet potato infant food have K' around 200-400 Pa s<sup>n'</sup> and K'' around 30-70 Pa s<sup>n''</sup> with n' smaller than n'' (Ahmed and Ramaswamy, 2007a, 2006). Rice pastes have power law parameters similar to 10% XG and 15% MS. Depending on type of rice K' range from 1100-2800 Pa s<sup>n'</sup> and n' range from 0.072- 0.137 (Li et al., 2016). Rice with higher amylose content and longer amylopectin branches leads to higher K' and lower n' (Li et al., 2016; Lu et al., 2009). In a 3D printing study, glutinous rice paste which has low amylose content was too sticky to be extruded. On the other hand, rice powder from non-glutinous rice has poor shape retention (Tanaka et al., 2015). The differences in 3D printability may be explained by K' and n'.

The weak gel model and its parameters (Equation 4-3) of food inks may be used to evaluate the suitability for 3D food printing. The parameters  $A_f$  and  $z$  of XG and S pastes and for foods are summarized in Table 13. The literature data was categorized into five different groups based on their average  $A_f$  (Table 13). In general, pudding has  $A_f < 10^3$ , purée has  $A_f$  from  $10^3 - 2 \times 10^3$ , soft gel has  $A_f$  from  $2 \times 10^3 - 10^4$ , hard gel has  $A_f$  from  $10^4 - 4 \times 10^4$ , and dough has  $A_f > 4 \times 10^4$ . The parameters were obtained directly from the publication or calculated from the reported  $G'$  and  $G''$  using Equation 4-3.

Table 13 Parameters of the weak gel model for different food reported in the literature. Rheology measurement conducted at 20 - 25 °C

Food Groups	Material	$A_f$ (Pa s <sup>1/z</sup> )	$z$	Reference
Hydrocolloids	XG paste	320-1200	11-13	This study
	MS paste	800-1070	13-14	
Pudding	yoghurt	150	6.93	Gabriele et al., 2001
	fruit jams	505-750	3.6-6	Gabriele et al., 2001 Peressini et al., 2002
Purée	carrot purée	900-1200	11	Moelants et al., 2013
	beef, chicken, lamb purée	970-2900	8.27-8.97	Ahmed and Ramaswamy, 2007b
	mayonnaise	900-2000	8.34-11.32	Mancini et al., 2002
Soft Gel	mashed potatoes	2350-7450	5.1-6.1	Alvarez et al., 2012
	salmon baby food	2800-6500	8.9-7	Ramamoorthi et al., 2009
	tofu (salt-induced)	2300-3600	8.9-9.5	Murekatete et al., 2014
	cheese and lemon cream	5520-6560	4.87-5.09	Peressini et al., 2002
Hard Gel	alginate gel	1500-3700	25-50	Moresi et al., 2004
	surimi gel	7900-22000	10.1-10.6	Campo and Tovar, 2009, 2008
	tofu (acid-induced)	13000-18000	7.6-7.7	Murekatete et al., 2014
	pork liver pâtés	29000-41000	8-9	Delgado-Pando et al., 2012
Dough	pasta dough	46250	4.43	Gabriele et al., 2001
	cereal-blend dough	97700	5.03	Peressini et al., 2002
	maize dough	52500-106000	8.9-16.5	Moreira et al., 2015

Looking at the values of  $A_f$  and  $z$ , representing gel strength and the degree of viscoelasticity respectively, one can assess the potential suitability of these foods for 3D printing extrusion applications.

The foods classified as pudding possess  $A_f$  values within the lower range of XG and MS pastes and their  $z$  is lower so it will likely end up spreading and are not 3D printable. The observation is consistent with a recent study where chocolate jam and Greek yogurt are evaluated for 3D food printing with cylinder printing experiment and show significant deformation even at the low height of 20 mm (Kim et al., 2017).

The foods classified as purée are characterized by  $A_f$  and  $z$  similar to the 10% XG and 20% MS paste suggesting that these foods could be suitable for 3D printing. Pumpkin, beet, and tuna purée have recently been 3D printed although the printed object was fairly flat (~1 cm) (Kouzani et al., 2017). Additionally, we have recently demonstrated that carrot purée can be 3D printed as cylinders with an extrusion system in the lab (data not shown). Vegetable and meat food products are of particular interest since these products are essential elements of a balanced diet. Puréed vegetable and meat products are likely candidates when 3D food printing is to be used for regular “main-course” type meals as opposed to desserts and cake decoration applications.

The foods classified as soft gel possess a wide range of  $A_f$  and  $z$  values. Many of these foods have been investigated in 3D food printing studies. Cheese cream, lemon cream, and mashed potatoes have the lowest  $z$ . Compared to XG and MS pastes their  $A_f$  is higher but  $z$  is lower. It is likely suitable for 3D printing since the lower elasticity balances out with the high network strength. Mashed potato with added potato starch was successfully 3D printed in a recent study (Liu et al., 2017). When fitted to the weak gel model, the potato mixture with both good extrudability and shape retention has  $A_f$  of 4300 Pa s<sup>1/z</sup> and  $z$  of 6 (Liu et al., 2017). The higher  $z$  range (7.6-9.5) foods include salmon-based baby food and salt-induced tofu. The salmon-based baby food have similar  $z$  and higher  $A_f$  compared to other meat-based baby food (Ahmed and Ramaswamy, 2007b). Salt-induced tofu  $A_f$  is almost a magnitude lower than that of acid-induced tofu (Murekatete et al., 2014). Soft gels are likely suitable for 3D printing since the lower elasticity balances out with the high network strength. Tofu paste with methyl cellulose has been used to 3D print decorative coral reef like structures (Mizrahi et al., 2016).

The foods classified as hard gel have  $A_f$  between  $10^4$  to  $4 \times 10^4$  with the exception of alginate gel. Alginate is classified as hard gel because it has high  $z$  value (25-50) and a reported low  $\tan \delta$  of 0.05 (Moresi et al., 2004). Recent study on extrusion-based 3D printing indicate that gels with low  $\tan \delta$  may be harder to extrude and produce broken lines due to poor fluidity (Liu et al., 2017; L. Wang et al., 2017). Surimi gel was reported to have  $z$  value around 10 by Campo and Tovar (2008; 2009). In a recent study, surimi gels with different levels of salt were shown to be suitable for creating 3D printed foods (L. Wang et al., 2017).

$A_f$  was estimated from the published experimental data and  $A_f$  for surimi gel with 1.5% salt ( $10^4 \text{ Pa s}^{1/2}$ ) is a magnitude lower than that with no added salt ( $10^5 \text{ Pa s}^{1/2}$ ) (L. Wang et al., 2017). The gel strength,  $A_f$ , of surimi gel can be manipulated by changing starch and egg white protein levels (Campo and Tovar, 2009, 2008). Compared to XG and MS pastes,  $A_f$  for surimi gel is much higher. In the 3D printing study of surimi gel, a conveying screw extrusion mechanism was used (L. Wang et al., 2017) instead of a syringe and plunger system. Study conducted by Wang and colleagues indicates that hard gels can be 3D printed by extrusion when the system is adapted for these types of foods.

The foods classified as dough have  $A_f$  around  $4 \times 10^4 \text{ Pa s}^{1/2}$  or higher, more than a magnitude higher compared to XG and MS pastes. The high  $A_f$  values are indicative of high gel strength and strong network development which for such dough type material, extrusion with a syringe and plunger system could be very difficult. Similar limitations were observed in a recent study with protein and fiber-rich pastes. The protein paste with  $A_f$  of  $3.7 \times 10^4 \text{ Pa s}^{1/2}$  could not be extruded even with a high pressure of 600 kPa and wide syringe nozzle of 1.19 mm (Lille et al., 2017).

## 4.5. Conclusion

The rational development of 3D printable food inks requires knowledge of how composition, rheology, and printability relate to each other. 3D printing studies establish the printability window by identifying key parameters such as  $G^*$ , yield stress, and their ranges. Print tests with xanthan gum (XG) and modified starch (MS) pastes show that the printable paste have  $G^*$  at 1 Hz from 300 to 1200 Pa and yield stress from 60 to 730 Pa.

3D printable inks should be extrudable and maintain their shapes. Foods can be compared based on their network strength and degree of viscoelasticity. XG and MS pastes were used as reference due to their simple composition. Compared to the classification of dysphagia foods, XG and MS pastes have  $G^*$  between the honey and pudding class but have  $\tan \delta$  smaller than pâté class. The pastes are very elastic but not as stiff.

The parameters ( $A_f$  and  $z$ ) weak gel model for a wide range of food texture studies were compared. The  $A_f$  values was used to classify foods in five groups (pudding, purée, soft gel, hard gel, and dough). XG and MS pastes are similar to purée group in terms of network strength but are more elastic.

The overall network strength and degree of viscoelasticity balance each other when it comes to 3D printability. Soft pastes that are highly elastic (e.g. XG and MS pastes) and stiff pastes that flow easily (e.g. carrot purée, mashed potato) could be 3D printed. It only works up to a certain degree since cookie or pasta dough with low  $z$  but high  $A_f$  ( $> 4 \times 10^4$  Pa) cannot be 3D printed without the use of a more powerful extruder.

The next steps in developing predictive models for formulating 3D printable recipes would involve relating the rheological parameters to food composition. Furthermore, composition can be related to nutritional content as well as sensory properties.

## **Chapter 5. 3D printing of hydrocolloids and texture modified food**

This chapter addresses the third objective of my work, determining suitable 3D printer settings for good print object quality. Printing experiments included extrusion tests as well as line and cylinder printing experiments. The experiments determine appropriate printer settings including extrusion lag time, extrusion rate, nozzle speed, layer height, and infill level for the ink type. I would like to state the contributions of Madhu Sharma for conducting the rheological experiments presented in this chapter. This chapter was written as a manuscript intended for submission to publication in the *Journal of Food Engineering*.

### **5.1. Introduction**

3D printing has the potential to transform the landscape of the manufacturing industry. This technology could provide on-demand low volume products and a great degree of customization. Instead of using molds and dies, objects with complex geometry can be fabricated by a 3D printer in a layer-by-layer fashion. Furthermore, the object can be directly generated from a computer created design. In terms of foods, 3D printing offers the ability to achieve personalized nutrition and customizable design (Sun et al., 2015a).

Food can be 3D printed either by fusing loose powders such as spice and sugar with a binder or through extrusion deposition (Sun et al., 2015a). Extrusion-based 3D printing is more versatile and can handle a wide variety of food. They range from confectionary items such as chocolate (Hao et al., 2010; Lanaro et al., 2017) and cookies (Vancauwenberghe et al., 2017a) to foods such as rice (Tanaka et al., 2015), mashed potato (Liu et al., 2017), turkey and scallop purée (Lipton et al., 2010), fish gel (L. Wang et al., 2017) to novelty foods like insect flour (Severini and Derossi, 2016; Soares and Forkes, 2014) and self-folding pasta (W. Wang et al., 2017). These types of food products are suitable because they can be extruded and can maintain their shapes after deposition.

Approaches to characterizing the quality of the printed object have relied predominantly on visual observation of the printed object with simple geometry such as a cube, pyramid, or lattice. A few methods have been proposed for quantifying the quality of the object of such as line diameters for given printer settings (Hao et al., 2010; Lanaro et al., 2017; L. Wang et al., 2017). Ouyang et al (2016) proposed a method based on image analysis of the pore shapes in a lattice design of alginate and gelatin inks where the circularity of the pore would reflect spreading. A gel that spreads more would have circular pore as opposed to a gel with less spreading which would possess square pores (Ouyang et al., 2016).



When considering food products for personalized nutrition and 3D printing extrusion deposition operations, textured foods products such as those foods for people with chewing or swallowing difficulties have attracted attention. This application, which consists in shaping puréed foods with defined texture attributes, has been discussed in several recent reviews (Aguilera and Park, 2016; Lipton, 2017; Sun et al., 2017; Tian et al., 2016). The use of 3D printing for improving the aesthetics of puréed foods was recently addressed for pumpkin, beet, and fish purée foods (Kouzani et al., 2017). The ability to produce a broad variety of personalised meals and food products for the elderly using 3D printing technology was the focus of the EU funded PERFORMANCE project (Kück, 2015).

Most studies on 3D printing extrusion deposition are trial and error experimentation with different types of food inks and recipes. This trial-and-error approach does not transfer easily to new ink formulations or different types of inks where additional testing would be required. There is need to develop a method that possesses predictability power to assist with development of ink formulation. Such method could be developed from the rheological properties of the food ink. Hydrocolloids can be used to simulate a range of food textures. Different ratios of xanthan gum and gelatin are used to create cubes with different texture and mouthfeel (Vesco et al., 2009). Recent studies have used pectin (Vancauwenberghe et al., 2017b) and methyl cellulose (Kim et al., 2017) to study 3D printing extrusion system and the microstructure, texture, and dimensional stability of the printed object.

This study aims to determine the range of rheological parameters for an ink and 3D printer settings for achieving suitable object geometry. Modified starch (MS) and xanthan gum (XG) were used to create inks with different consistency and study relationships between ink rheology and 3D printer settings. Selected XG and MS pastes also served as reference for evaluating the 3D printing of modified carrot purée as ink.

## **5.2. Material and methods**

### **5.2.1. Materials and paste preparation**

Modified corn starch (MS) (Uni-Pure® D2560, Ingredion) and xanthan gum (XG) (Duinkerken Foods, Canada) and deionized water were first mixed with a spoon. Once a paste was formed, blue food coloring (McCormick Canada) was added and the mixture was blended with a food processor (BlenderPro) for 2 min. Three concentrations of MS (10, 15, 20% w/w) and XG (5, 7.5, 10% w/w) were prepared. The concentration were selected so the paste could be extruded and hold its shape after deposition.

Carrots were purchased from local supermarket (Waterloo, Ontario) and prepared according to methods described in (Sharma et al., 2017). Briefly summarized, carrots were cubed and cooked in a food steamer before being puréed in a food processor with modified starch or xanthan gum. Unmodified carrot purée,

purée with 2% w/w MS, and purée with 1.2% w/w XG were prepared. The XG and MS concentrations were selected from study by (Sharma et al., 2017). All samples were stored at 4 °C and warmed up to room temperature prior to 3D printing.

### **5.2.2. Rheology measurement**

Viscoelasticity of the modified starch and xanthan gum pastes were obtained with Paar Physica MCR-301 rheometer (Anton Paar GmbH, Germany) operated at 25 °C. Parallel plates with a diameter of 50 mm and gap distance of 2 mm were used. Shear stress ramp was conducted from 1 to 1000 Pa at frequency of 1 Hz to determine the yield stress. The yield stresses of the pastes was estimated using a method recently proposed in literature (Cyriac et al., 2015). Briefly, oscillatory strain was plotted against shear stress and the point where the curve starts to deviate from linearity was determined as the yield stress. Each analysis was conducted in triplicates.

### **5.2.3. Food texture**

The food texture measurements were based on the methods describes in the International Dysphagia Diet Standardisation Initiative (IDDSI) (Cichero et al., 2017). The IDDSI framework group thickened liquids and texture-modified food into levels from 0 to 7 according to consistency and texture. Specifically, level 4 (puréed/extremely thick) and 5 (minced and moist) are of interest for 3D printing applications since these classes are described as food that can be layered, molded, or shaped.

The texture measurements were conducted with fork and spoon. A standard stainless steel dinner fork with four prongs and 4 mm gaps was used for the fork drip test. One tablespoon (approximately 15 mL) of sample was placed on top of the fork. For the spoon tilt test a standard stainless steel dinner spoon was used. After placing the sample on the spoon, the spoon was turned sideways and lightly tapped. Photographs were taken and the results were compared visually with focus on shape retention, dripping through fork prongs, and amount of residue left the on the tilted spoon.

### **5.2.4. 3D printing**

#### ***5.2.4.1. 3D Printer and extruder***

A desktop 3D printer (Rostock Max V2, SeeMeCNC) and a stepper motor driven paste extruder (Discov3ry, Structur3D Printing) were used for all printing experiments. The printer was controlled by an open-source slicer called MatterControl (MatterHackers). A syringe with a 1.54 mm polypropylene diameter nozzle was used. The nozzle height was set to equal the nozzle diameter unless stated otherwise. All experiments were conducted at constant stepper motor speed of 48 RPM. The nozzle speed was adjusted for each test. All 3D printing tests were conducted at room temperature.

#### 5.2.4.2. Extrusion test

The amount of material exiting the nozzle were recorded over a period of 10 minutes at 48 RPM stepper motor speed to investigate changes in extrusion rate over time. The data were fitted to a Weibull distribution function (Equation 5-1). While this equation has been traditionally used to model fungal microbial growth (Peleg and Normand, 2013), it was recently used to model the changes in height of a 3D printed object over time (Derossi et al., 2017).

$$M(t) = M_{\infty}[1 - \exp(-kt^n)] \quad \text{Equation 5-1}$$

$M(t)$  is the extrusion rate at time  $t$  and  $M_{\infty}$  is the extrusion rate at the plateau (g/min). The constants  $k$  ( $s^{-1}$ ) and  $n$  (dimensionless) provide a measure of the steepness and the width of the extrusion rate according to time (Peleg and Normand, 2013).

The steady state extrusion rate was calculated from the plateau value. The extrusion lag time was calculated as the time required for the extrusion rate to reach 90% of the steady state extrusion rate according to Equation 5-2.

$$t_{lag} = \left( \frac{\ln 0.1}{-k} \right)^{1/n} \quad \text{Equation 5-2}$$

#### 5.2.4.3. Line printing tests

Straight lines were printed and photographed to evaluate print accuracy based on the diameter of the printed line, i.e. its circularity. If a line displayed significant spread, the diameter would not have a circular cross-section and could be captured by elliptical dimensions, height and width. Nozzle speeds, ranging from 2 to 10 mm/s, were used at 48 RPM stepper motor speed. Image analysis software ImageJ (National Institutes of Health) was used to estimate the diameter of the printed line.

Assuming that the diameter of the printed line is controlled by the nozzle speed and the extrusion rate, one can obtain a theoretical line diameter by considering a given volumetric extrusion rate and an elliptical cross-section of the line:

$$\frac{Q}{v} = A = \frac{\pi ab}{4} \quad \text{Equation 5-3}$$

Where  $Q$  is the volumetric extrusion rate ( $\text{mm}^3/\text{s}$ ),  $v$  is the nozzle speed (mm/s), and  $a$  and  $b$  are the width and height of an elliptical cross-section (mm), respectively. The aspect ratio  $c$  is defined as the height over width ( $c = b/a$ ). If the cross-section is a circle then  $c = 1$ , but if there is spreading of the line,  $c < 1$ .

Equation 5-3 can be rearranged to estimate the line width  $a$  as function of  $Q$  and  $v$  (Equation 5-4).

$$a = \sqrt{\frac{4}{\pi c}} \sqrt{\frac{Q}{v}} \quad \text{Equation 5-4}$$

Linear regression was performed to determine the value of  $c$  for each type of ink.

#### **5.2.4.4. Cylinder printing tests**

The ability of an ink to produce an object which can hold its shape was obtained by printing cylinders with different infill levels. A cylinder, 20 mm in diameter and 40 mm in height, was generated using the slicer program MatterControl (MatterHackers). Three different infill levels (0, 25, and 50%) were used. Infill level represents the amount of internal structure. A cylinder with 0% infill is hollow whereas a cylinder with 100% infill is solid. Video of the cylinder printing process was captured with a digital camera. A snapshot was taken before the cylinder collapsed and the height of the cylinder was deduced from image analysis using ImageJ.

## 5.3. Results and discussion

### 5.3.1. Rheology of starch and xanthan gum pastes

Inks suitable for 3D printing should be easy to extrude through the nozzle and cohesive enough to hold its shape after deposition. The ease of extrusion and the structural stability of the shaped object are related to the rheology of the ink, the storage modulus and the yield stress. Two hydrocolloid pastes, xanthan gum (XG) and modified starch (MS), were selected as model ink to understand the relationship between their rheological characteristics and their 3D printability window. These pastes can display a wide range of rheological behaviors by adjusting their concentration.

When the ink experiences mechanical deformation, its elastic and viscous responses are represented by its storage modulus ( $G'$ ) and the loss modulus ( $G''$ ), respectively.  $G'$  represents the amount of the energy stored during shearing and can serve as an indicator of the material's stiffness (Steffe, 1996). In contrast,  $G''$  represents the amount of energy dissipated due to the ink flowing. An ink suitable for 3D printing should possess high  $G'$  to provide shape retention. Stiffer material can build more geometrically complex structures with overhangs and bridges without collapse. Furthermore, a suitable ink should possess low  $G''$  to prevent spreading but if it's too low the ink may fracture instead of flows during the extrusion process.

The yield stress is defined as the point where the internal structure of the ink starts to break down (Steffe, 1996). In other words, the ink goes from behaving like an elastic solid to flowing like a fluid. An ink suitable for 3D printing should possess a yield stress low enough to ensure adequate extrusion but not too low to avoid spreading of the printed object under its own weight.

The concentration of XG and MS pastes suitable for 3D printing with the Discov3ry extruder system was identified from the printing of a 20 x 20 x 10 mm solid cube without the base spreading more than 2 mm.

$G'$  and  $G''$  as function of shear stress obtained from oscillatory stress sweep and are shown in Figure 16.

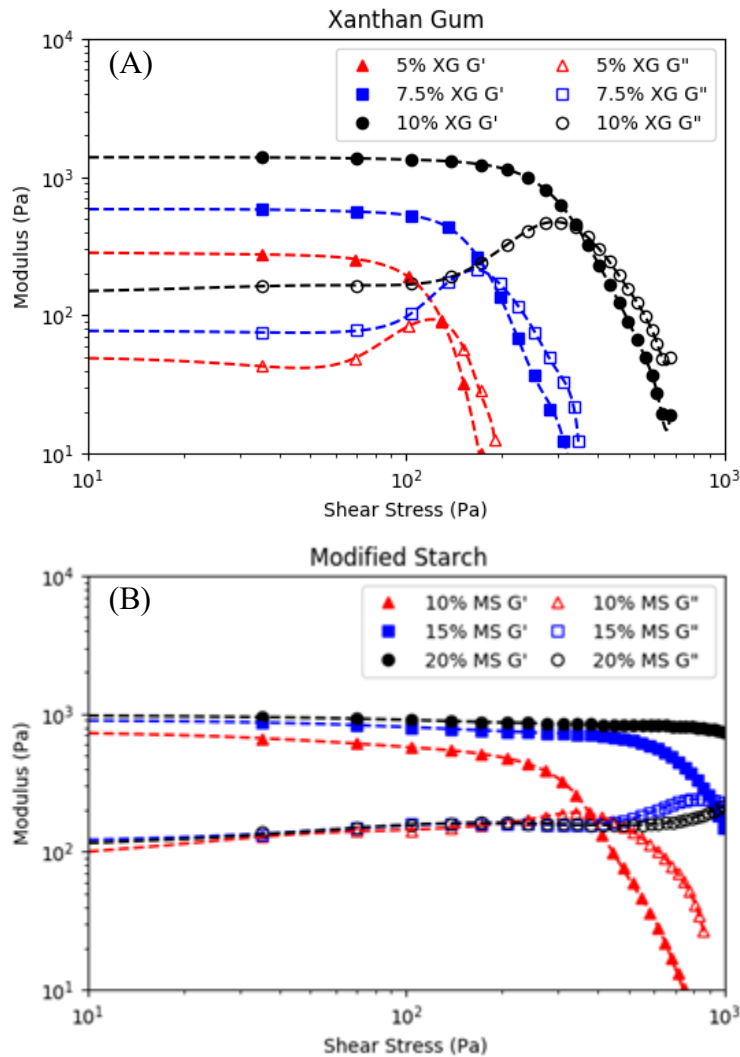


Figure 16 Oscillatory stress sweep for (A) xanthan gum (XG) and (B) modified starch (MS) pastes. Each data point is the average of three measurements and the dotted lines are the fitted cubic spline functions

At low shear stress,  $G'$  is higher than  $G''$  for all pastes which indicates a predominantly elastic response. Within the linear viscoelastic region (LVR),  $G'$  and  $G''$  remained relatively constant. As shear stress increased,  $G'$  decreased indicating a breakdown of the internal structure of the material. For all XG pastes,  $G''$  showed a slight increase before crossover with  $G'$  (Figure 16A). Such strain-overshoot phenomena has been reported for concentrated XG solutions (Hyun et al., 2002; Song et al., 2006). For MS pastes, strain-overshoot was observed at 15% and 20%. Above the cross-over stress,  $G''$  exceeded  $G'$  which indicates the transition from predominantly solid to liquid.

The degree of viscoelasticity of the material was obtained from the loss tangent ( $\tan \delta$ ), defined as the ratio of  $G''$  to  $G'$ . The XG and MS pastes investigated in this study have  $\tan \delta$  ranged from 0.1-0.2 within the LVR and can be classified as weak gels (Dolz et al., 2006; Vancauwenberghe et al., 2017b). Recent

study on extrusion-based 3D printing indicates that inks with  $\tan \delta < 0.1$  may be harder to extrude and produce broken lines due to poor fluidity (Liu et al., 2017; L. Wang et al., 2017). Broken lines were not observed in the case of XG and MS pastes since their  $\tan \delta$  was higher than 0.1.

Table 14 Oscillatory stress sweep (1-1000 Pa) at 25 C for XG and MS pastes.  $G'$  and  $G''$  are values within LVR. Results reported as average  $\pm$  standard deviation. (N = 3).

Material	Yield Stress (Pa)	$G'$ (Pa)	$G''$ (Pa)
5% XG	62 $\pm$ 4	283 $\pm$ 17	47 $\pm$ 9
7.5% XG	78 $\pm$ 13	572 $\pm$ 29	80 $\pm$ 9
10% XG	169 $\pm$ 11	1350 $\pm$ 146	175 $\pm$ 28
10% MS	141 $\pm$ 8	755 $\pm$ 7	82 $\pm$ 4
15% MS	446 $\pm$ 63	899 $\pm$ 119	138 $\pm$ 31
20% MS	730 $\pm$ 116	925 $\pm$ 102	140 $\pm$ 21

The yield stress,  $G'$  and  $G''$  (Table 14) showed distinct characteristics according to the type of paste. For XG pastes, the yield stress ranged from 62 to 169 Pa which was lower than all the MS pastes. For MS pastes  $G'$  were similar for all concentrations. There is a linear relationship between the yield stress and XG concentration where every 5% increase in concentration resulted in 300 Pa increase in yield stress. The 10% XG and 10% MS paste were unique in that their yield stresses were similar while their  $G'$  was significantly different with  $G'$  for XG twice that of MS.

Based on the above rheology characteristics, the minimum yield stress was around 60 Pa and its maximum around 730 Pa. These yield stress estimates are in the same range as those reported in recent studies investigating the suitability of food inks for 3D printing extrusion deposition, namely 312-370 Pa for mashed potatoes (Liu et al., 2017) and 419 to 1419 Pa for vegemite and marmite (Hamilton et al., 2017). However, caution should be exercised when comparing yield stress data. The published data were obtained from viscosity data while oscillatory rheology was used in the current study. The yield point measured with oscillatory measurements is the static yield stress whereas the yield stress obtained from flow curves is the dynamic yield stress (Steffe, 1996). Static yield stress is generally higher than dynamic yield stress since the shear stress required to initiate flow is higher than the shear stress required to maintain flow at low shear rates (Moelants et al., 2013).

Based on the yield stress and  $G'$  characteristics, the 5% XG (5XG), 10% starch (10MS), and 15% starch (15MS) were selected to represent model foods with low, medium, and high yield stress and  $G'$  characteristics for assessing their printability of an object.

### **5.3.2. Texture measurement**

Texture modified food products for dysphagia often lose their shape and have limited visual appeal which may affect the intake of these foods ultimately leading to reduce nutrient intake and poor health conditions. 3D printing could provide shape to these texture modified food products and ultimately improve nutrient intake.

Not all texture modified foods will be suitable for 3D printing extrusion deposition. Only those foods that can be extruded and cohesive enough to hold their shape after extrusion will be suitable.

With this in mind, the IDDSI framework and methodology were used to assess and classify potential ink candidates for 3D printing. The IDDSI methodology consisted of the fork drip test and the tilt spoon test where the behavior of an amount of food is visually characterized. The spoon tilt test was used as a measure of the adhesiveness of the paste where an ink with high adhesiveness would be more resistant to flow and may require higher extrusion force. The ideal texture for safe swallowing should be cohesive and slippery (Cichero, 2016). Once tilted the sample should slide off spoon with minimal residue.

Level 3 (thickened liquids) represents materials that will continuously drip through the prongs of the fork which will not be suitable for 3D printing besides single layer designs. Level 4 (purée) represents materials that may flatten out and form a small tail through the prongs without flowing through. Level 5 (minced and moist) represents materials where the pile will retain its shape while sitting on top of the fork. Level 4 and 5 are likely suitable for 3D printing.



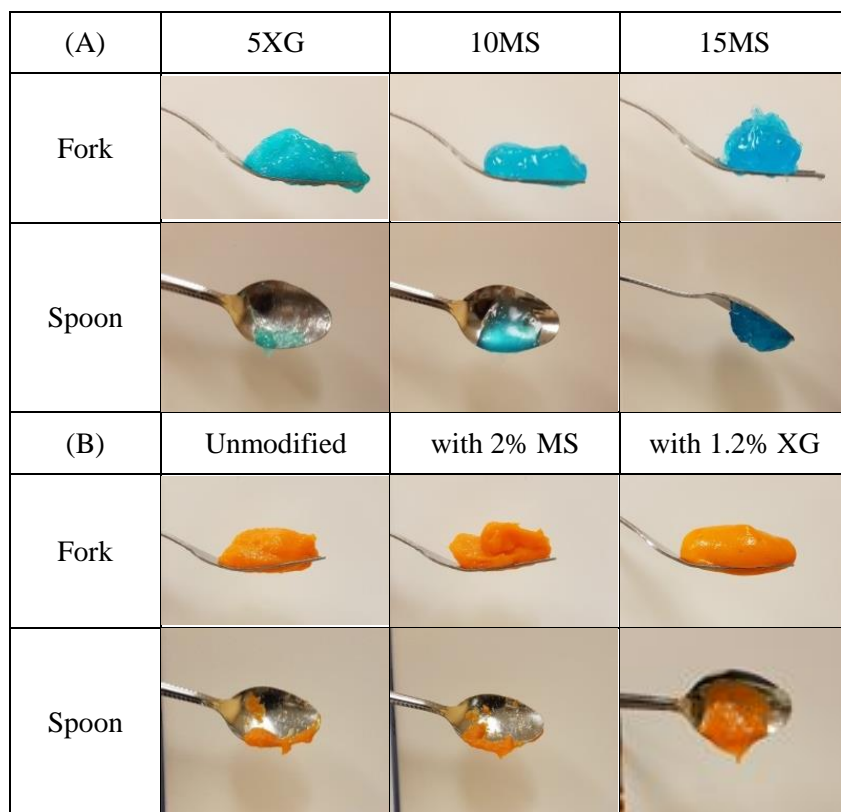


Figure 17 Results of fork drip and spoon tilt test based on IDDSI for (A) XG and MS pastes and (B) carrot purée.

As illustrated in Figure 17, all XG and MS pastes and carrot purée remained on top of the fork without dripping. The behavior of the XG and MS pastes agreed with their yield stress and  $G'$  characteristics. The 15MS paste which had the highest yield stress and  $G'$ , retained its shape without spreading when placed on the fork while the 10MS and 5XG pastes spread out into a pile. The 5XG paste, which had the lowest yield stress and  $G'$ , showed a slight tail forming below the fork. The carrot purée with 1.2% XG and without XG behaved similarly to the 5XG. In contrast, the carrot purée with 2% MS retained its shape and behaved as the 15MS paste.

The residual amount of food remaining on the spoon was used as an indicator of the adhesiveness of the material. The 5XG and 10MS were able to slide off the spoon. The 5XG slipped off easily while there was some residue left on the spoon for the 10MS. In contrast, the 15MS was quite adhesive and did not fall off spoon even when inverted. For the carrot purée without and with 2% MS, the residue remaining on the spoon was similar to the 5XG whereas the carrot purée with 1.2% XG behaved as the 10MS. A recent study on thickened carrot purée show that sensory adhesiveness has strong negative correlation to yield point (Sharma et al., 2017). A similar correlation was observed in this study for the 5XG paste with the lowest yield stress showed the lowest adhesiveness from the spoon tilt test.

### 5.3.3. 3D Printing test

3D printing tests were performed with 5XG, 10MS, 15MS, carrot purée without hydrocolloid, carrot purée with 2% MS, and carrot purée with 1.2% XG. The purpose of the tests was to assess and relate the printability of an object to the rheological characteristics of the ink. Printability of an object was obtained from measured extrusion rate, the spreading of a printed line, and the height prior to collapse of a cylinder with different infill levels.

#### 5.3.3.1. Extrusion test as measure of extrusion rate and lag time

The evolution with time of the extrusion rate, defined as mass of ink exiting the nozzle per unit time, was used to understand the time required to reach constant extrusion rate and consequently uniform printing.

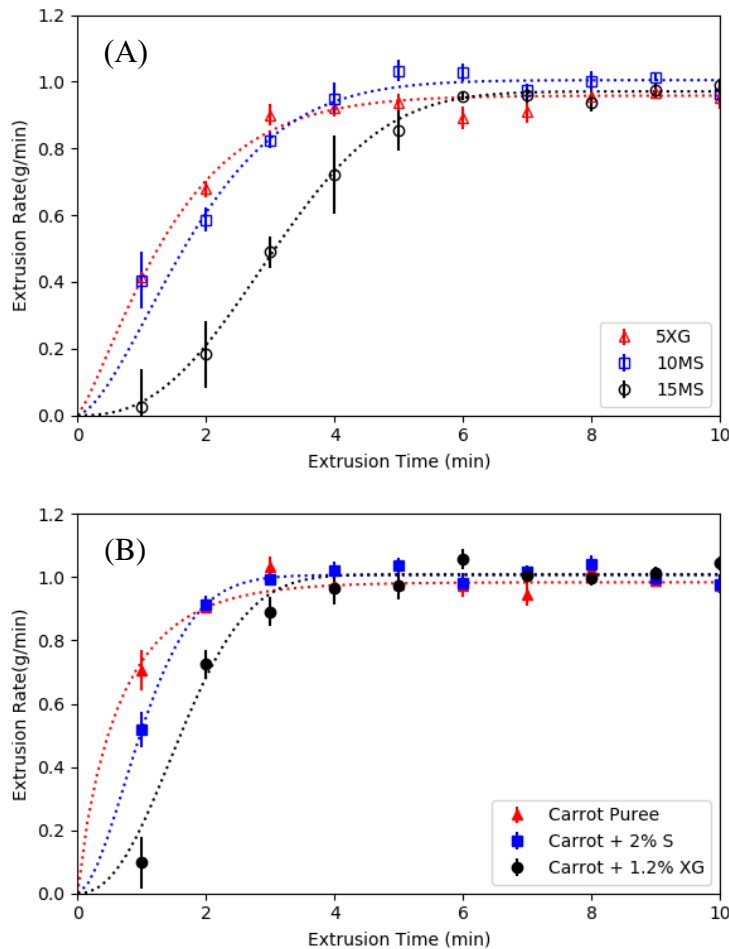


Figure 18 Extrusion rate over time for (A) and carrot purée samples (B). Each point represents the average of 3 measurements with standard deviation represented as error bars

Similar extrusion rate profile with time was observed for all inks with an initial increase before reaching a similar plateau value (Figure 18). The extrusion rate at steady state was approximately 1 g/min for all inks. The carrot purée inks reached the plateau faster than the XG and MS pastes.

The extrusion rate profiles were fitted to Equation 5-1 with  $R^2$  values ranged from 0.88 to 0.99 (Table 15). The parameters  $M_\infty$  were similar for all inks. The parameter  $k$  decreased while  $n$  increased as concentration increased. The lag time (estimated with Equation 5-2 and reported in Table 15) which reflects the time required to reach steady state, could be related to the yield stress of the XG and MS pastes. The 5XG with a low yield stress of 62 Pa reached steady state after 3 minutes. In comparison, the 15MS with a yield stress of about 450 Pa needed 5 minutes to reach steady state. The 10MS which has an intermediate yield stress value, 144 Pa, reached steady state in 3.6 minutes. Since the carrot purée inks reached steady state in about 2 minutes, one can suspect that their yield stress is lower than that of the 5XG. In a recent study, the yield stress for carrot purée with added hydrocolloids is reported to be around 20 Pa (Sharma et al., 2017).

Table 15 Parameters obtained when fitting extrusion rates to Equation 5-1 for XG and MS pastes and carrot purée. Extrusion lag time ( $t_{lag}$ ) calculated with Equation 5-2

Parameters	Reference Hydrocolloids			Carrot Purée		
	5XG	10MS	15MS	Unmodified	2% MS	1.2% XG
$M_\infty$ (g/min)	0.96	1.00	0.97	0.98	1.01	1.01
$k$	0.56	0.31	0.04	1.37	0.72	0.24
$n$	1.25	1.57	2.52	0.87	1.72	2.25
$t_{lag}$ (min)	3.1	3.6	5.0	1.8	2.0	2.7
$R^2$	0.97	0.94	0.99	0.88	0.98	0.97

### 5.3.3.2. Line printing as measure of print quality

Print quality is directly related to the extrusion conditions, namely extrusion rate, nozzle speed, and nozzle diameter. Previous studies have related extrusion rate and nozzle speed by matching the line diameter to the nozzle diameter (Hao et al., 2010; Yang et al., 2018). In this study, we have investigated the print quality and spreading of lines. Line spreading should give a better measure of the print quality as not all applications will require that there is no spreading (i.e. the diameter of the printed line is exactly that of the nozzle diameter). Printed lines as a zigzag pattern were produced for different combinations of extrusion rate ( $Q$ ) and nozzle speed ( $v$ ). The width of the line was measured and related to  $Q$  and  $v$  using Equation 5-4 (Figure 19).

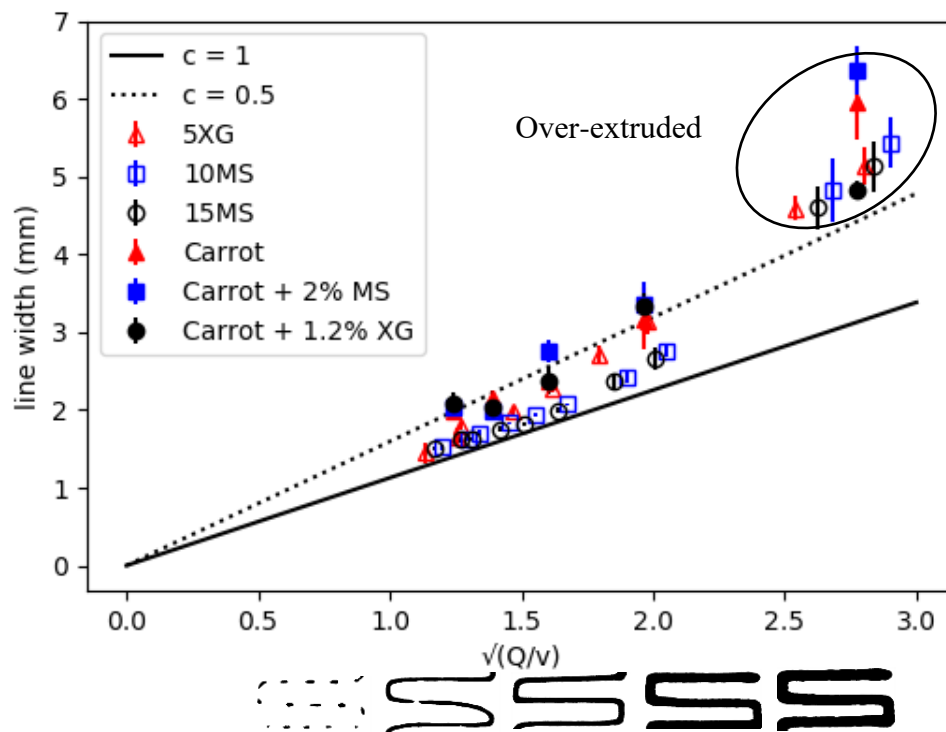


Figure 19 Line width as a function of extrusion rate ( $Q$ ) and nozzle speed ( $v$ ) for a syringe with a 1.54 mm diameter nozzle. Images represent typical printed lines at each condition. The solid line ( $c = 1$ ) represents the aspect ratio of a line with a circular cross-section. The dotted line ( $c = 0.5$ ) represents aspect ratio for a line with an elliptical cross-section (height is half the width of the line). Each point represents the average of 6 measurements with standard deviation represented as error bars.

At  $\sqrt{(Q/v)} < 1$ , discontinuous lines were produced. The pressure supplied by the extruder was insufficient to push adequate amount of material and keep up with the nozzle speed. In contrast, when  $\sqrt{(Q/v)} > 2.5$ , the nozzle speed was not sufficient to handle all the material pushed by the extruder and over extrusion was observed (Figure 19). For over-extrusion conditions, the printed lines were flattened by the nozzle tip dragging through them and were no longer elliptical in cross-sectional area.

At  $\sqrt{(Q/v)}$  around 1, the corners are rounded. Slight under extrusion may not have the same obvious effect as discontinuous lines but sharp angles in design will be rounded out due to printed line being dragged around (Figure 19). In order to ensure that sharp angles can be 3D printed, the line width should be slightly higher than the nozzle diameter for proper adhesion between layers. By considering a desired line width to be 2 mm (130% of the nozzle diameter), the  $\sqrt{(Q/v)}$  should be 1.2 to 1.6.

In addition to measuring print quality from line width, line spreading measured from the aspect ratio ( $c$ ) was investigated. An aspect ratio of 1 and 0.5 are represented in Figure 19 as solid and dotted lines, respectively. Spreading may occur due to gravity or weight of subsequent layers on top. Inks with low yield stress and  $G'$  should be more prone to spreading. Linear regression was performed on data points within printable range (excluding over-extrusion data points) to obtain the aspect ratio according to Equation 5-4 (Table 16).

Table 16 Aspect ratios ( $c$ ) for XG and MS pastes and carrot purée obtained from linear regression of the line widths for  $\sqrt{(Q/v)}$  from 1 to 2.5.

Material	5XG	10MS	15MS	Carrot purée	Carrot + 2% MS	Carrot + 1.2% XG
$c$	0.61	0.78	0.80	0.52	0.47	0.50
$R^2$	0.92	0.98	0.97	0.96	0.90	0.89

The XG and MS pastes spread less compared to the carrot purée inks. For the 5XG paste spread the most with a  $c$  of 0.6 and the 15MS paste spread the least with a  $c$  of 0.8. The carrot purée inks all have  $c$  around 0.5 and showed no noticeable differences. If the design of the printed object had fine details, the nozzle size should be equal or smaller than the desired resolution multiplied by the material's  $c$  value.

### 5.3.3.3. Cylinder printing quality

The quality of the 3D characteristics of the printed products was obtained by printing a cylinder with different infill level and estimating the height of the cylinder prior to its collapse. This information provided a measure of the shape retention of the ink once printed into a 3D object. Potential relationships with the rheological characteristics of the ink were investigated. The operating parameters of the 3D printing system were selected based on the investigation reported in the previous section. For a stepper motor speed of 48 RPM, the nozzle speed was calculated as 8 mm/s (i.e.  $\sqrt{(Q/v)} = 1.5$ ) and the estimated layer height as 1 mm for the 1.54 mm nozzle diameter assuming  $c = 0.65$ .

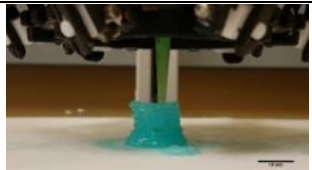
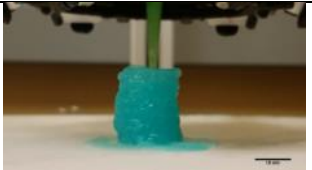
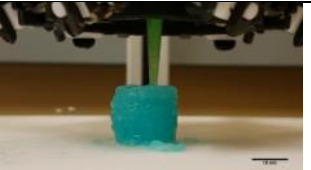
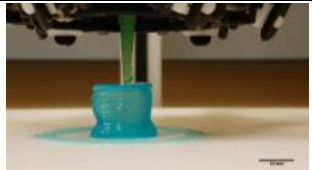
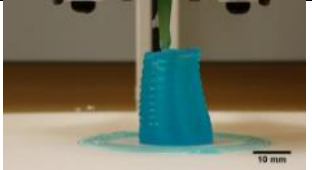
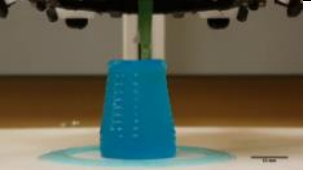

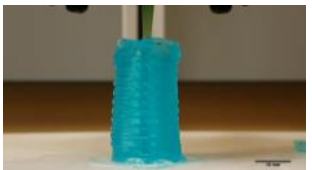
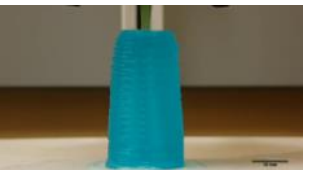
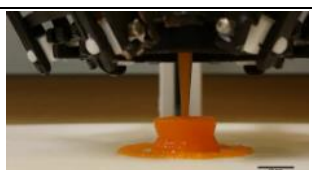
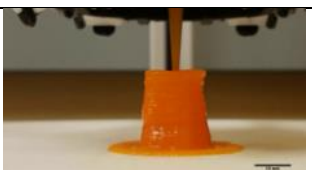
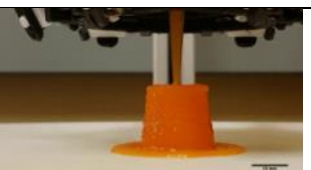

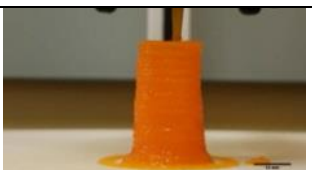

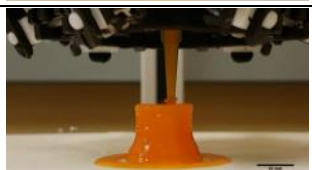

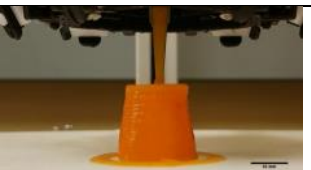
Inks	Infill		
	0%	25%	50%
5XG			
10MS			
15MS			
Carrot Purée			
Carrot + 2% MS			
Carrot + 1.2% XG			

Figure 20 Images of cylinder printing experiments for XG and MS pastes and carrot purée at three infill levels

The maximum height of the cylinder prior to collapse was obtained from the analysis of snapshots of the printed cylinder over time (Figure 20). During the printing process the cylinder is subjected to stress from gravity, subsequent layers, and the moving print head. There will be a time and height at which an additional layer can no longer be supported by the existing cylinder. At this point the cylinder will collapse. Three modes of collapse were observed in the cylinder printing process

The first type of collapse was bottom spreading. The lower layers of the cylinder deform under gravity and excessive weight. Such collapse was observed for cylinders with unmodified carrot purée and with 1.2% XG. In this case the material itself was not rigid enough so only flat designs can be printed. The second type of collapse was when the walls of the cylinder fold inwards. Such collapse was observed for cylinders with 0% infill and the 5XG and 10MS ink where the bottom portion started to pinch indicating a lack of internal support. The third type of collapse was when the printed object fell sideways which was observed for 15MS as well as for the carrot purée with 2% MS. The object usually collapsed due to the movement of the nozzle. One solution would be to lower the nozzle speed and avoid crossing over printed areas.

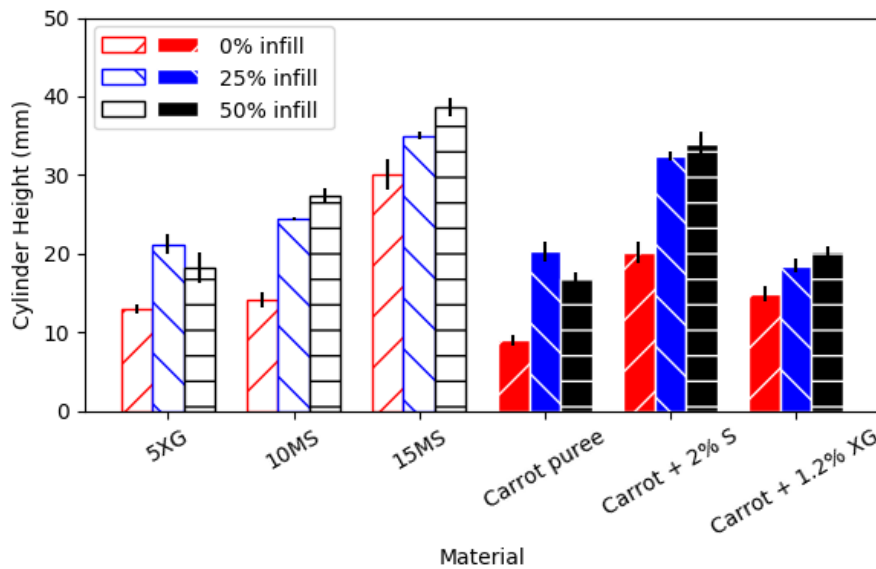


Figure 21 Height of printed cylinders before collapse at three infill levels. Each column represents the average with standard deviation represented as error bars (N =3).

The height of the cylinder prior to collapse estimated by image analysis is presented in Figure 21. Overall the unmodified carrot purée had the lowest cylinder height at all infill levels and the 15MS had the highest cylinder height. The cylinder height of unmodified carrot purée and purée with 1.2% XG were similarly to 5XG. The bottom layers started to spread out after the cylinder reached around 15 mm. Both 15MS and carrot purée with 2% starch produced the tallest cylinders. These two inks also held their shape

the best in the fork drip test. The 15MS ink had high adhesiveness and an extrusion lag time of 5 minutes. In contrast, the carrot purée with 2% starch showed low adhesiveness and a shorter lag time (2 minutes).

Using paired student's t-test with  $\alpha = 0.01$ , the differences in cylinder heights between 0% and 25% infills as well as 0% and 50% infills were significant except for the 15MS ink. There was no statistically significant difference between 25% and 50% infill. This suggests that having some internal support prevented the cylinder from folding inwards; however, further increasing infill did not provide significantly more support where total print time increased from 9 to 12 minutes. Long print time may pose a food safety hazard due to microbial growth. A cooking step afterwards or refrigerated printing chamber may be required for printing large objects.

The inks that were able to print the tallest cylinder without collapse had high  $G'$  ( $>900$  Pa). Carrot purée with 2% MS was sufficiently stiff but had low yield stress evident by its short extrusion lag time. The  $G'$  of the inks within LVR was a better predictor of maximum cylinder height than its yield stress.

## 5.4. Conclusions

Extrusion-based 3D printing was evaluated with modified starch (MS) and xanthan gum (XG) pastes as well as carrot purée. IDDSI tests with fork and spoon, originally designed to evaluate texture-modified foods used in dysphagia management, were useful tools in evaluating the 3D printability of the inks. The yield stress for a printable paste ranged from 60 to 730 Pa and its  $G'$  ranged from 300 to 900 Pa.

For a stepper motor driven extruder, there is typically a lag time anywhere from 2 to 5 minutes at the start of the printing process. The lag time was correlated with the yield stress and the adhesiveness of the ink as measured by the spoon test. The higher the yield stress and adhesiveness, the longer the time required for the material to reach steady state extrusion rate. The optimal 3D printer settings were determined from line printing tests. Volume conservation was used to estimate the width of a printed line as a function of the ratio of extrusion rate over nozzle speed. Objects with sharp angles can be 3D printed when the line diameter is 130% of the nozzle diameter. Slightly thicker lines ensure proper layer adhesion without compromising print accuracy. The spreading of the ink was obtained by assuming an elliptical cross-section of the line. Cylinder printing tests were used to estimate the maximum height and the height prior to collapse was found to be related to  $G'$ . The paste with  $G'$  of around 300 Pa could only print cylinder up to 20 mm prior to collapse whereas paste with  $G'$  around 900 Pa could print cylinder with twice the height. The approach developed in this study could be extended to the characterization of 3D printers and other paste-like inks including ceramics, elastomers, and cells.



## **Chapter 6. Conclusions and recommendations**

### **6.1. Conclusions**

3D printing food can offer several significant advantages over traditional food preparation process. It can automate the cooking process to save time, produce meals on-demand to minimize food waste, and customize nutritional content. One potential application is to 3D print food for those suffering from dysphagia, a condition that makes it difficult to swallow. Texture modified food products for dysphagia often lose their shape and have limited visual appeal which may affect the intake of these foods ultimately leading to reduce nutrient intake and poor health conditions. 3D printing could provide shape to these texture modified food products and ultimately improve nutrient intake. One of the limitations currently preventing wide adaption of this technology is the lack of understanding of the effect of food properties on the 3D printing process. The work presented in this thesis considered room temperature extrusion-based 3D printing with a desktop 3D printer and a syringe extrusion system and rheological characterization of food inks to assess their suitability.

The first objective of this work was to understand how desktop 3D printer could be adopted for paste extrusion. The slicer settings (filament diameter, layer height, and extruder steps per mm) were first investigated by incrementally adjusting individual setting and measuring their effects on the printing process. Afterwards, the machine command (G-code) was investigated to understand the effect of the slicer settings on the extrusion rate and the nozzle speed. The nozzle speed could be controlled by the extrusion multiplier while the extrusion rate could be controlled by the stepper motor speed provided that the nozzle diameter, filament diameter, layer height, print speed remained constant. The predicted extrusion rate and nozzle speed were assessed by conducting printing experiments. Extrusion tests showed that 2-5 minutes were required before stable extrusion rate was achieved. The extrusion lag time increased with increased yield stress of the ink and decreased with increased motor speed.

The second objective focused on the ink properties. The suitable textures and rheology characteristics for a 3D printable ink were investigated with xanthan gum (XG) and modified starch (MS) pastes and compared to other food systems. Food texture measurements based on the methods described in the International Dysphagia Diet Standardisation Initiative (IDDSI) were conducted with fork and spoon. All XG and MS pastes could sit on top the fork without dripping indicative of IDDSI purée level consistency. The 5% XG paste slide off the spoon with minimum residue indicating low adhesiveness while the 15% MS paste did not fall off spoon even when inverted indicating high adhesiveness. Oscillatory rheology provided insight on the response of the inks to deformation. A 3D printable ink should be extrudable and produce an object that holds its shape. The rheological characteristics that allowed for an ink to be

extruded were identified as yield stress between 60-730 Pa and  $\tan \delta$  between 0.1-0.2. Frequency sweep results of XG and MS pastes were analyzed with the weak gel model and compared to published data. In the weak gel model, the complex modulus ( $G^*$ ) is expressed in terms of the constant ( $A_f$ ) representing the network strength and the exponent ( $z$ ) represents frequency dependency or the degree of viscoelasticity. XG and MS pastes having  $A_f$  from 320 to 1200 Pa s<sup>1/2</sup> and  $z$  between 11 and 14 and are suitable for 3D printing since they are extrudable and retain their shape after deposition. In comparison, puréed carrot has higher  $A_f$  but lower  $z$ . Puréed carrot was suitable for 3D printing because it has higher stiffness despite its low elasticity. However, the current extruder was unable to handle food such as cookie dough with  $A_f > 2 \times 10^5$  Pa s<sup>1/2</sup>.

The third and final objective of this work focused on the shape of printed objects with simple geometry, lines, lattices, and cylinders using XG and MS pastes and carrot purée as ink. Quantitative evaluation was obtained by image analysis. Line printing tests were used to identify the combination of volumetric extrusion rate, nozzle speed, and spreading of the ink after deposition. Continuous lines and sharp angles were 3D printed when the line diameter was 130% of the nozzle diameter. Slightly thicker line diameters ensure proper layer adhesion without compromising print accuracy. The aspect ratio ( $c$ ), calculated as ratio between the height and diameter of the printed line, was used to assess spreading of a printed object. The 5% XG paste displayed the most spreading ( $c = 0.6$ ) and the 15% MS paste displayed the least spreading ( $c = 0.8$ ). All puréed carrot had similar spreading ( $c = 0.5$ ). Cylinder printing was conducted to find the maximum built height for different inks and infill level, representing the fraction of the interior of the object to be filled with material when printed. Cylinders 20 mm in diameter and 40 mm in height at 0, 25, and 50% infill were printed. From the cylinder printing experiments, ink with  $G'$  around 300 Pa produces cylinder up to its diameter before collapse whereas the ink with  $G'$  around 900 Pa could print cylinder up to twice its diameter. Increasing infill levels provided additional internal support but subjected the print to more stress due to nozzle movement.

## **6.2. Recommendations for future work**

Based on the work completed in this thesis, the following work is proposed as next steps:

On the hardware side, alternative extruder systems such as pneumatic or conveying screw extruder should be explored to expand the types of inks and to improve the efficiency of the printing process. A pneumatic extruder system could provide faster response time and the conveying screw could allow for continuous loading as well as higher extrusion force. Temperature control devices such as a heated syringe or a thermoelectric cooling built plate could be implemented for printing phase-changing food such as chocolate and gelatin. Additionally, larger nozzle diameter and tubing would be desirable in food printing to shorten print time as well as allow for printing of food with bigger particles.

On the software side, slicer software with more customization options such as Simplify3D should be explored. A primary requirement for 3D printing paste is to have slicing algorithm that allows continuous extrusion and minimize crossover. A G-code generating script for paste extrusion could be written in Python similar to mecode developed by the Lewis Lab at Harvard University.

Texture profile analysis should be conducted to further characterize the inks investigated in this study. In addition, the effect of temperature on the inks should also be investigated. The gelation kinetics for phase-changing inks could be measured with a rheometer using temperature sweeps.

The types of printed food objects could be further explored. Post-printing modifications such as steaming, frying, or baking could be employed; however, the effect of cooking on product shape and texture should be taken into account. Texture profile analysis or sensory panels should also be considered to evaluate the effect of the 3D process on these food attributes.

# Letters of Copyright Permission

## TERMS AND CONDITIONS

Nov 11, 2017

This Agreement between Ms. Chu yin Huang ("You") and Elsevier ("Elsevier") consists of your license details and the terms and conditions provided by Elsevier and Copyright Clearance Center.

License Number	4226230780340
License date	Nov 11, 2017
Licensed Content Publisher	Elsevier
Licensed Content Publication	Journal of Food Engineering
Licensed Content Title	Extrusion-based food printing for digitalized food design and nutrition control
Licensed Content Author	Jie Sun, Weibiao Zhou, Liangkun Yan, Dejian Huang, Lien-ya Lin
Licensed Content Date	Available online 6 March 2017
Licensed Content Volume	n/a
Licensed Content Issue	n/a
Licensed Content Pages	1
Start Page	0
End Page	0
Type of Use	reuse in a thesis/dissertation
Portion	figures/tables/illustrations
Number of figures/tables/illustrations	1
Format	both print and electronic
Are you the author of this Elsevier article?	No
Will you be translating?	No
Original figure numbers	Figure 4. Extrusion mechanisms
Title of your thesis/dissertation	Extrusion-based 3D Printing and Characterization of Edible Materials
Expected completion date	Dec 2017
Estimated size (number of pages)	100
Requestor Location	Ms. Chu yin Huang 86 Annina crescent  Markham, ON L3R4S6 Canada Attn: Ms. Chu yin Huang
Total	0.00 CAD

Letter of copyright permission for

Figure 2 Different types of extrusion mechanisms reproduced with permission from (Sun et al., 2017)

ELSEVIER LICENSE  
TERMS AND CONDITIONS

Nov 13, 2017

This Agreement between Ms. Chu yin Huang ("You") and Elsevier ("Elsevier") consists of your license details and the terms and conditions provided by Elsevier and Copyright Clearance Center.

License Number	4227151236976
License date	Nov 13, 2017
Licensed Content Publisher	Elsevier
Licensed Content Publication	Carbohydrate Polymers
Licensed Content Title	Structure and physicochemical properties of octenyl succinic anhydride modified starches: A review
Licensed Content Author	Michael C. Sweedman, Morgan J. Tizzotti, Christian Schäfer, Robert G. Gilbert
Licensed Content Date	Jan 30, 2013
Licensed Content Volume	92
Licensed Content Issue	1
Licensed Content Pages	16
Start Page	905
End Page	920
Type of Use	reuse in a thesis/dissertation
Portion	figures/tables/illustrations
Number of figures/tables/illustrations	1
Format	both print and electronic
Are you the author of this Elsevier article?	No
Will you be translating?	No
Original figure numbers	Fig. 1. Schematic of structural and chemical composition of amylose and amylopectin.
Title of your thesis/dissertation	Extrusion-based 3D Printing and Characterization of Edible Materials
Publisher of new work	University of Waterloo
Author of new work	Christine Moresoli
Expected completion date	Dec 2017
Estimated size (number of pages)	100
Requestor Location	Ms. Chu yin Huang 86 Annina crescent  Markham, ON L3R4S6 Canada Attn: Ms. Chu yin Huang

Letter of copyright permission for Figure 4 Structure of amylose and amylopectin in starch (Sweedman et al., 2013). Reproduced with permission



Confirmation Number: 11681012  
Order Date: 11/13/2017

Customer Information

Customer: Chu Yin Huang  
Account Number: 3001216683  
Organization: Chu Yin Huang  
Email: cy3huang@uwaterloo.ca  
Phone: +1 (416) 300-6722  
Payment Method: Invoice

This is not an invoice

Order Details

Biofabrication

Billing Status:  
N/A

Order detail ID: 70789822  
ISSN: 1758-5090  
Publication Type: e-Journal  
Volume:  
Issue:  
Start page:  
Publisher: IOP Publishing

Permission Status: **Granted**  
Permission type: Republish or display content  
Type of use: Thesis/Dissertation  
Order License Id: 4227150321002

Requestor type: Academic institution  
Format: Print, Electronic  
Portion: chart/graph/table/figure  
Number of charts/graphs/tables/figures: 1  
The requesting person/organization: University of Waterloo  
Title or numeric reference of the portion(s): Chapter 2, Figure 3. Evaluating 3D printability of gel...image analysis of lattice structures  
Title of the article or chapter the portion is from: Extrusion-based 3D printing  
Editor of portion(s): N/A  
Author of portion(s): N/A  
Volume of serial or monograph: N/A  
Page range of portion: 18  
Publication date of portion: December 2017  
Rights for: Main product  
Duration of use: Current edition and up to 5 years  
Creation of copies for the disabled: no  
With minor editing privileges: no  
For distribution to: Worldwide  
In the following language(s): Original language of publication  
With incidental promotional use: no  
Lifetime unit quantity of new product: Up to 499

Title: Extrusion-based 3D Printing and Characterization of Edible Materials  
Instructor name: Christine Moresoli  
Institution name: University of Waterloo  
Expected presentation date: Dec 2017

Letter of copyright permission for Figure 5 Evaluating 3D printability of gel through image analysis of lattice structures (Ouyang et al., 2016). Reproduced with permission of IOP Publishing in the format Thesis/Dissertation via Copyright Clearance Center.

ELSEVIER LICENSE  
TERMS AND CONDITIONS

Nov 13, 2017

This Agreement between Ms. Chu yin Huang ("You") and Elsevier ("Elsevier") consists of your license details and the terms and conditions provided by Elsevier and Copyright Clearance Center.

License Number	4227241171656
License date	Nov 13, 2017
Licensed Content Publisher	Elsevier
Licensed Content Publication	Food Hydrocolloids
Licensed Content Title	Factors influencing the physico-chemical, morphological, thermal and rheological properties of some chemically modified starches for food applications—A review
Licensed Content Author	Jaspreet Singh, Lovdeep Kaur, O.J. McCarthy
Licensed Content Date	Jan 1, 2007
Licensed Content Volume	21
Licensed Content Issue	1
Licensed Content Pages	22
Start Page	1
End Page	22
Type of Use	reuse in a thesis/dissertation
Intended publisher of new work	other
Portion	figures/tables/illustrations
Number of figures/tables/illustrations	1
Format	both print and electronic
Are you the author of this Elsevier article?	No
Will you be translating?	No
Original figure numbers	table 2
Title of your thesis/dissertation	Extrusion-based 3D Printing and Characterization of Edible Materials
Publisher of new work	University of Waterloo
Author of new work	Christine Moresoli
Expected completion date	Dec 2017
Estimated size (number of pages)	100
Requestor Location	Ms. Chu yin Huang 86 Annina crescent  Markham, ON L3R4S6 Canada Attn: Ms. Chu yin Huang

Letter of copyright permission for Table 1 Health Canada approved chemically modified starch and their properties adapted from (Singh et al., 2007) with permission

## Bibliography

3DFP Ventures Ltd, 2017. Food Ink. [WWW Document]. URL <http://foodink.io/> (accessed 6.19.17).

Ağar, B., Gençcelep, H., Sarıcaoğlu, F.T., Turhan, S., 2016. Effect of sugar beet fiber concentrations on rheological properties of meat emulsions and their correlation with texture profile analysis. *Food and Bioprocess Processing* 100, 118–131. doi:10.1016/j.fbp.2016.06.015

Aguilera, J.M., Park, D.J., 2016. Texture-modified foods for the elderly: Status, technology and opportunities. *Trends in Food Science & Technology* 57, 156–164. doi:10.1016/j.tifs.2016.10.001

Ahmed, J., Ramaswamy, H.S., 2007a. Dynamic and steady shear rheology of fruit puree based baby foods. *Food Science & Technology* 44, 579–585.

Ahmed, J., Ramaswamy, H.S., 2007b. Dynamic rheology and thermal transitions in meat-based strained baby foods. *Journal of Food Engineering* 78, 1274–1284. doi:10.1016/j.jfoodeng.2005.12.035

Ahmed, J., Ramaswamy, H.S., 2006. Viscoelastic properties of sweet potato puree infant food. *Journal of Food Engineering* 74, 376–382. doi:10.1016/j.jfoodeng.2005.03.010

Akkineni, A.R., Ahlfeld, T., Lode, A., Gelinsky, M., 2016. A versatile method for combining different biopolymers in a core/shell fashion by 3D plotting to achieve mechanically robust constructs. *Biofabrication* 8, 45001. doi:10.1088/1758-5090/8/4/045001

Alvarez, M.D., Canet, W., 1999. Rheological properties of mashed potatoes made from dehydrated flakes: effect of ingredients and freezing. *European Food Research and Technology* 209, 335–342. doi:10.1007/s002170050505

Alvarez, M.D., Fernández, C., Olivares, M.D., Canet, W., 2012. A rheological characterisation of mashed potatoes enriched with soy protein isolate. *Food Chemistry* 133, 1274–1282. doi:10.1016/j.foodchem.2011.05.111

Anzalone, G.C., Wijnen, B., Pearce, J.M., 2015. Multi-material additive and subtractive prosumer digital fabrication with a free and open-source convertible delta RepRap 3-D printer. *Rapid Prototyping Journal* 21, 506–519. doi:10.1108/RPJ-09-2014-0113

Avery, M.P., Klein, S., Richardson, R., Bartlett, P., Adams, G., Dickin, F., Simske, S., 2014. The Rheology of Dense Colloidal Pastes Used in 3D-Printing. HP Tech Report HPL-2014-2.

Barui, S., Chatterjee, S., Mandal, S., Kumar, A., Basu, B., 2017. Microstructure and compression



- properties of 3D powder printed Ti-6Al-4V scaffolds with designed porosity: Experimental and computational analysis. *Materials Science and Engineering C* 70, 812–823.  
doi:10.1016/j.msec.2016.09.040
- Bégin-Drolet, A., Dussault, M.-A., Fernandez, S.A., Larose-Dutil, J., Leask, R.L., Hoesli, C.A., Ruel, J., 2017. Design of a 3D printer head for additive manufacturing of sugar glass for tissue engineering applications. *Additive Manufacturing* 15, 29–39. doi:10.1016/j.addma.2017.03.006
- Benson, J., 2014. Chow from a 3-D printer? Natick researchers are working on it. *Army Technology Magazine* 22.
- Brand-Miller, J.C., Atkinson, F.S., Gahler, R.J., Kacinik, V., Lyon, M.R., Wood, S., 2010. Effects of PGX, a novel functional fibre, on acute and delayed postprandial glycaemia. *European Journal of Clinical Nutrition* 64, 1488–1493. doi:10.1038/ejcn.2010.199
- Cai, K., Román-Manso, B., Smay, J.E., Zhou, J., Osendi, M.I., Belmonte, M., Miranzo, P., 2012. Geometrically complex silicon carbide structures fabricated by robocasting. *Journal of the American Ceramic Society* 95, 2660–2666. doi:10.1111/j.1551-2916.2012.05276.x
- Campo, L., Tovar, C., 2009. The effect of egg albumen on the viscoelasticity of crab sticks made from Alaska Pollock and Pacific Whiting surimi. *Food Hydrocolloids* 23, 1641–1646.  
doi:10.1016/j.foodhyd.2009.03.013
- Campo, L., Tovar, C., 2008. Influence of the starch content in the viscoelastic properties of surimi gels. *Journal of Food Engineering* 84, 140–147. doi:10.1016/j.jfoodeng.2007.05.011
- Carmona, J.A., Ramirez, P., Calero, N., Garcia, M.C., Munoz, J., 2014. Non-Linear Dynamic Viscoelasticity of Xanthan Gum Solutions, in: Williams, P.A., Phillips, G.O. (Eds.), *Gums and Stabilisers for the Food Industry 17-The Changing Face of Food Manufacture: The Role of Hydrocolloids*. Royal Society of Chemistry, pp. 176–183.
- Casanovas, A., Hernández, M.J., Martí-Bonmatí, E., Dolz, M., 2011. Cluster classification of dysphagia-oriented products considering flow, thixotropy and oscillatory testing. *Food Hydrocolloids* 25, 851–859. doi:10.1016/j.foodhyd.2010.07.029
- Chung, J.H.Y., Naficy, S., Yue, Z., Kapsa, R., Quigley, A., Moulton, S.E., Wallace, G.G., 2013. Bio-ink properties and printability for extrusion printing living cells. *Biomaterials Science* 1, 763.  
doi:10.1039/c3bm00012e

- Cichero, J.A.Y., 2016. Adjustment of Food Textural Properties for Elderly Patients. *Journal of Texture Studies* 47, 277–283. doi:10.1111/jtxs.12200
- Cichero, J.A.Y., Lam, P., Steele, C.M., Hanson, B., Chen, J., Dantas, R.O., Duivesteyn, J., Kayashita, J., Lecko, C., Murray, J., Pillay, M., Riquelme, L., Stanschus, S., 2017. Development of International Terminology and Definitions for Texture-Modified Foods and Thickened Fluids Used in Dysphagia Management: The IDDSI Framework. *Dysphagia* 32, 293–314. doi:10.1007/s00455-016-9758-y
- Contractor, A., Irvin, D.J., Prouty, M.D., Ward, K.A., McDaniel, J.B., 2016. Additive Manufacturing For Producing Edible Composition. US 2016/0106142 A1.
- Creative Machines Lab, 2017. Digital Food [WWW Document]. URL <http://www.creativemachineslab.com/digital-food.html> (accessed 6.19.17).
- Cyriac, F., Lugt, P.M., Bosman, R., 2015. On a New Method to Determine the Yield Stress in Lubricating Grease. *Tribology Transactions* 58, 1021–1030. doi:10.1080/10402004.2015.1035414
- D’Angelo, G., Hansen, H.N., Hart, A.J., Angelo, G.D., Hansen, H.N., Hart, A.J., 2016. Molecular Gastronomy Meets 3D Printing: Layered Construction via Reverse Spherification. *3D Printing and Additive Manufacturing* 3, 152–159. doi:10.1089/3dp.2016.0024
- De Graef, V., Depypere, F., Minnaert, M., Dewettinck, K., 2011. Chocolate yield stress as measured by oscillatory rheology. *Food Research International* 44, 2660–2665. doi:10.1016/j.foodres.2011.05.009
- Delgado-Pando, G., Cofrades, S., Ruiz-Capillas, C., Triki, M., Jiménez-Colmenero, F., 2012. Low-fat pork liver pâtés enriched with n-3 PUFA/konjac gel: Dynamic rheological properties and technological behaviour during chill storage. *Meat Science* 92, 44–52. doi:10.1016/j.meatsci.2012.04.002
- Derossi, A., Caporizzi, R., Azzollini, D., Severini, C., 2017. Application of 3D printing for customized food. A case on the development of a fruit-based snack for children. *Journal of Food Engineering* 1–11. doi:10.1016/j.jfoodeng.2017.05.015
- Dolz, M., Hernández, M.J., Delegido, J., 2006. Oscillatory measurements for salad dressings stabilized with modified starch, xanthan gum, and locust bean gum. *Journal of Applied Polymer Science* 102, 897–903. doi:10.1002/app.24125
- Dorj, B., Park, J.-H., Kim, H.-W., 2012. Robocasting chitosan/nanobioactive glass dual-pore structured

- scaffolds for bone engineering. *Materials Letters* 73, 119–122. doi:10.1016/j.matlet.2011.12.107
- Dupuis, J.H., Liu, Q., Yada, R.Y., 2014. Methodologies for Increasing the Resistant Starch Content of Food Starches: A Review. *Comprehensive Reviews in Food Science and Food Safety* 13, 1219–1234. doi:10.1111/1541-4337.12104
- Faes, M., Valkenaers, H., Vogeler, F., Vleugels, J., Ferraris, E., 2015. Extrusion-based 3D printing of ceramic components. *Procedia CIRP* 28, 76–81. doi:10.1016/j.procir.2015.04.028
- Feilden, E., Blanca, E.G.T., Giuliani, F., Saiz, E., Vandeperre, L., 2016. Robocasting of structural ceramic parts with hydrogel inks. *Journal of the European Ceramic Society* 36, 2525–2533. doi:10.1016/j.jeurceramsoc.2016.03.001
- Funami, T., 2011. Next target for food hydrocolloid studies: Texture design of foods using hydrocolloid technology. *Food Hydrocolloids* 25, 1904–1914. doi:10.1016/j.foodhyd.2011.03.010
- Furukawa, H., Kawakami, M., Gong, J., Makino, M., Kabir, M.H., Saito, A., 2015. 3D gel printing for soft-matter systems innovation, in: *The International Society for Optical Engineering*. pp. 1–6. doi:10.1117/12.2084472
- Gabriele, D., de Cindio, B., D’Antona, P., 2001. A weak gel model for foods. *Rheologica Acta* 40, 120–127. doi:10.1007/s003970000139
- Gao, C., Rahaman, M.N., Gao, Q., Teramoto, A., Abe, K., 2013. Robotic deposition and in vitro characterization of 3D gelatin–bioactive glass hybrid scaffolds for biomedical applications. *Journal of Biomedical Materials Research Part A* 101A, 2027–2037. doi:10.1002/jbm.a.34496
- Ghazanfari, A., Li, W., Leu, M.C., Hilmas, G.E., 2017. A novel freeform extrusion fabrication process for producing solid ceramic components with uniform layered radiation drying. *Additive Manufacturing* 15, 102–112. doi:10.1016/j.addma.2017.04.001
- Godoi, F.C., Prakash, S., Bhandari, B.R., 2016. 3d printing technologies applied for food design: Status and prospects. *Journal of Food Engineering* 179, 44–54. doi:10.1016/j.jfoodeng.2016.01.025
- Gong, J., Shitara, M., Serizawa, R., Makino, M., Kabir, M.H., Furukawa, H., 2014. 3D Printing of Meso-Decorated Gels and Foods. *Materials Science Forum* 783–786, 1250–1254. doi:10.4028/www.scientific.net/MSF.783-786.1250
- Hamilton, C.A., Alici, G., in het Panhuis, M., 2017. 3D printing Vegemite and Marmite: Redefining

- “breadboards.” *Journal of Food Engineering* 1–6. doi:10.1016/j.jfoodeng.2017.01.008
- Hao, L., Mellor, S., Seaman, O., Henderson, J., Sewell, N., Sloan, M., 2010. Material characterisation and process development for chocolate additive layer manufacturing. *Virtual and Physical Prototyping* 5, 57–64. doi:10.1080/17452751003753212
- He, Y., Yang, F., Zhao, H., Gao, Q., Xia, B., Fu, J., 2016. Research on the printability of hydrogels in 3D bioprinting. *Scientific Reports* 6, 29977. doi:10.1038/srep29977
- Health Canada, 2016. 13. List of Permitted Starch-Modifying Agents [WWW Document]. URL <http://www.hc-sc.gc.ca/fn-an/securit/addit/list/13-starch-modif-amidon-eng.php> (accessed 12.18.16).
- Hinton, T.J., Hudson, A., Pusch, K., Lee, A., Feinberg, A.W., 2016. 3D Printing PDMS Elastomer in a Hydrophilic Support Bath via Freeform Reversible Embedding. *ACS Biomaterials Science & Engineering* 2, 1781–1786. doi:10.1021/acsbiomaterials.6b00170
- Hinton, T.J., Jallerat, Q., Palchesko, R.N., Park, J.H., Grodzicki, M.S., Shue, H.-J., Ramadan, M.H., Hudson, A.R., Feinberg, A.W., 2015. Three-dimensional printing of complex biological structures by freeform reversible embedding of suspended hydrogels. *Science Advances* 1, e1500758–e1500758. doi:10.1126/sciadv.1500758
- Hözl, K., Lin, S., Tytgat, L., Van Vlierberghe, S., Gu, L., Ovsianikov, A., 2016. Bioink properties before, during and after 3D bioprinting. *Biofabrication* 8, 32002. doi:10.1088/1758-5090/8/3/032002
- Horvath, J., 2014. The Desktop 3D Printer, in: *Mastering 3D Printing*. Apress, Berkeley, CA, pp. 11–20. doi:10.1007/978-1-4842-0025-4\_2
- Hung, K.-C., Tseng, C.-S., Hsu, S., 2014. Synthesis and 3D Printing of Biodegradable Polyurethane Elastomer by a Water-Based Process for Cartilage Tissue Engineering Applications. *Advanced Healthcare Materials* 3, 1578–1587. doi:10.1002/adhm.201400018
- Hyun, K., Kim, S.H., Ahn, K.H., Lee, S.J., 2002. Large amplitude oscillatory shear as a way to classify the complex fluids. *Journal of Non-Newtonian Fluid Mechanics* 107, 51–65. doi:10.1016/S0377-0257(02)00141-6
- Jakus, A.E., Secor, E.B., Rutz, A.L., Jordan, S.W., Hersam, M.C., Shah, R.N., 2015a. Three-Dimensional Printing of High-Content Graphene Scaffolds for Electronic and Biomedical Applications. *ACS Nano* 9, 4636–4648. doi:10.1021/acsnano.5b01179

- Jakus, A.E., Taylor, S.L., Geisendorfer, N.R., Dunand, D.C., Shah, R.N., 2015b. Metallic Architectures from 3D-Printed Powder-Based Liquid Inks. *Advanced Functional Materials* 25, 6985–6995. doi:10.1002/adfm.201503921
- Jones, E., Oliphant, T., Peterson, P., Others, 2001. SciPy: Open Source Scientific Tools for Python [WWW Document]. URL <https://www.scipy.org/> (accessed 9.25.17).
- Keller, H.H., Locher, J.L., Steele, C.M., 2014. Translational Advancements in Applications of Pureed Food. *Journal of Nutrition in Gerontology and Geriatrics* 33, 135–138. doi:10.1080/21551197.2014.943635
- Khot, R.A., Aggarwal, D., Pennings, R., Hjorth, L., Mueller, F.F., 2017. EdiPulse: Investigating a Playful Approach to Self-monitoring through 3D Printed Chocolate Treats, in: *Proceedings of the 2017 CHI Conference on Human Factors in Computing Systems - CHI '17*. ACM Press, Denver, CO, USA, pp. 6593–6607. doi:10.1145/3025453.3025980
- Kim, H.W., Bae, H., Park, H.J., 2017. Classification of the printability of selected food for 3D printing: Development of an assessment method using hydrocolloids as reference material. *Journal of Food Engineering*. doi:10.1016/j.jfoodeng.2017.07.017
- Kirchmajer, D.M., Gorkin III, R., in het Panhuis, M., 2015. An overview of the suitability of hydrogel-forming polymers for extrusion-based 3D-printing. *Journal of Materials Chemistry B* 3, 4105–4117. doi:10.1039/C5TB00393H
- Koenig, N., 2016. How 3D printing is shaking up high end dining. *BBC News*.
- Kouzani, A.Z., Adams, S., J. Whyte, D., Oliver, R., Hemsley, B., Palmer, S., Balandin, S., 2017. 3D Printing of Food for People with Swallowing Difficulties, in: *The International Conference on Design and Technology*. KnE Engineering, pp. 23–29. doi:10.18502/keg.v2i2.591
- Kouzani, A.Z., Adams, S., Oliver, R., Nguwi, Y.Y., Hemsley, B., Balandin, S., 2016. 3D printing of a pavlova, in: *2016 IEEE Region 10 Conference (TENCON)*. IEEE, pp. 2281–2285. doi:10.1109/TENCON.2016.7848435
- Kück, M., 2015. 3D-printed food to help patients with dysphagia [WWW Document]. *CORDIS*. URL [http://cordis.europa.eu/news/rcn/124181\\_en.html](http://cordis.europa.eu/news/rcn/124181_en.html) (accessed 8.30.17).
- Kuo, C.-J., Huang, S.-H., Hsu, T.-H., Rodriguez, L., Olivé, X., Ching-Yi, M., Chang, C.-T., Shih-Chang, C., Sepulveda, E., Delgado, V., 2016. Apparatus, Method and System for Manufacturing Food

Using Additive Manufacturing 3D Printing Technology. US 2016/0135493 A1.

- Kuo, C.C., Liu, L.C., Teng, W.F., Chang, H.Y., Chien, F.M., Liao, S.J., Kuo, W.F., Chen, C.M., 2016. Preparation of starch/acrylonitrile-butadiene-styrene copolymers (ABS) biomass alloys and their feasible evaluation for 3D printing applications. *Composites Part B: Engineering* 86, 36–39. doi:10.1016/j.compositesb.2015.10.005
- Lanaro, M., Forrestal, D.P., Scheurer, S., Slinger, D.J., Liao, S., Powell, S.K., Woodruff, M.A., 2017. 3D printing complex chocolate objects: Platform design, optimization and evaluation. *Journal of Food Engineering*. doi:10.1016/j.jfoodeng.2017.06.029
- Le Tohic, C., O’Sullivan, J.J., Drapala, K.P., Chartrin, V., Chan, T., Morrison, A.P., Kerry, J.P., Kelly, A.L., 2017. Effect of 3D printing on the structure and textural properties of processed cheese. *Journal of Food Engineering*. doi:10.1016/j.jfoodeng.2017.02.003
- Lehner, B.A.E., Schmieden, D.T., Meyer, A.S., 2017. A Straightforward Approach for 3D Bacterial Printing. *ACS Synthetic Biology* A-G. doi:10.1021/acssynbio.6b00395
- Leung, P.Y.V., 2017. Sugar 3D Printing: Additive Manufacturing with Molten Sugar for Investigating Molten Material Fed Printing. *3D Printing and Additive Manufacturing* 4, 13–18. doi:10.1089/3dp.2016.0045
- Li, H., Prakash, S., Nicholson, T.M., Fitzgerald, M.A., Gilbert, R.G., 2016. Instrumental measurement of cooked rice texture by dynamic rheological testing and its relation to the fine structure of rice starch. *Carbohydrate Polymers* 146, 253–263. doi:10.1016/j.carbpol.2016.03.045
- Li, H., Zhu, Y., Jiao, A., Zhao, J., Chen, X., Wei, B., Hu, X., Wu, C., Jin, Z., Tian, Y., 2013. Impact of  $\alpha$ -amylase combined with hydrochloric acid hydrolysis on structure and digestion of waxy rice starch. *International Journal of Biological Macromolecules* 55, 276–281. doi:10.1016/j.ijbiomac.2013.01.021
- Li, W., Ghazanfari, A., Leu, M.C., Landers, R.G., 2015. Methods of extrusion on demand for high solids loading ceramic paste in freeform extrusion fabrication, in: *International Solid Freeform Fabrication Symposium*. pp. 332–345.
- Lille, M., Nurmela, A., Nordlund, E., Metsä-Kortelainen, S., Sozer, N., 2017. Applicability of protein and fiber-rich food materials in extrusion-based 3D printing. *Journal of Food Engineering* 1–8. doi:10.1016/j.jfoodeng.2017.04.034

- Linden, D. Van Der, 2015. 3D Food printing: Creating shapes and textures [WWW Document]. TNO. URL [https://www.tno.nl/media/5517/3d\\_food\\_printing\\_march\\_2015.pdf](https://www.tno.nl/media/5517/3d_food_printing_march_2015.pdf) (accessed 10.7.15).
- Lipton, J., Arnold, D., Nigl, F., Lopez, N., Cohen, D., Norén, N., Lipson, H., 2010. Multi-material food printing with complex internal structure suitable for conventional post-processing, in: Proceedings of the 21st International Solid Freeform Fabrication Symposium. Austin, U.S., pp. 809–815. doi:10.1.1.375.7717
- Lipton, J.I., 2017. Printable food: the technology and its application in human health. *Current Opinion in Biotechnology* 44, 198–201. doi:10.1016/j.copbio.2016.11.015
- Lipton, J.I., Lipson, H., 2016. 3D Printing Variable Stiffness Foams Using Viscous Thread Instability. *Nature Publishing Group* 6, 2–7. doi:10.1038/srep29996
- Liu, Z., Zhang, M., Bhandari, B., Yang, C., 2017. Impact of rheological properties of mashed potatoes on 3D printing. *Journal of Food Engineering*. doi:10.1016/j.jfoodeng.2017.04.017
- Lu, Z.-H., Sasaki, T., Li, Y.-Y., Yoshihashi, T., Li, L.-T., Kohyama, K., 2009. Effect of amylose content and rice type on dynamic viscoelasticity of a composite rice starch gel. *Food Hydrocolloids* 23, 1712–1719. doi:10.1016/j.foodhyd.2009.01.009
- Malone, E., Lipson, H., 2007. Fab@Home: the personal desktop fabricator kit. *Rapid Prototyping Journal* 13, 245–255. doi:10.1108/13552540710776197
- Mancini, F., Montanari, L., Peressini, D., Fantozzi, P., 2002. Influence of Alginate Concentration and Molecular Weight on Functional Properties of Mayonnaise. *LWT - Food Science and Technology* 35, 517–525. doi:10.1006/fstl.2002.0899
- Mantell, D.A., Hays, A.W., Langford, Z.C., 2015. Printing 3D Tempered Chocolate. US 9185923 B2.
- McKenna, B.M., Lyng, J.G., 2003. Introduction to food rheology and its measurement, in: *Texture in Food, Volume 1: Semi-Solid Foods*. Woodhead Publishing, Boston, pp. 130–160. doi:<http://dx.doi.org/10.1533/9781855737082.1.130>
- Meza, B.E., Verdini, R.A., Rubiolo, A.C., 2011. Effect of freezing on the viscoelastic behaviour during the ripening of a commercial low-fat soft cheese. *International Dairy Journal* 21, 346–351. doi:10.1016/j.idairyj.2010.12.003
- Mizrahi, M., Golan, A., Mizrahi, A.B., Gruber, R., Lachnise, A.Z., Zoran, A., 2016. Digital Gastronomy:

- Methods & Recipes for Hybrid Cooking, in: Proceedings of the 29th Annual Symposium on User Interface Software and Technology - UIST '16. Association for Computing Machinery, Inc, Tokyo, Japan, pp. 541–552. doi:10.1145/2984511.2984528
- Moelants, K.R.N., Cardinaels, R., Jolie, R.P., Verrijssen, T.A.J., Van Buggenhout, S., Zumalacarregui, L.M., Van Loey, A.M., Moldenaers, P., Hendrickx, M.E., 2013. Relation Between Particle Properties and Rheological Characteristics of Carrot-derived Suspensions. *Food and Bioprocess Technology* 6, 1127–1143. doi:10.1007/s11947-011-0718-0
- Moreira, R., Chenlo, F., Arufe, S., Rubinos, S.N., 2015. Physicochemical characterization of white, yellow and purple maize flours and rheological characterization of their doughs. *Journal of Food Science and Technology* 52, 7954–7963. doi:10.1007/s13197-015-1953-6
- Moresi, M., Bruno, M., Parente, E., 2004. Viscoelastic properties of microbial alginate gels by oscillatory dynamic tests. *Journal of Food Engineering* 64, 179–186. doi:10.1016/j.jfoodeng.2003.09.030
- Murekatete, N., Hua, Y., Chamba, M.V.M., Djakpo, O., Zhang, C., 2014. Gelation Behavior and Rheological Properties of Salt- or Acid-Induced Soy Proteins Soft Tofu-Type Gels. *Journal of Texture Studies* 45, 62–73. doi:10.1111/jtxs.12052
- Muth, J.T., Vogt, D.M., Truby, R.L., Mengüç, Y., Kolesky, D.B., Wood, R.J., Lewis, J.A., 2014. Embedded 3D Printing of Strain Sensors within Highly Stretchable Elastomers. *Advanced Materials* 26, 6307–6312. doi:10.1002/adma.201400334
- N. Turner, B., Strong, R., A. Gold, S., 2014. A review of melt extrusion additive manufacturing processes: I. Process design and modeling. *Rapid Prototyping Journal* 20, 192–204. doi:10.1108/RPJ-01-2013-0012
- Namasivayam-MacDonald, A.M., Morrison, J.M., Steele, C.M., Keller, H., 2017. How Swallow Pressures and Dysphagia Affect Malnutrition and Mealtime Outcomes in Long-Term Care. *Dysphagia*. doi:10.1007/s00455-017-9825-z
- Norton, I.T., Spyropoulos, F., Cox, P., 2011. *Practical Food Rheology: An Interpretive Approach*. Wiley-Blackwell, Oxford, UK. doi:10.1002/9781444391060
- O'Bryan, C.S., Bhattacharjee, T., Hart, S., Kabb, C.P., Schulze, K.D., Chilakala, I., Sumerlin, B.S., Sawyer, W.G., Angelini, T.E., 2017. Self-assembled micro-organogels for 3D printing silicone structures. *Science Advances* 3, e1602800. doi:10.1126/sciadv.1602800



- Ouyang, L., Yao, R., Zhao, Y., Sun, W., 2016. Effect of bioink properties on printability and cell viability for 3D bioplotting of embryonic stem cells. *Biofabrication* 8, 35020. doi:10.1088/1758-5090/8/3/035020
- Peleg, M., Normand, M.D., 2013. Modeling of Fungal and Bacterial Spore Germination under Static and Dynamic Conditions. *Applied and Environmental Microbiology* 79, 6765–6775. doi:10.1128/AEM.02521-13
- Peressini, D., Sensidoni, A., Pollini, C.M., Gabriele, D., Migliori, M., de Cindio, B., 2002. Filled-snacks production by co-extrusion-cooking. Part 3. A rheological-based method to compare filler processing properties. *Journal of Food Engineering* 54, 227–240. doi:10.1016/S0260-8774(01)00208-4
- Postiglione, G., Natale, G., Griffini, G., Levi, M., Turri, S., 2015. Conductive 3D microstructures by direct 3D printing of polymer/carbon nanotube nanocomposites via liquid deposition modeling. *Composites Part A: Applied Science and Manufacturing* 76, 110–114. doi:10.1016/j.compositesa.2015.05.014
- Potter, A.L., Hassid, W.Z., 1948. Starch. II. Molecular weights of amyloses and amylopectins from starches of various plant origins. *Journal of the American Chemical Society* 70, 3774–3777. doi:10.1021/ja01191a069
- Ramamoorthi, L., Lee, Y., Brewer, S., 2009. Effect of food matrix and heat treatment on the rheological properties of salmon-based baby food. *Journal of Food Engineering* 95, 432–437. doi:10.1016/j.jfoodeng.2009.06.004
- Ren, L., Zhou, X., Song, Z., Zhao, C., Liu, Q., Xue, J., Li, X., 2017. Process Parameter Optimization of Extrusion-Based 3D Metal Printing Utilizing PW–LDPE–SA Binder System. *Materials* 10, 305. doi:10.3390/ma10030305
- RepRapWiki, 2017. G-code [WWW Document]. URL <http://reprap.org/wiki/G-code> (accessed 10.25.17).
- Rodgers, S., 2016. Minimally Processed Functional Foods: Technological and Operational Pathways. *Journal of Food Science* 0, 1–11. doi:10.1111/1750-3841.13422
- Schutyser, M.A.I., Houlder, S., de Wit, M., Buijsse, C.A.P., Alting, A.C., 2017. Fused deposition modelling of sodium caseinate dispersions. *Journal of Food Engineering* 1–7. doi:10.1016/j.jfoodeng.2017.02.004

- Seisun, D., 2012. Overview of the Food Hydrocolloids Market, in: Williams, P.A., Phillips, G.O. (Eds.), *Gums and Stabilisers for the Food Industry 16*. Royal Society of Chemistry, pp. 3–8.
- Serizawa, R., Shitara, M., Gong, J., Makino, M., Kabir, M.H., Furukawa, H., 2014. 3D jet printer of edible gels for food creation, in: Goulbourne, N.C., Naguib, H.E. (Eds.), *Proceedings of the International Society for Optical Engineering*. pp. 1–5. doi:10.1117/12.2045082
- Severini, C., Derossi, A., 2016. Could the 3D Printing Technology be a Useful Strategy to Obtain Customized Nutrition? *Journal of Clinical Gastroenterology* 50, S175–S178. doi:10.1097/MCG.0000000000000705
- Severini, C., Derossi, A., Azzollini, D., 2016. Variables affecting the printability of foods: Preliminary tests on cereal-based products. *Innovative Food Science & Emerging Technologies* 38, 281–291. doi:10.1016/j.ifset.2016.10.001
- Shahiri Tabarestani, H., Mazaheri Tehrani, M., 2014. Optimization of physicochemical properties of low-fat hamburger formulation using blend of soy flour, split-pea flour and wheat starch as part of fat replacer system. *Journal of Food Processing and Preservation* 38, 278–288. doi:10.1111/j.1745-4549.2012.00774.x
- Sharma, M., Kristo, E., Corredig, M., Duizer, L., 2017. Effect of hydrocolloid type on texture of pureed carrots: Rheological and sensory measures. *Food Hydrocolloids* 63, 478–487. doi:10.1016/j.foodhyd.2016.09.040
- Shih, W.Y., Shih, W.-H., Aksay, I.A., 2004. Elastic and Yield Behavior of Strongly Flocculated Colloids. *Journal of the American Ceramic Society* 82, 616–624. doi:10.1111/j.1151-2916.1999.tb01809.x
- Shin, S.R., Farzad, R., Tamayol, A., Manoharan, V., Mostafalu, P., Zhang, Y.S., Akbari, M., Jung, S.M., Kim, D., Comotto, M., Annabi, N., Al-Hazmi, F.E., Dokmeci, M.R., Khademhosseini, A., 2016. A Bioactive Carbon Nanotube-Based Ink for Printing 2D and 3D Flexible Electronics. *Advanced Materials* 28, 3280–3289. doi:10.1002/adma.201506420
- Singh, J., Kaur, L., McCarthy, O.J., 2007. Factors influencing the physico-chemical, morphological, thermal and rheological properties of some chemically modified starches for food applications—A review. *Food Hydrocolloids* 21, 1–22. doi:10.1016/j.foodhyd.2006.02.006
- Soares, S., Forkes, A., 2014. *Insects Au Gratin - An investigation into the experiences of developing a 3D printer that uses insect protein based flour as a building medium for the production of sustainable*

- food, in: Proceedings of the 16th International Conference on Engineering and Product Design Education. pp. 426–431.
- Song, K.W., Kuk, H.Y., Chang, G.S., 2006. Rheology of concentrated xanthan gum solutions: Oscillatory shear flow behavior. *Korea Australia Rheology Journal* 18, 67–81. doi:10.1007/BF02908257
- Statistics Canada, 2016. Table 105-0501 Health indicator profile, annual estimates, by age group and sex, Canada, provinces, territories, health regions (2013 boundaries) and peer groups [WWW Document]. CANSIM (database). URL <http://www5.statcan.gc.ca/cansim/a26?lang=eng&retrLang=eng&id=1050501&&pattern=&stByVal=1&p1=1&p2=37&tabMode=dataTable&csid=> (accessed 10.18.17).
- Steffe, J.F., 1996. Rheological methods in food process engineering, 2nd ed, Agricultural Engineering. East, Lansing, MI.
- Sun, J., Peng, Z., Yan, L., Fuh, J., Hong, G.S., 2015a. 3D food printing—An innovative way of mass customization in food fabrication. *International Journal of Bioprinting* 1, 27–38. doi:10.18063/IJB.2015.01.006
- Sun, J., Zhou, W., Huang, D., Fuh, J.Y.H., Hong, G.S., 2015b. An Overview of 3D Printing Technologies for Food Fabrication. *Food and Bioprocess Technology* 8, 1605–1615. doi:10.1007/s11947-015-1528-6
- Sun, J., Zhou, W., Yan, L., Huang, D., Lin, L., 2017. Extrusion-based food printing for digitalized food design and nutrition control. *Journal of Food Engineering* 1–11. doi:10.1016/j.jfoodeng.2017.02.028
- Sweedman, M.C., Tizzotti, M.J., Schäfer, C., Gilbert, R.G., 2013. Structure and physicochemical properties of octenyl succinic anhydride modified starches: A review. *Carbohydrate Polymers* 92, 905–920. doi:10.1016/j.carbpol.2012.09.040
- Sworn, G., 2009. Xanthan gum, in: *Handbook of Hydrocolloids*. Woodhead Publishing, pp. 186–203.
- Takizawa, C., Gemmell, E., Kenworthy, J., Speyer, R., 2016. A Systematic Review of the Prevalence of Oropharyngeal Dysphagia in Stroke, Parkinson’s Disease, Alzheimer’s Disease, Head Injury, and Pneumonia. *Dysphagia* 31, 434–441. doi:10.1007/s00455-016-9695-9
- Tanaka, H., Asano, Y., Watanabe, M., Masumori, A., 2015. Food Printing technologies out of white rice, in: *International Conference on Digital Printing Technologies*. pp. 289–292.

- Tian, J. (Jingxin), Bryksa, B.C., Yada, R.Y., 2016. Feeding the world into the future – food and nutrition security: the role of food science and technology. *Frontiers in Life Science* 3769, 1–12.  
doi:10.1080/21553769.2016.1174958
- Tunick, M.H., 2011. Small-Strain Dynamic Rheology of Food Protein Networks. *Journal of Agricultural and Food Chemistry* 59, 1481–1486. doi:10.1021/jf1016237
- Tyers, P., 2017. Dysphagia no longer a bitter pill to swallow with 3D printed food - CSIRO blog [WWW Document]. CSIRO blog. URL <https://blog.csiro.au/dysphagia-no-longer-bitter-pill-to-swallow-3d-printed-food/> (accessed 6.7.17).
- Vancauwenberghe, V., Delele, M.A., Aregawi, W., Verboven, P., Bongaers, E., 2017a. Characterization and model-based design validation of 3D printed cookies, in: 7th Conference on Industrial Computed Tomography. Leuven, Belgium, pp. 1–9.
- Vancauwenberghe, V., Katalagarianakis, L., Wang, Z., Meerts, M., Hertog, M., Verboven, P., Moldenaers, P., Hendrickx, M.E., Lammertyn, J., Nicolaï, B., 2017b. Pectin based food-ink formulations for 3-D printing of customizable porous food simulants. *Innovative Food Science & Emerging Technologies* 42, 138–150. doi:10.1016/j.ifset.2017.06.011
- Vesco, A., Lipson, H., Cohen, D.L., Lipton, J.I., Cutler, M., Coulter, D., 2009. Hydrocolloid Printing: A Novel Platform for Customized Food Production, in: *Proceedings of the 20th International Solid Freeform Fabrication Symposium*. pp. 807–818. doi:10.1017/CBO9781107415324.004
- Viebke, C., Al-Assaf, S., Phillips, G.O., 2014. Food hydrocolloids and health claims. *Bioactive Carbohydrates and Dietary Fibre* 4, 101–114. doi:10.1016/j.bcdf.2014.06.006
- von Hasseln, K.W., von Hasseln, E.M., Williams, D.X., 2014. Apparatus and Method for Producing A Three-Dimensional Food Product. US 2014/0154378 A1.
- VormVrij 3D, 2016. LUTUM® – Clay and Ceramics 3dprinters [WWW Document]. URL <http://lutum.vormvrij.nl/> (accessed 7.5.17).
- Wang, G., Yao, L., Wang, W., Ou, J., Cheng, C.-Y., Ishii, H., 2016. xPrint: A Modularized Liquid Printer for Smart Materials Deposition, in: *Proceedings of the 2016 CHI Conference on Human Factors in Computing Systems - CHI '16*. ACM Press, San Jose, CA, USA, pp. 5743–5752.  
doi:10.1145/2858036.2858281
- Wang, J., Shaw, L.L., 2005. Rheological and extrusion behavior of dental porcelain slurries for rapid

- prototyping applications. *Materials Science and Engineering A* 397, 314–321.  
doi:10.1016/j.msea.2005.02.045
- Wang, L., Zhang, M., Bhandari, B., Yang, C., 2017. Investigation on fish surimi gel as promising food material for 3D printing. *Journal of Food Engineering* 1–8. doi:10.1016/j.jfoodeng.2017.02.029
- Wang, P.W., Chou, C.S., Wei, W.C.J., Liu, B.H., Liu, A., Wang, A.B., Luo, R.C., 2016. Glass and hot extrusion by ME module for 3D additive manufacturing, in: 2016 IEEE International Conference on Industrial Technology (ICIT). IEEE, pp. 1167–1171. doi:10.1109/ICIT.2016.7474920
- Wang, S., Lee, J.M., Yeong, W.Y., 2015. Smart hydrogels for 3D bioprinting. *International Journal of Bioprinting* 1, 3–14. doi:10.18063/IJB.2015.01.005.
- Wang, W., Yao, L., Zhang, T., Cheng, C., Levine, D., Ishii, H., 2017. Transformative Appetite, in: *Proceedings of the 2017 CHI Conference on Human Factors in Computing Systems - CHI '17*. ACM Press, Denver, CO, USA, pp. 6123–6132. doi:10.1145/3025453.3026019
- Williams, P.A., 2006. An Overview of the Structure-Function Relationships of Hydrocolloids, in: *Gums and Stabilisers for the Food Industry* 13. pp. 15–29.
- Wittbrodt, B.T., Glover, A.G., Laureto, J., Anzalone, G.C., Oppliger, D., Irwin, J.L., Pearce, J.M., 2013. Life-cycle economic analysis of distributed manufacturing with open-source 3-D printers. *Mechatronics* 23, 713–726. doi:10.1016/j.mechatronics.2013.06.002
- Yang, F., Zhang, M., Bhandari, B., 2015. Recent development in 3D food printing. *Critical Reviews in Food Science and Nutrition* 57, 3145–3153. doi:10.1080/10408398.2015.1094732
- Yang, F., Zhang, M., Bhandari, B., Liu, Y., 2018. Investigation on lemon juice gel as food material for 3D printing and optimization of printing parameters. *LWT - Food Science and Technology* 87, 67–76. doi:10.1016/j.lwt.2017.08.054
- Yang, J., Wu, L., Liu, J., 2001. Method For Rapidly Making A 3-D Food Object. US 6280784 B1.
- Yi, Y., Jeon, H.J., Yoon, S., Lee, S.M., 2015. Hydrocolloids decrease the digestibility of corn starch, soy protein, and skim milk and the antioxidant capacity of grape juice. *Preventive Nutrition and Food Science* 20, 276–283. doi:10.3746/pnf.2015.20.4.276
- Zargaraan, A., Rastmanesh, R., Fadavi, G., Zayeri, F., Mohammadifar, M.A., 2013. Rheological aspects of dysphagia-oriented food products: A mini review. *Food Science and Human Wellness* 2, 173–178.

doi:10.1016/j.fshw.2013.11.002

Zargaraan, A., Saghafi, Z., Hasandokht Firouz, M., Fadavi, G., Ghorbani Gorji, S., Mohammadifar, M.A., 2015. Effect of Rheological Properties on Sensory Acceptance of Two-Model Dysphagia-Oriented Food Products. *Journal of Texture Studies* 46, 219–226. doi:10.1111/jtxs.12131

Zhao, Y., Li, Y., Mao, S., Sun, W., Yao, R., 2015. The influence of printing parameters on cell survival rate and printability in microextrusion-based 3D cell printing technology. *Biofabrication* 7, 45002. doi:10.1088/1758-5090/7/4/045002

Zhong, J., Zhou, G.X., He, P.G., Yang, Z.H., Jia, D.C., 2017. 3D printing strong and conductive geopolymer nanocomposite structures modified by graphene oxide. *Carbon* 117, 421–426. doi:10.1016/j.carbon.2017.02.102

Zimmerman, A., Walczyk, D.F., Crump, S.S., Batchelder, J.S., 2015. Additive Manufacturing System and Method for Printing Customized Chocolate Confections. US 9215882 B2.

## Appendix A. Slicer setting design of experiments

This section documents early attempts at modifying 3D printer settings for paste extrusion. The initial approach was to use design of experiment to investigate the effect of key printer settings and visually inspect the finished print.

At first the slicer settings didn't have the expected effect on nozzle speed and extrusion rate. The software has an "printing speed" option to but changing the number from 40 mm/s to as low as 5 mm/s did not make a noticeable difference to the nozzle speed. Instead, decreasing parameters seemingly unrelated to the printing speed such as filament diameter significantly slowed down the nozzle.

The proposed  $2^3$  full factorial DOE is proposed in table 1A and 2A.

Table 1A Design of Experiment Variables

Factors	+1	-1
A - Layer Height	1.5 mm	1 mm
B - Extruder steps per mm	1000	800
C - Filament Diameter	1 mm	0.75 mm

Table 2A Detailed Full Factorial DOE for Printer Parameters

$2^3$ factorial	A	B	C	Weight (g)	Print Time (min)	Print Quality Ranking (best = 8, worst = 1)
run #1	1	1	1	10.34	25	7
run #2	-1	1	1	9.24	22	8
run #3	1	-1	1	8.55	25	5
run #4	-1	-1	1	7.7	22	4
run #5	1	1	-1	9.37	27	2
run #6	-1	1	-1	19.88	45	1
run #7	1	-1	-1	7.56	27	3
run #8	-1	-1	-1	16.3	45	6

The final weight of the printed object and printing time were selected as measured variables to observe the effect of printer parameter on extrusion rate and printing speed. Print quality of a 3D object was more difficult to measure numerically so a ranking method was adopted instead. The print with the best quality was ranked as 8 while the worst one was ranked as 1. Photos of the actual print are shown in the table 3A.

Table 3A Photos of printed object using carrot purée thickened with 5% w/w modified food starch

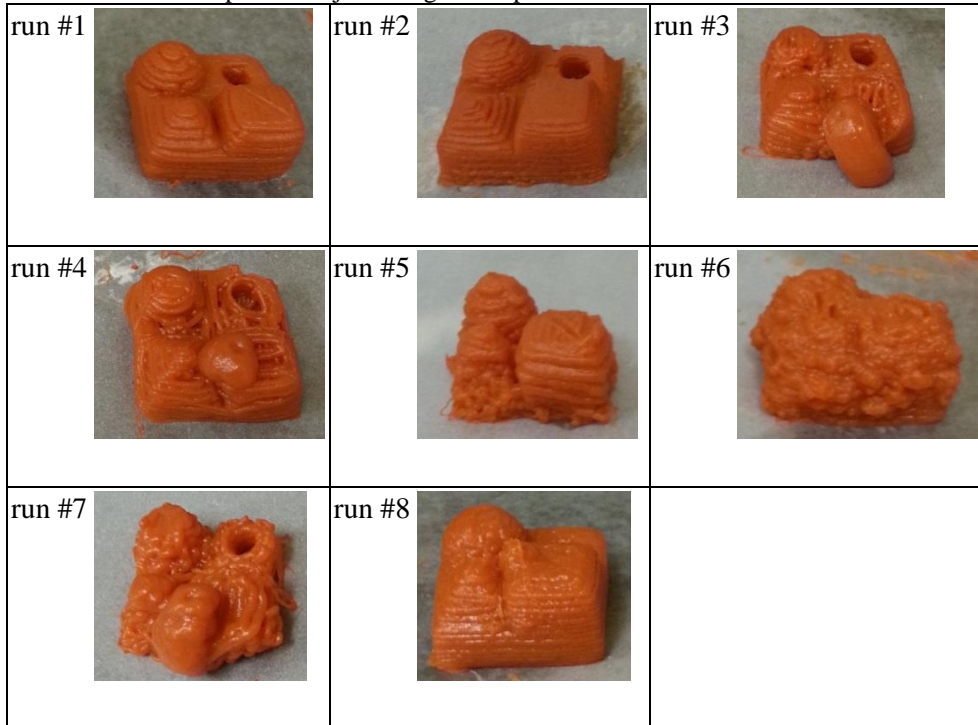


Figure 1A, 2A and 3A show the effect of layer height (A), extruder steps per mm (B), filament diameter (C), and their interactions (AB, BC, and AC). The three factor interaction (ABC) was usually assumed to be negligible. If the magnitude of the effect for a factor was smaller than that of the three factor interaction then it was deemed to be non-significant.

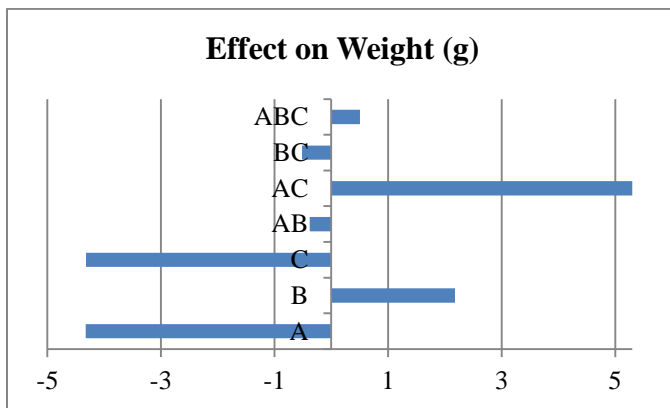


Figure 1A Parameter Effect on Weight of Printed Object

The most significant factors shown in figure 1A were layer height, filament diameter, and their interaction term. Increasing the two factors individually resulted in decreased weight; however, if both factors were increased or decreased simultaneously there would be an increase in the amount extruded. One thing to note was that inconsistent extrusion occurred when layer height was at 1.5 mm and filament diameter was



set to 0.75 mm. The printer would move through a portion of the layer with nothing extruding and then extrude a large amount while moving slowly through the remaining portion.

Increasing the extruder steps per mm increased the weight of the final print. This effect was expected since the stepper motor controls how fast the syringe pushes out material.

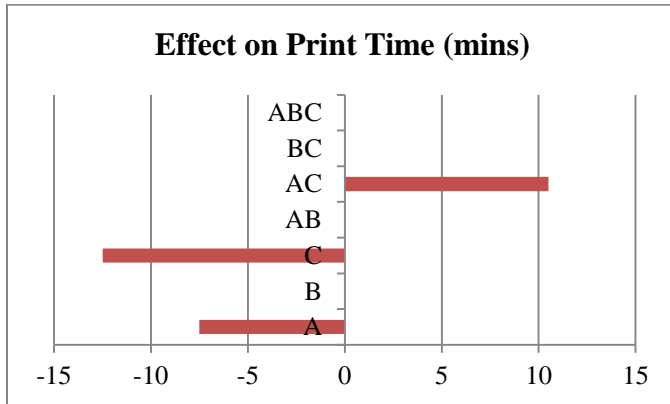


Figure 2A Parameter Effect on Printing Time

Figure 2A shows a similar pattern between printing time and printed object weight. Increase in layer height and filament diameter reduced printing time. It was expected since taller layers means there was less of them to print. However, print speed at 1.5 mm layer height was slower compared to that of 1.0 mm layer height at the same filament diameter.

Decreasing both simultaneously increased the print time by slowing down the print speed. Slower movement allows for increased print accuracy since paste material doesn't handle sharp turns very well. In addition, some material such as cookie dough requires the slower speed for proper layer adhesion.

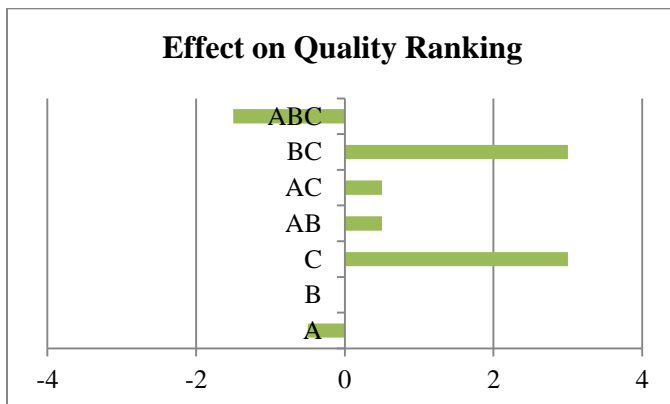


Figure 3A Parameter Effect on Print Quality

Figure 3A shows that the filament diameter and its interaction term with extruder steps per mm have the most significant effect on the print quality. It was surprising since layer height was expected to have the most impact according to conventional 3D printing: lower layer height gives better print resolution. This was observed somewhat by comparing run #1 and run #2 from table 3A. The second run has decreased layer height and the final print has better defined geometry.

Overall increasing filament diameter gives better print. When filament diameter is set to 0.75 mm the extrusion was inconsistent and the print speed was very slow. If the slow print speed was matched with a slow extrusion rate then the object turns out ok (run # 8), otherwise it only produces a blob (run #6).

After this initial set of experiments it was decided that the machine command G-code should be investigated in more detail and the results are available in section G-code and slicer settings.

## Appendix B. 3D printing experiment slicer settings

The table below list slicer settings, target motor speed, and target nozzle speed used during printing experiments. Motor speed is controlled by EEPROM extruder steps per mm (e-steps) and nozzle speed is controlled by extrusion multiplier. This section shows calculations required to find the appropriate e-steps and extrusion multiplier to enter into the slicer software.

Slicer Setting	
Filament Diameter (mm)	3.125
Nozzle Diameter (mm)	1.54
Layer Height (mm)	1
Printing speed (mm/s) = $f$	10

Targets	
Motor speed (RPM)	48
Nozzle speed (mm/s)	8

Rearrange Equation 3-3 to calculate e-steps

$$e\text{-step} = \frac{\text{motor speed} \times \text{motor steps per rev}}{f}$$

$$e\text{-step} = \frac{48 \text{ RPM} \times 20000 \frac{\text{steps}}{\text{rev}}}{10 \frac{\text{mm}}{\text{s}} \times \frac{60 \text{ s}}{\text{min}}} = 1600 \text{ steps/mm}$$

Combine Equation 3-1 and Equation 3-2 and rearrange to calculate extrusion multiplier

$$\text{extrusion multiplier} = \frac{D_{\text{nozzle}}}{\text{layer height}} \times \frac{(D_{\text{filament}})^2}{(D_{\text{nozzle}})^2} \times \frac{1}{1.273} \times \frac{f}{\text{nozzle speed}}$$

$$\text{extrusion multiplier} = \frac{1.54 \text{ mm}}{1 \text{ mm}} \times \frac{(3.125 \text{ mm})^2}{(1.54 \text{ mm})^2} \times \frac{1}{1.273} \times \frac{10 \frac{\text{mm}}{\text{s}}}{8 \frac{\text{mm}}{\text{s}}} = 6.22$$

With the given slicer settings: for motor speed of 48 RPM the e-step should be set to 1600 steps per mm. For nozzle speed of 8 mm/s the extrusion multiplier should be set to 6.22.